Impact of Cyclic Loads and Subsurface Weaknesses on the Behavior of a Deep-Sea Quay Wall

Ammaan Chat

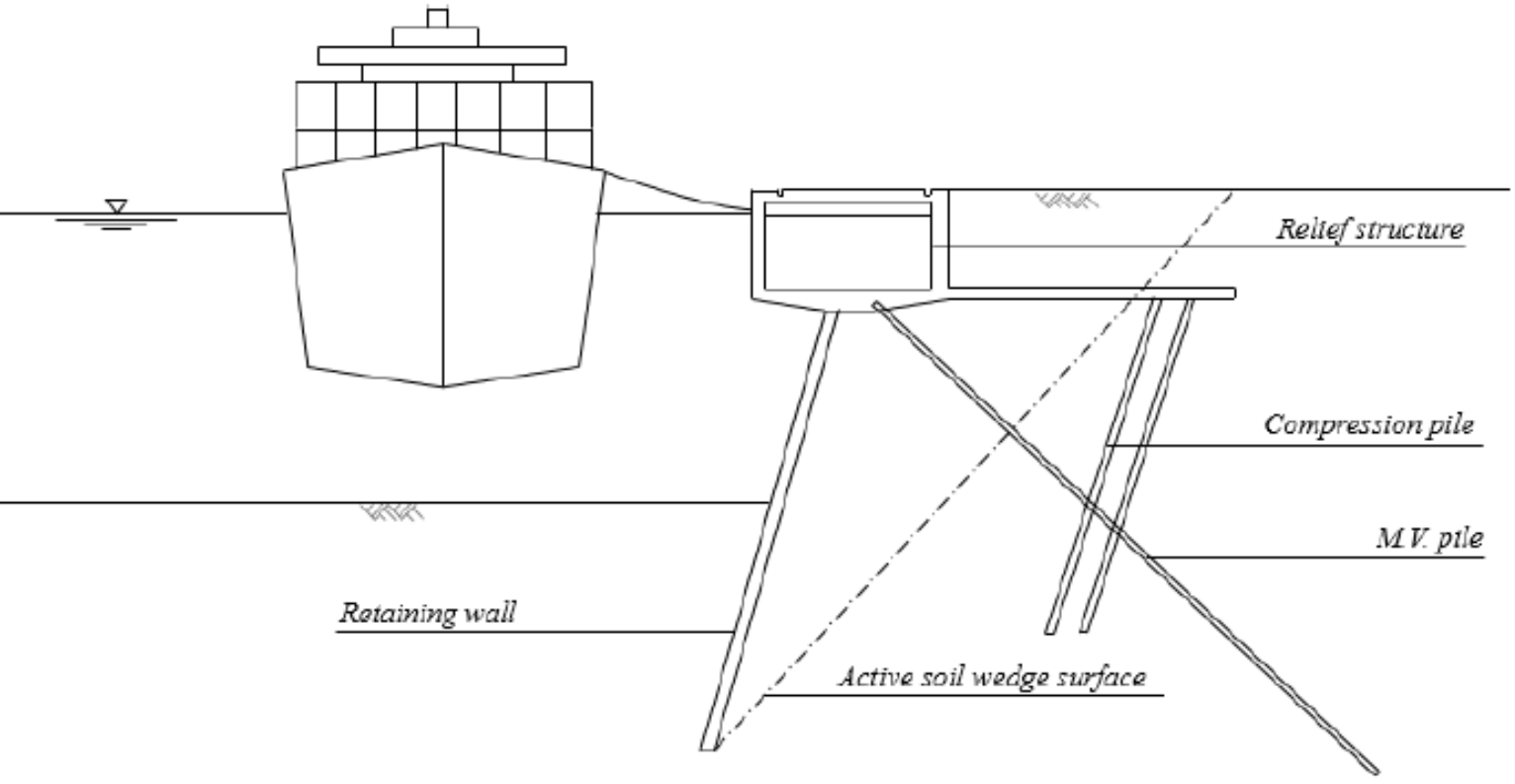

TU Delft

Impact of Cyclic Loads and Subsurface Weaknesses on the Behavior of a Deep-Sea Quay Wall

by

Ammaan Chat

to obtain the degree of Master of Science

at the Delft University of Technology,

Student number: 5047587

Project duration: April, 2024 – , – April, 2025

Thesis committee: Prof. dr. ir. K. Gavin (Chair), TU Delft, Geo-Engineering

Prof. dr. ir. M. van Koningsveld, TU Delft, Hydraulic Engineering

This thesis is confidential and cannot be made public until April 23, 2025.

TU Delft

Abstract

Deep-sea quay walls in the Port of Rotterdam have been extensively constructed in the last 150 years and have been subjected to cycles of unload and reload of surcharge load along with fluctuating water levels. These cyclic load conditions significantly impact the continuous development of deformations in the quay walls and the forces in the structural elements over a long term. This study presents a detailed analysis of the long-term behavior of the quay wall located in the Hartel Tank Terminal at the Port of Rotterdam. This study also considers the effect of deeply embedded thin clay layers on the bearing capacity of the screw injection (SI) piles. Previous research by Rica and Van Baars (2018) and Chai et al. (2022), among many others, have shown that the subsurface weaknesses, especially due to presence of deep clay layers, have a significant impact on the end bearing capacity of the closed ended piles loaded under compression. This effect depends on the location of the clay layer with respect to the zone of influence of the pile.

The quay walls nowadays are modelled with finite element method to better understand the elasto-plastic response of the soil and the intricate soil-structure interactions in detail. The advanced soil constitutive models consider the dependence of various parameters of the soil conditions on the stress and strain development in the soil, such as shear strength parameters and stiffness parameters.

For this research, the quay wall is modelled in Plaxis 2D and is then validated using real time measurement data from the smart sensors installed in the sub-structure. Changes in water levels are obtained through piezometers, and their influence on the combined wall displacement and the anchor force is examined with finite element analysis. The load combinations presented in design reports of the project were used to simulate the realistic unload-reload conditions in the model. The future modifications planned for HTT quay wall will introduce a crane load instead of a liquid storage tank load. The future scenario loading has also been analysed for the long-term behaviour of the wall. In addition, the effect of the presence of clay layers in the soil profile on the end bearing capacity of the SI piles is analysed.

The two major structural responses observed in the behaviour of the quay wall is the accumulation of horizontal wall displacements and continuously increasing anchor forces in the tension piles over long-term application of the cyclic surcharge loads. The progressive increase in the anchor force is a direct result of the continuously increasing horizontal displacements of the wall. The maximum allowed horizontal displacement of the wall is 1% of the total retaining height, as stated in the project design report by Imbrechts et al. (2017a). The accumulation of displacement in the wall was maximum after the first cycle of loading for both the current and future scenarios of loading, and the rate of accumulation of displacement dropped exponentially after the initial load cycles due to densification of the soil. In the current scenario, after 40 cycles of unloading and reloading, the total accumulated displacement of the wall after 22.2 mm, which resulted in the total wall displacement of 20% of the maximum allowed wall displacement. In the Future loading scenario, the additional horizontal load from the crane resulted in much larger accumulation in wall displacements, taking the total wall displacements to 33% of the max displacement value after 40 load cycles. The rate of accumulation of displacement after 40 cycles of loading in the current loading scenario converged at 0.1 mm per load cycle towards the end of loading cycles. The anchor forces generated in the MV pile also showed a similar trend in accumulation of anchor forces with repeated unloading and reloading on top of the wall. The anchor force generated in the MV pile is a measure of the pulling force that the MV pile experiences. This pulling force is balanced by the shaft friction mobilised in the bearing stratum. The mobilised anchor force capacity and the mobilised shaft capacity of the tension piles proved to be more critical for the stability analysis of the quay wall, as around 62% of anchor force capacity along with 73% of shaft capacity were mobilised after the load cycles from the future load scenario. The water level fluctuations did not impact the performance of the quay in terms of horizontal displacement of the wall or anchor forces in the MV piles as the soil profile is dominated by highly permeable cohesionless soils and the scale of water level fluctuations was not significant.

Clay layer present in the deep Pleistocene sand in the vicinity of the tips of the bearing piles was shown to

have a negative impact on the mobilised base resistance of the piles. In the case of a quay wall with a relieving platform and a bearing and tension pile trestle with inclined pair of bearing piles, where the complete load bearing capacity is derived only from the deep bearing sand layers, the impact was most significant i.e. at least a 10% reduction, when the clay layer was present from 3D below the pile tip to 1.5D above the pile tip, D being the equivalent diameter of the SI piles. The maximum reduction in the mobilised base resistance was observed to be 38% when the pile tips were in the middle of the clay layer, with half the clay layer above and half below the pile tips. Given the smaller magnitude of the current operational loads, the thin clay layer did not have a significant impact on the deformation behaviour of the quay wall as the reduction in the end bearing resistance of SI piles was compensated by the increase in the mobilised shaft capacity observed near the toe of the SI piles. However, the increase in the mobilised shaft capacity in presence of clay layer at +0.5D was more than 80% as compared to a case with no clay layer. This drastic increase in the mobilised shaft capacity poses a serious concern for the stability of the pile system. In the case of presence of a thicker clay layer, or the presence of multiple clay layers around the pile tips, the mobilised shaft capacity could reach the failure point which would lead to plunging of the SI piles leading to large settlements of the relieving platform and possibly to larger bending moments generated in the combined wall

This study provided valuable insights into the long-term deformation behaviour of the quay wall under cyclic operational and water loads. It also provided critical reasons to enhance site investigations to look for any subsurface weaknesses in the vicinity of structural elements and to optimise the pile design, such as embedment length, as per the actual subsurface conditions.

Contents

1 Introduction **1**
- 1.1 Motivation for research . . . 1
- 1.2 Research Objectives . . . 2
- 1.3 Research Methodology . . . 3

2 Background Information **5**
- 2.1 History of Quays in The Netherlands . . . 5
- 2.2 Calculation Methods . . . 8
  - 2.2.1 The Blum Method . . . 8
  - 2.2.2 Spring Supported Beam Method . . . 9
  - 2.2.3 Finite Element Method . . . 10
- 2.3 Loads acting on the quay . . . 15
- 2.4 Influence of thin clay layer presence on SI piles . . . 19

3 Case Study **24**
- 3.1 Case Description . . . 24
- 3.2 Elements of quay wall . . . 25

4 Numerical Model **31**
- 4.1 Soil Profile . . . 32
- 4.2 Soil Parameters . . . 35
- 4.3 Structural Elements Model Input Paramenters . . . 38
- 4.4 Simulating Construction Phases . . . 41
- 4.5 Validation of the Plaxis Model with Measurement Data . . . 44

5 Modeling the Cyclic Loading Behaviour **47**
- 5.1 Introduction . . . 47
- 5.2 Unload-Reload Behaviour of the Quay wall . . . 47
  - 5.2.1 Design Load Cases . . . 50
  - 5.2.2 Unload-Reload Simulation Method . . . 55
  - 5.2.3 Wall Horizontal Displacement Results . . . 56
  - 5.2.4 Anchor Force Results . . . 60
- 5.3 Behaviour of Quay Wall under Cyclic Water Level Fluctuations . . . 64
  - 5.3.1 Monitoring Data of Water Level . . . 66
  - 5.3.2 Water Level Fluctuation Simulation Method . . . 66
  - 5.3.3 Results of Water Level Fluctuation Simulations . . . 67
- 5.4 Discussion . . . 68
  - 5.4.1 Cyclic Surcharge Loading . . . 68
  - 5.4.2 Cyclic Water Level Fluctuations . . . 69
  - 5.4.3 Comparing the impact of Cyclic Surcharge Loads and Cyclic Water Loads . . . 70

6 Soil profile with Deep Clay Layer **72**
- 6.1 Presence of Deep Embedded Clay Layer in Pleistocene Sand . . . 72
- 6.2 Method of Simulating Influence of Clay Layer on SI Piles . . . 74
- 6.3 Influence of Clay layer on base resistance of SI Piles . . . 76
- 6.4 Discussion . . . 79

7 Conclusions and Recommendations **83**
- 7.1 Conclusions . . . 83
  - 7.1.1 Impact of Cyclic Loads . . . 84

7.1.2 Influence of Subsurface Weakness on SI Piles 85
7.2 Recommendations 86
7.2.1 Design Considerations for Cyclic Loading 86
7.2.2 Design Considerations for Subsurface Weaknesses 87
7.2.3 Future Research 87

A Drawing of Section B4 **91**

B Cone Penetration Test Data **93**
B.1 CPTs used for soil parameter determination 93
B.2 CPTs from zone B showing presence of deep clay layer 103

List of Figures

2.1 Progressive increase of water depth in the port of Rotterdam (De Gijt & Broeken, 2013) 5
2.2 Gravity Quay on shallow foundation (De Gijt & Broeken, 2013) 6
2.3 Pile supported masonry block wall, 1854 6
2.4 Caisson wall, 1913 (De Gijt & Broeken, 2013) 7
2.5 Combined wall with pile trestle and sand drains 7
2.6 Combined wall with a deep relieving platform 8
2.7 Soil stress-displacement diagram according to Blum 1931 (Korff, 2018) 9
2.8 Soil stress-displacement diagram for spring supported beam method (Korff, 2018) 10
2.9 Finite element mesh for the quay wall at HTT (left), and finite elements with nodes around the bearing piles (right) 11
2.10 Three independent stiffness moduli for different types of loading in HS model (Brinkgreve, 2019) 11
2.11 Hyperbolic stress-strain relationship in triaxial loading (Duncan & Chang, 1970) 12
2.12 Shear Hardening in the HS Model (Brinkgreve, 2019a) 12
2.13 Cap and Shear yield surfaces in HS model (Brinkgreve, 2019a) 13
2.14 Stiffness modulus variation with shear strain amplitudes (Obrzud & Truty, 2018) 14
2.15 Shear modulus reduction curve adopted in the HSsmall model (Obrzud & Truty, 2018) 15
2.16 Shear loading on the ground caused by heaped bulk storage (De Gijt & Broeken, 2013) 16
2.17 Time-dependent deformation of the wall (De Gijt et al., 2011) 18
2.18 Development of wall displacement in time due to cyclic surcharge loads (De Gijt et al., 2011) . 19
2.19 Effect of partial embedment on the base resistance of a pile (White & Bolton, 2005) 21
2.20 Influence of weak clay layer on the bearing capacity of a pile in sand (Chai et al., 2022) 22

3.1 HTT Quay wall after the construction of storage tanks enclosed within bund walls 24
3.2 Combined wall with steel tubular piles and triple PU28 sheet piles (De Gijt & Broeken, 2013) . 26
3.3 Cast iron saddle eccentrically placed on tubular pile (De Gijt & Broeken, 2013) 26
3.4 MV pile tip with grout pipe (Spruit et al., 2019) 27
3.5 Soil arches around the bearing piles (Qiu & Grabe, 2012) 28
3.6 Principle of a deep relief floor (De Gijt & Broeken, 2013) 29
3.7 Placement of FBG sensors in the H-profile MV Piles 30

4.1 Drawing of the cross-section at zone B4 of HTT quay wall (Putteman et al., 2017) 32
4.2 Locations of CPTs around zone B4 (Imbrechts et al., 2017a) 33
4.3 CPT DKM032B from axis X-2 taken from the report Geotechnisch Onderzoek VN-66080-1 by Dijkstra (2016) 34
4.4 Shaft friction around MV pile mobilised in the Pleistocene sand (Imbrechts et al., 2017c) 40
4.5 Dredging steps at zone B4 of HTT quay wall (Schouten, 2020) 43
4.6 Water levels before and after the dredging of Wijchen layer (Putteman et al., 2017) 44
4.7 Validation of FE model with inclinometer measurement data 45
4.8 Validation of FE Model with anchor force data 46

5.1 : Loads acting on the quay wall in current loading scenario (Tank load) and future loading scenario (Crane load) 50
5.2 The bending moment in the compression pile for design case 1 (left) and design case 2 (right) 53
5.3 Anchor Forces mobilised in the two design cases OG1 and OG2 54
5.4 Combi-wall displacement at the end of dredging and in design cases OG1 and OG2 54
5.5 Maximum horizontal displacement in the combi-wall with unload-reload cycles in the current and future loading scenarios 57
5.6 Horizontal Displacement of the wall with load cycles in current and future scenario 58
5.7 Incremental horizontal displacements of combi-wall with reloading steps 60
5.8 Tensile force (left) and skin friction (right, in Pleistocene sand) vs. Depth at the final load step of MV piles load tests at HTT quay wall (Spruit et al., 2019) 61

5.9 Mobilisation of anchor forces with unload-reload cycles in current and future loading scenario . 62
5.10 Mobilisation of shaft resistance in MV pile with unload-reload cycles in current and future loading scenario 63
5.11 Increments in anchor force with load cycles in current and future scenarios 64
5.12 Comparison between Harbour water level and Ground water level at HTT quay wall in early operational phase (Schouten, 2020) 65
5.13 Groundwater level fluctuations at zone B4 of HTT quay wall 66
5.14 Effect of water level fluctuations on the horizontal displacement of combi-wall 67
5.15 Plastic points (red) generated in the soil after final dredging phase 68
5.16 Evolution of plastic points in the soil behind the top part of the wall with load cycles in current and future loading scenarios 69
5.17 Comparison of wall displacement response for cyclic surcharge loading and cyclic water loading 70

6.1 CPTs depicting presence of deep weak layers (red) in the Pleistocene sand (Imbrechts et al., 2017b) 73
6.2 Locations of CPTs that recorded deep clay layers around zone B4 (Imbrechts et al., 2017b) . . 73
6.3 CPT DKM53 showing deeply embedded clay layer (red) in Pleistocene sand (Imbrechts et al., 2017b) 74
6.4 Representation of soil parameters for the deep clay layer along with the Plaxis model overview 75
6.5 Plaxis model output showing axial forces in the waterside SI pile with no clay layer (left) and clay layer at +0.5D from pile tip (right) 76
6.6 Influence of clay layer on the mobilised base resistance of the waterside SI pile 77
6.7 Influence of clay layer on the mobilised base resistance of the landside SI pile 78
6.8 Influence of clay layer on the average mobilised base resistance of both SI piles 79
6.9 Skin fiction generated along SI piles for the case of no deep clay layer (left) and a clay layer at +0.5 D (right) 80
6.10 Overview of the Plaxis 3D model created to simulate pile load test in presence of weak soil layer (Chai et al., 2022) 81
6.11 Load frame for pile load tests of 4 SI piles (Matic et al., 2019) 81

B.1 CPTs along axis-3 with deep clay layers [red] recorded around zone B of HTT quay wall (Imbrechts et al., 2017b) 103
B.2 Locations of CPTs that recorded deep clay layers around zone B4 (Imbrechts et al., 2017b) . . 103

List of Tables

2.1 Representative hawser force for different ships (De Gijt & Broeken, 2013) 17
2.2 Container Crane loads for existing cranes at the Port of Rotterdam (De Gijt & Broeken, 2013) . 17

3.1 Zones A to D at HHTT quay and their specifications (Schouten, 2020) 25

4.1 Soil parameters as per design report (Imbrechts et al., 2017a) 33
4.2 Soil layer description 34
4.3 Soil input parameters for the Plaxis model 37
4.4 Additional soil material parameters for the model 37
4.5 Model input parameters of structural elements 38
4.6 Additional model input for plate elements 39
4.7 Embedded beam elements strength properties 41

5.1 Description of crane load cases (Imbrechts et al., 2017a) 49
5.2 Loads applied to validate design cases with the FE model 52
5.3 Comparison between the maximum field moment in the combi-wall in design cases OG1 and OG2 53
5.4 Summary of loads activated to simulate the cyclic surcharge loading behaviour of quay wall . . 56
5.5 Summary of maximum horizontal wall displacements with load cycles 59

Chapter 1

Introduction

Quay walls are geotechnical earth-retaining structures built along harbours or docks to hold back the earth and water pressures, and to facilitate berthing of ships for transshipment of goods. Quay walls are an essential infrastructure for maritime trade, facilitating the transhipment of goods in the form of dry or liquid freight. The main functions of Quay wall include the retaining of earth behind the quay, bearing of loads imposed by the shipment and operational activities, navigation facilities for the ships and the safety function.

In these modern engineering times, quay walls are usually founded on a network of tension and compression piles connected to a relieving platform. The front wall consists of a combination of sheet piles and tubular piles interlocked to form a wall. This combined wall serves as part of the foundation of the quay system due to the axial and flexural rigidity of the tubular piles. In the Netherlands, the quay system must overcome various challenges imposed by the weak soil conditions, changing surcharge load and water levels and the increasing draught of the Post Panamax shipping vessels that lead to increasing retaining heights (De Gijt & Broeken, 2013). The design life of most quay walls is around 100 years, and it is often expected that the design requirements will change in the lifespan. The geotechnical requirements in the functionality of quay wall include primarily the retaining height and the load bearing capacity. The functional requirements may also change in the nature of the use of the quay. For instance, in the case of HTT quay, it is also designed for a future modification of being used as a container terminal instead of liquid bulk storage terminal.

1.1. Motivation for research

The displacements of a quay wall are not always instantaneous for a given surcharge load. Often, the quay wall displacements keep continuously developing for the same surcharge loads if they are loaded and unloaded repeatedly. In the port of Rotterdam itself, multiple quay walls, such as the Brittanie Harbour Quay wall, have shown continuously developing wall displacements over time. De Gijt et al. (2011) and Tolba et al. (2020) have shown that two of the major reasons for this continuous development of wall displacement is the continuous regeneration of plastic strains and redistribution of stresses in the soil due to repeated loading and unloading of surcharge loads. These cycles of loading and unloading are usually not considered during the design of the quay structures. Moreover, all the design reports and the literature related to quay walls usually consider the surcharge loads as instantaneous in time and only study the effect of a single application of that load under different limit states or load combinations, hence disregarding the continuous redistribution of stresses and evolution of plastic strains in soil behind the wall which happens due to load-unload cycles.

The quay wall at the Hartel Tank Terminal in the Port of Rotterdam is chosen as the site to be studied in this

thesis. The design reports of the HTT quay wall have considered various design cases in ultimate limit state as well as the serviceability limit state. However, the effect of repeated cycles of unload and reload have not been included in the design reports.

HTT quay wall provides scope to study the effects of varying geotechnical conditions on the quay wall system including the loading and unloading of the surcharge on the quay wall. This quay wall has also been designed for a future modification into a container crane terminal, which leads to application of a container crane load on top of the wall. This adds a significant horizontal load on top of the quay wall and helps to better assess the impact of loading cycles on the development of horizontal displacements of the wall over long term. This thesis attempts to comprehend this long-term non-linear behaviour of the quay wall system, including the soil behind it, and the effect of the probable future modification into a container terminal port instead of a petrochemical storage and transhipment port. The key aspects studied in this thesis, due to loading and unloading of the wall, include the horizonal deformations in the wall and the anchor forces in the tension piles.

The changes in the loads experienced by the quay are also in the form of water loads. The fluctuating water levels in the harbour lead to corresponding changes in the ground water level behind the quay wall. This affects the stress conditions in the soil behind the wall in terms of total stress and effective stress in the soil. The changes in effective stress in the soil directly affect the lateral earth pressure experienced by the quay wall. These repeated water level fluctuations may also be a factor in the continuous development of displacements of the quay walls as they ultimately lead to loading and unloading of the wall.

Another aspect related to the quay walls, or any retaining wall in general, which demands serious consideration is the soil conditions experienced by the structure. The zone B of HTT quay wall is constructed with a relieving platform supported horizontally and vertically by the combined wall, the compression piles, and the tension piles. The soil conditions around the compression piles, especially the part of piles embedded in the load bearing soil layer, greatly influence the base capacity offered by the compression piles. Numerous studies have been conducted to show the effect of weak soil conditions around the tips of axially loaded compression piles. The presence of thin clay layers in the vicinity of the tips of compression piles reduces the base resistance mobilised by the piles, as shown by Chai et al. (2022) and Rica and Van Baars (2018). As per the CPT findings presented in the design report HHTT-DZK_RAP-DO-0303 by Imbrechts et al. (2017b), intermediate clay layers are present in the Pleistocene sand, where the compression piles get most of their shaft friction as well as all the end bearing capacity. These clay lenses are also present around the zone of influence of the compression piles. The geotechnical soil profiles extended from the available soil survey show the spatial extent of these clay layers to be less than 25 meter in the Pleistocene sand, with the CPT grid during soil investigations being 25m*25m. Hence, there is a chance of clay lenses smaller than 25m*25m to be present around the zone of influence of compression piles. This makes it crucial to also evaluate the stability of the quay wall in presence of these deep clay layers present in the bearing stratum. In this thesis, an attempt is made to study the influence of these deeply embedded clay layers on the end bearing resistance of the SI piles.

1.2. Research Objectives

The main objective of this is to analyse the effect of cyclic loading on top of the quay wall and the influence of subsurface weaknesses on the foundational capacity of the quay wall. The research question is presented as:

’How do operational cyclic loads and subsurface weaknesses impact the performance of a deep-sea quay wall?’

This study will investigate the structural response of a quay wall under cyclic surcharge and cyclic water loads, along with the assessment of foundational capacity of the quay wall in presence of deeply embedded clay layers in the bearing strata. To assess the quay wall in these aspects, the finite element modelling

software Plaxis-2D will be used with its advanced soil structure interaction analyses to acquire insights into the deformation behaviour and overall stability of the quay wall.

The main research question is divided into two sub questions as follows:

1. **What is the impact of cyclic surcharge and cyclic water loads on the deformation behaviour of the quay wall?**

The cyclic loading of surcharge loads refers to their repeated application and removal. The frequency and duration of these loads is not definite and has been estimated using similar cases around the Port of Rotterdam. These cyclic loads also consist of water loads due to changing water levels in the harbour and ground water. Over time, these cyclic loads can lead to progressive displacements of the front wall. To answer the first research sub-question, realistic cyclic loading scenarios will be simulated in the finite element model and the deformation behaviour of the quay wall along with the development of anchor forces in the tension piles will be analysed.

2. **What is the impact of subsurface weaknesses on the end-bearing resistance of the screw injection piles?**

Subsurface weaknesses refer to the presence of the deeply embedded clay layers in the Pleistocene sand. The localised regions of weak soil in an otherwise dense sand can affect the load bearing resistance offered by the compression piles. Such weak zones will be simulated in the finite element model to assess the behaviour of the compression piles in terms of their foundational capacity.

1.3. Research Methodology

This sub chapter presents the layout of the research. This thesis is divided into two parts. In the first part, an attempt is made to analyse the long-term behaviour of the quay wall under surcharge cyclic loading conditions and the effect of fluctuating water levels. The second part consists of design analysis to check for the effect of the spatially varying clay layers on the forces in the compression piles and the tension piles and how these forces translate to the horizontal displacement and bending moments in the wall.

After introducing the motivation for this research and the research questions in chapter 1, chapter 2 gives insight into the background knowledge about quay walls including history and calculation methods. It will also elaborate the load conditions present at the HTT quay wall and explain some literature related to the effect of clay layers on the end bearing resistance of the compression piles. Chapter 3 will introduce the HTT quay wall case study along with details on the structural components of the quay wall system. Chapter 4 explains how the quay wall is modelled in the finite element software Plaxis-2D. It elaborates how the input soil and structural properties of the model are calculated and later validates the simulated construction phases of the quay wall with measurement data from the site. Chapter 5 begins with introduction to the design load cases at the quay wall as per the design reports and progresses into how the load cases, including water loads, are simulated in the model. It ends with results and discussions on simulations. Chapter 6 begins with showing the presence of clay layers in the Pleistocene sand and explains the simulations of spatially varying clay layers around pile tips. It ends with results and discussion on the effect seen on screw injection piles. Finally, chapter 7 concludes the whole thesis and poses recommendations for future considerations.

For the implementation of the research, the following steps are followed:

Step 1: Creating and validating an a-priori finite element model to simulate the construction phase

For simulating the construction phases of the quay wall, a Plaxis model is created and validated using the measurement data from the fibre optic sensors and the inclinometers installed in the quay system that provide information about the Anchor forces in the MV piles and the horizontal deformation as well as the bending moments in the wall. The soil parameters to be input into the model are calculated using various empirical correlations with the cone tip resistance from the CPT data available. This is explained in detail in chapter 4.

Step 2: Simulating the loading and unloading conditions of surcharge and hydraulic loads

In this step, as explained in chapter 5, the most influential surface loading conditions are shown, inspired by the design report on the HTT quay wall by Mariteam and Port of Rotterdam. The design standard for Quay walls (De Gijt & Broeken, 2013) and the Design standard for sheet pile walls (CUR 166: Part-2, 2008) is also consulted in selecting the most suitable loads that would help predict the long-term behaviour of the quay. Along with this, the long-term influence of the daily changing water levels is also analysed in combination with the surface loads. The loading unloading and the water level changes are modelled using many different phases to activate and deactivate the said elements of the model. The current loading conditions are modelled first followed by the future modifications. Chapter 5 ends with discussion on the results.

Step 3: Model the spatially varying clay layers in the soil profile

As explained in chapter 6, this chapter will explain how the clay layers are chosen in the soil profile at various depths within and beyond the zone of influence for compression piles. The influence of these clay layers will also be studied on the shaft friction mobilisation of the tension piles. Finally, the result of such influences on the bearing and tension piles will be analysed for the quay wall system by looking into the differences into the horizontal deflection and the bending moment generated in the wall.

Chapter 2

Background Information

2.1. History of Quays in The Netherlands

The Port of Rotterdam is Europe's largest port for sea-going vessels and is the second largest port in the world. Quay walls play a crucial role in the functionality of this port. Approximately 80 km of quay wall length in total is presently in service at this port. According to the study from 2012, as reported in Handbook of Quay wall (De Gijt & Broeken, 2013), the port of Rotterdam is the busiest port in Europe in terms of the tonnage of the freight that is shipped annually.

In the 19th century, the maximum depth of the ports was not more than 10 meters. As the size of the ships increased, so did the need to deepen the ports. The Figure 2.1 below presents a timeline of increasing depths of different harbors over time in The Netherlands.

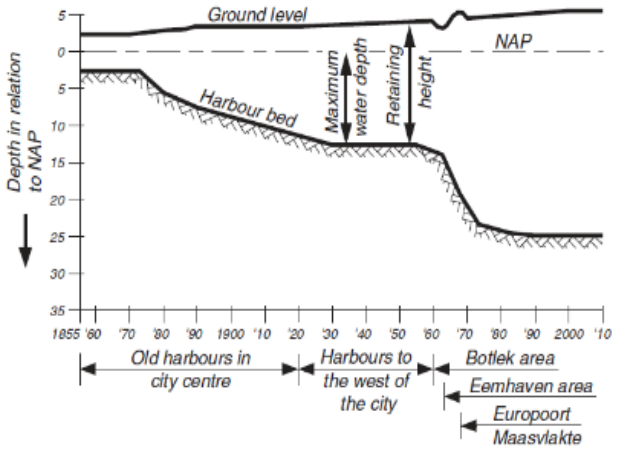

Figure 2.1: Progressive increase of water depth in the port of Rotterdam (De Gijt & Broeken, 2013)

The oldest quays in The Netherlands date from the beginning of the 17th century (De Gijt & Broeken, 2013). They were primarily all Gravity walls, with the soil retaining strength achieved out of their own structural weight and the weight of the soil above it. They served as fishing harbours in Blaakhaven, Nieuwehaven etc. The maximum retaining height that could be achieved during that period using brick masonry wall founded on

wooden grillage was merely 2.5 meter, which did not accommodate the draught of the ships, and so wooden piles were used in front of the quay structure to moor the ships and a gangway was used for loading and unloading of freight.

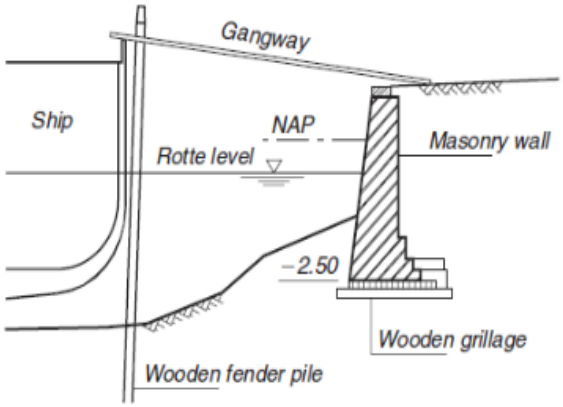

Figure 2.2: Gravity Quay on shallow foundation (De Gijt & Broeken, 2013)

To facilitate the berthing of ships adjacent to the quay, new development in the gravity quay construction took place. Wooden pile foundations were used to increase the retaining height. This type of quay construction was called Masonry Block Quay wall.

Figure 2.3: Pile supported masonry block wall, 1854

In 1905, RCC was introduced in the port construction. The wooden grillage and piles were replaced by RCC piles. Concrete caissons were then used as a shallow foundation instead of pile foundations, along with the replacement of the weaker soil with sand of sufficient bearing capacity. The caissons were filled with sand and served as the first prefabricated quay walls.

This method of construction of the quay proved to be economical in case of stronger subsoil where soil replacement is not needed. In fact, this method is still often used in the construction of quays. Caisson construction method could accommodate a retaining height of up to 15m, surcharge up to $150\,\text{kN/m}^2$ and a live load of up to 4500 kN, such as crane load (De Gijt & Broeken, 2013).

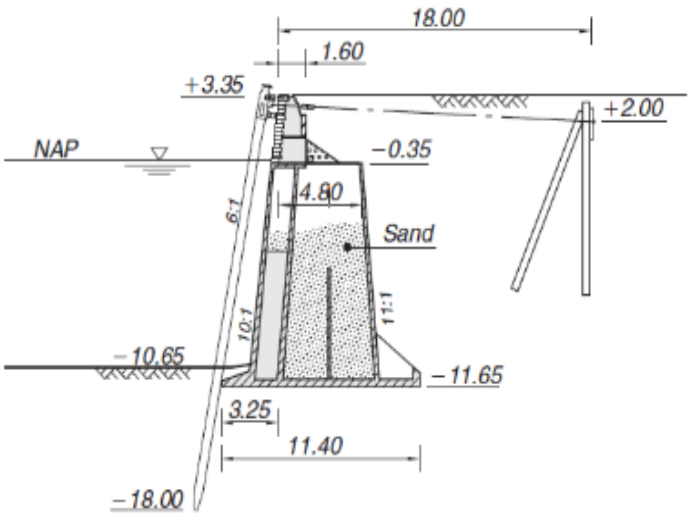

Figure 2.4: Caisson wall, 1913 (De Gijt & Broeken, 2013)

In 1927, steel sheet piles were used as a retaining wall at the Dokhaven harbour for the first time. This construction method did not necessarily require weaker soils at the top to be replaced as greater embedded depths in the stronger bearing soils could be achieved. The drivability of these sheet piles is easier in soft soil. In 1863, retaining height of about 18 meter was achieved using a pile trestle system with bearing and tension piles along with the sheet pile wall. Vertical sand drains were introduced to reduce excess pore pressure development in the soft soil and served as an economical soil improvement method.

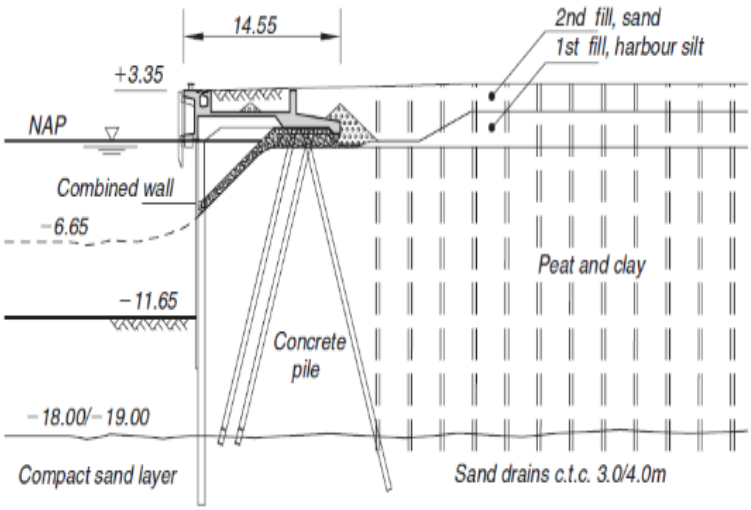

Figure 2.5: Combined wall with pile trestle and sand drains

The advances in the sheet pile wall led to the development of L-wall on piles. It was used in dry building pits and had a relieving structure. The front of the superstructure was supported by the bearing and retaining combined wall and the rear by bearing and tension piles. The relieving platform provided a relaxing effect on the horizontal earth pressures faced by the combined wall after placing load on top of it. As the need for greater retaining height increased, deeper relieving platforms were constructed which reduced the embedded depth required of the combined wall e.g. The relieving platform at the EMO Mississippi harbour has a retaining height of 26.50 m with the relieving platform constructed at -6.00 m.

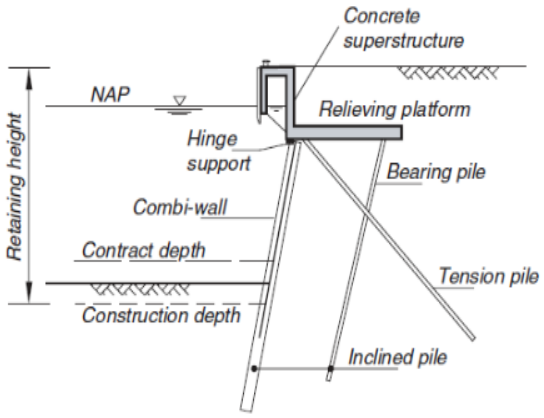

Figure 2.6: Combined wall with a deep relieving platform

2.2. Calculation Methods

There are many calculation models for retaining walls which are either analytical or empirical.

2.2.1. The Blum Method

The method of Blum published in 1931 (Korff, 2018) is an analytical model used for quick stability related calculations of the embedment depth of the retaining walls. This method assumes complete active and passive failure of soil regardless of the displacements and does not consider the elastic deformations in the soil. Hence, the deformations of the wall calculated with this method are not very realistic (Korff, 2018). This method serves as a rough approximation of the penetration depth of the retaining wall and does not consider the effect of stress or strain dependency of the stiffness of the soil. This method also does not consider the different excavation stages or building phases. For better understanding of the behaviour of the retaining wall, spring supported beam method and finite element method are used (De Gijt & Broeken, 2013).

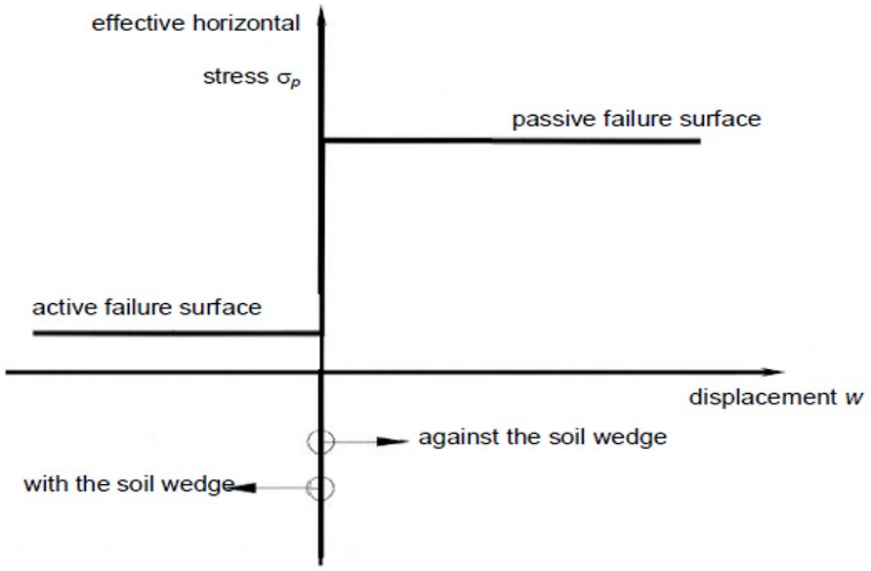

Figure 2.7: Soil stress-displacement diagram according to Blum 1931 (Korff, 2018)

2.2.2. Spring Supported Beam Method

This method of modeling the retaining wall as a beam on an elastic foundation is a standard method in the Netherlands. With this method, it is possible to consider the effect of staged excavation as well as multiple anchoring. The soil is modeled as elasto-plastic springs which enables to include the effect of displacement on the horizontal effective stresses generated in the soil. Unlike the Blum's method in which the soil yields abruptly on active or passive side, the spring method considers a transition between passive and active yielding which is based on the elastic relation between the soil stresses and displacement. This is done by assuming that the soil behaves as uncoupled springs on either side of the retaining wall with the spring coefficient represented by the horizontal coefficient of subgrade reaction k_h as shown in the Figure 2.8 below.

The governing equation for this model is:

$$\mathrm{EI}\,\frac{d^4w}{dx^4} + k(x,w)\cdot w = f(x) \tag{2.1}$$

EI is the flexural rigidity of the retaining wall, x is the height of the wall, k is the horizontal coefficient of subgrade reaction, f is the function for external loads on the wall, and w is the displacement.

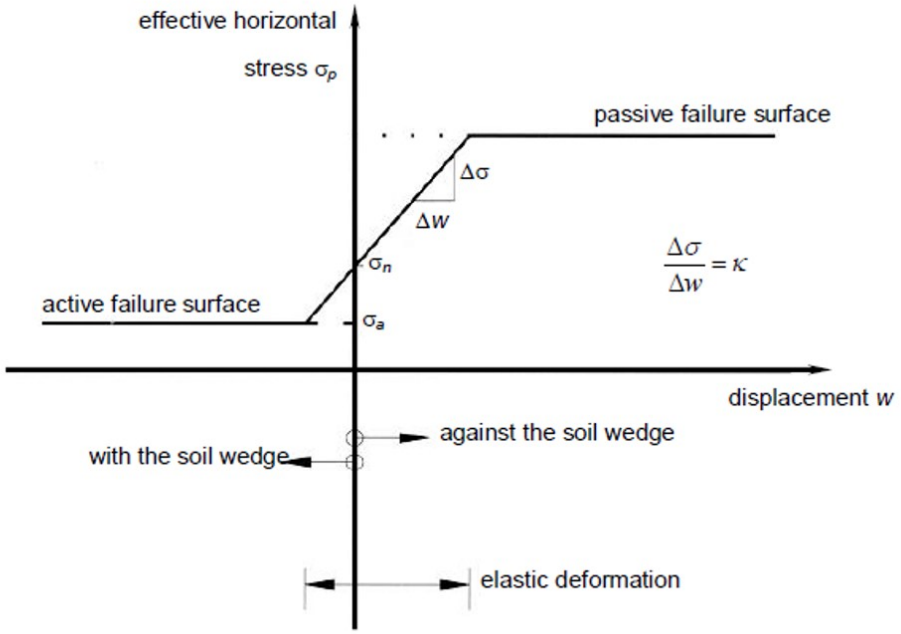

Figure 2.8: Soil stress-displacement diagram for spring supported beam method (Korff, 2018)

This basic Equation 2.1 is applied iteratively at various points on the wall to calculate the displacements, effective stresses, rotations of the wall, excess pore pressures, moments and shear forces, etc, until the results converge (Korff, 2018).

Advantages of the spring model include short calculation times, simple user-friendly input and soil schematization, incorporating the effect of anchors or struts, and implementation of stages of construction. The spring model also has significant limitations such as only considering the soil structure interaction of the wall and no other structural members, assuming a bilinear stress-displacement behavior of the soil which is multi-linear in reality (Korff, 2018). This model assumes linear failure surfaces in the active and passive zones which limit the accuracy of the results. It can only calculate stability of vertically inclined walls. The arching effect of soil around stiffer members of the retaining wall, such as tubular piles of the combined wall or the bearing piles, is not considered.

Considering these limitations, this model is only used for first approximation draft designs. For the complete design of the retaining structures, finite element method is most widely used with programs such as Plaxis, Diana, etc.

2.2.3. Finite Element Method

Finite element method calculates the stresses and deformations in the soil mass around the retaining structure as well as in all the structural members using a series of partial differential equations. These differential equations are solved with numerical iterations for two- and three-dimensional problems by dividing the whole soil mass and the structural members into triangular or rectangular finite elements. These elements contain nodes where the stress and displacement calculations are made. Each node has a degree of freedom which equals the number of unknowns, i.e., the primary variables to be calculated. The stress calculations are done based on the relative displacements of nodes with respect to each other and with respect to other elements through joint nodes. The nodes of the soil elements and structural elements are connected through interface elements. Together, all these elements constitute the finite element mesh.

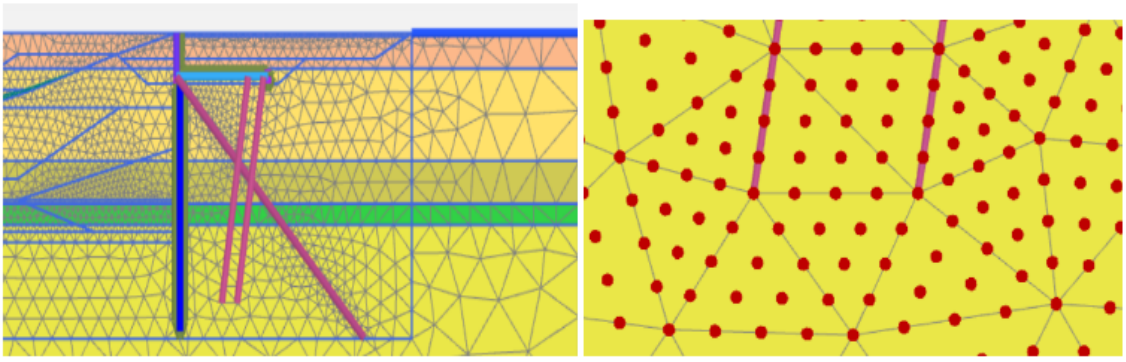

Figure 2.9: Finite element mesh for the quay wall at HTT (left), and finite elements with nodes around the bearing piles (right)

The advantages of this method are many compared to the previously mentioned methods. It is possible to include soil structure interaction in the calculations for all structural members. It is possible to model complex geometries such as relieving platforms and inclined walls. Dynamic calculations can also be performed, and no prescribed failure planes are used.

Hardening Soil Model

For modelling a retaining wall in a finite element program such as Plaxis, constitutive soil models are used to simulate the soil behaviour. The most suitable soil constitutive model for a retaining wall is Hardening Soil Model and it can be used to simulate the behaviour of both stiff and soft soils (Schanz et al., 1999). The Hardening soil model considers independent stiffness moduli for primary deviatoric loading, primary compression loading, and unloading/reloading. The stiffness moduli in the model are stress dependent. The stress dependency of stiffness is defined by an input parameter called power parameter ‘m’.

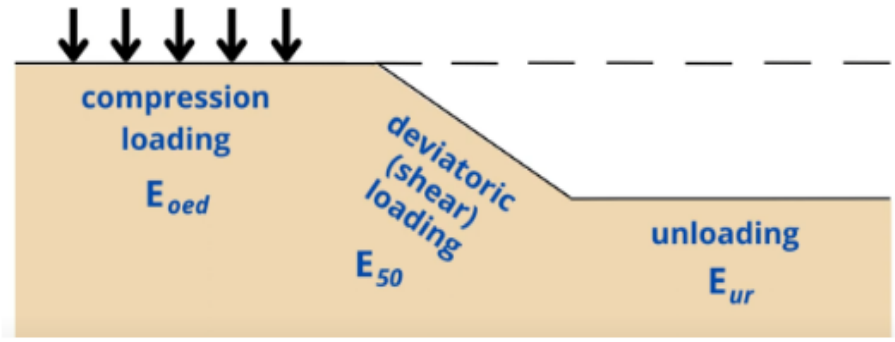

Figure 2.10: Three independent stiffness moduli for different types of loading in HS model (Brinkgreve, 2019)

The basic idea of the hardening soil model is that in a drained triaxial test, the relationship between stress and strain can be approximated with a hyperbolic function as was used by Kondner (1963) and later in the Duncan and Chang model (Duncan & Chang, 1970). This earlier hyperbolic model only used elasticity theory and could not produce dilatancy.

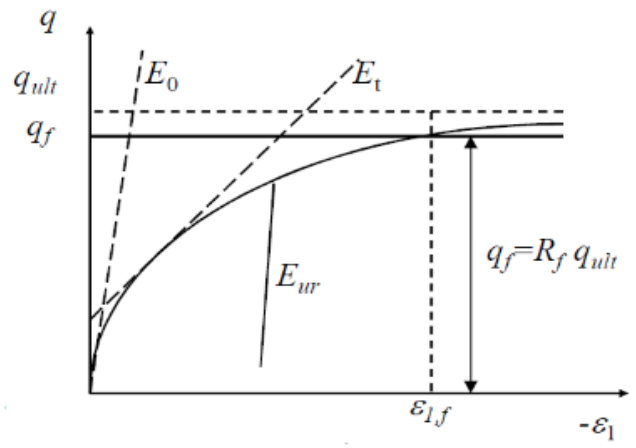

Figure 2.11: Hyperbolic stress-strain relationship in triaxial loading (Duncan & Chang, 1970)

The HS model is formulated around the theory of hardening plasticity of two types, namely, shear hardening and cap hardening. In shear hardening, a hyperbolic stress-strain relationship is seen as plastic strains develop due to deviatoric loading. The material under deviatoric loading starts mobilising its internal friction angle, also called mobilised shear strength, and starts yielding from the onset of loading. As the plastic strains (γ_p) increase with more mobilisation of the friction angle (ϕ_m), the stiffness decreases until maximum mobilisation of friction angle occurs where Mohr failure surface is reached.

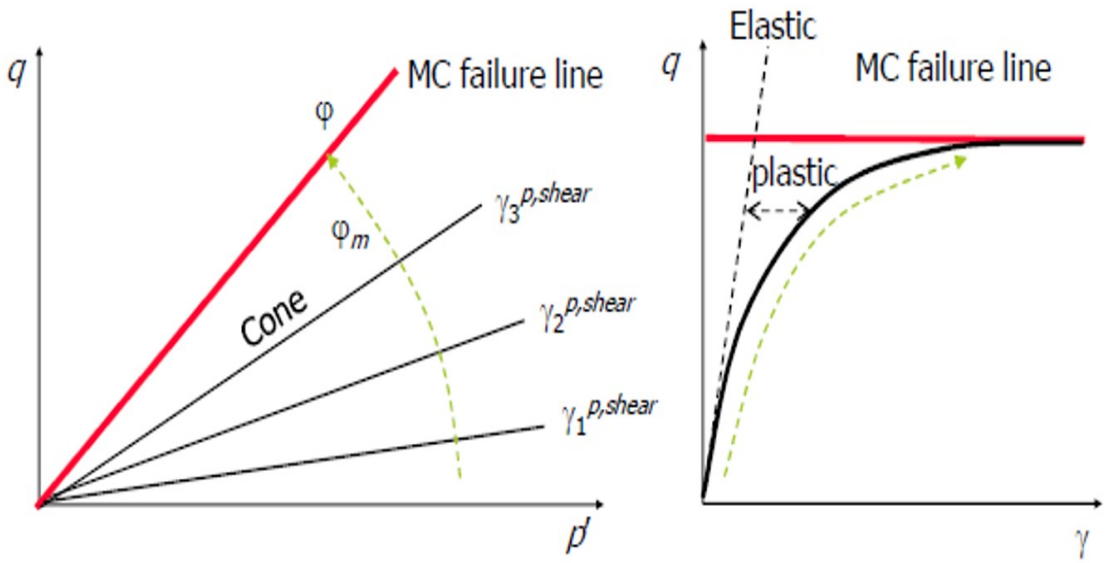

Figure 2.12: Shear Hardening in the HS Model (Brinkgreve, 2019a)

In the cap or compaction hardening, plastic volumetric strains are generated in primary compression. The cap extends when the mean effective stress surpasses the pre-consolidation stress, and so the compressive stiffness reduces.

The hardening surfaces in the HS model are better understood in the principal stress space. The top of the cone represents the cap yield surface, and the sides represent shear yield surfaces.

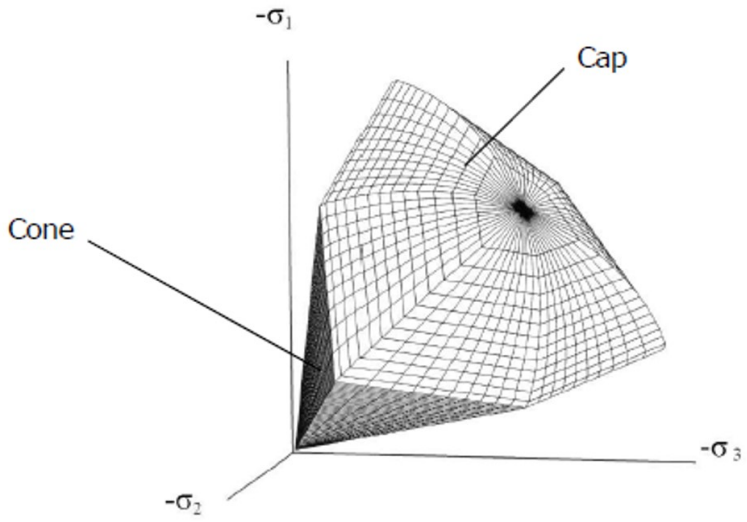

Figure 2.13: Cap and Shear yield surfaces in HS model (Brinkgreve, 2019a)

The input parameters for the hardening soil model are:

- E_{50}^{ref} for the plastic straining from primary deviatoric loads.
- E_{oed}^{ref} for the plastic straining from primary compressive loading in oedometer conditions.
- E_{ur}^{ref} and poisson's ratio ν_{ur} elastic unloading and reloading.
- c, ϕ and Ψ are the Mohr-Coulomb failure criteria parameters.
- m for the stress dependency of stiffness

Hardening Soil Model with Small Strain Stiffness

This soil constitutive model is an extension of the Hardening soil model in a way that it includes the strain dependency of soil stiffness as well as the stress dependency. The standard Hardening soil model considers the soil to act perfectly elastically during unload and reload. However, this is realistic only for very small shear strains ($< 10^{-6}$). As the shear strain increases, the soil stiffness decreases nonlinearly. As shown in the Figure 2.14, the typical range of shear strains in the case of retaining walls is 10^{-4} to 10^{-3}. Hence, for unload-reload of soils, plastic strain accumulation has to be considered in the case of larger than 10^{-6} shear strains. The hardening soil model with the small strain stiffness gives more realistic outputs for the deformations in retaining walls while modelling excavation problems (Obrzud & Truty, 2018).

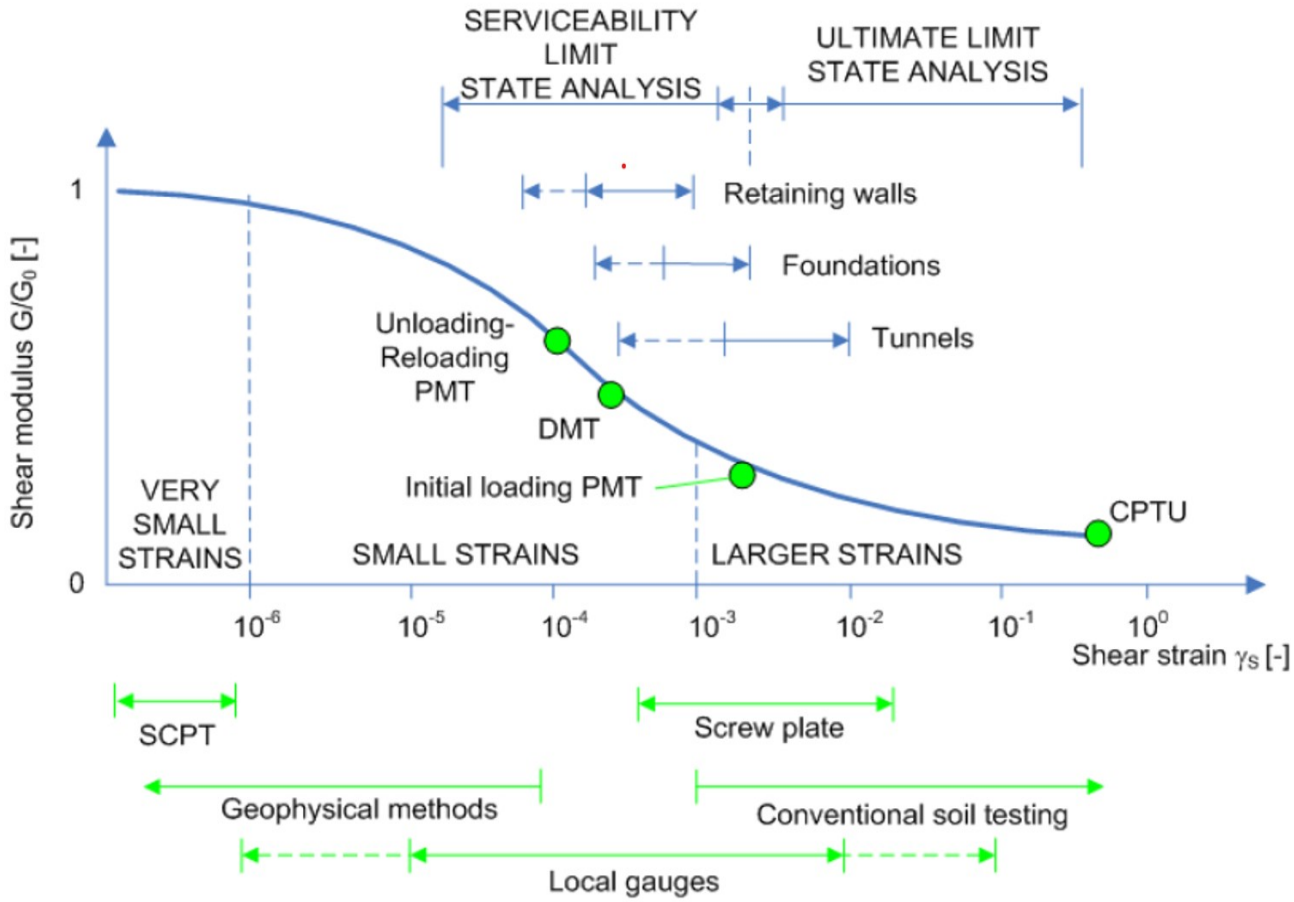

Figure 2.14: Stiffness modulus variation with shear strain amplitudes (Obrzud & Truty, 2018)

The small strain stiffness approach adds two more parameters to the standard Hardening soil model namely, the reference shear stiffness at small strains G_0^{ref} , which is the shear stiffness at very small strains in the order of 10^{-6}, and the threshold shear strain $\gamma_{0.7}$. The threshold shear strain is the shear strain from the modulus reduction curve at which the secant shear modulus G_s reduces to about 72.2 % of the initial small strain shear modulus G_0. The HS small strain model describes both stiff and soft soils with the hyperbolic equation:

$$G_s = \frac{G_0}{1 + 0.385\frac{\gamma}{\gamma_{0.7}}} \tag{2.2}$$

Initially, at very small shear strains, the soil behaves stiff in shearing, represented by the initial shear modulus G_0. As the shear strain increases, the secant shear stiffness G_s decreases. In the case of unloading, as the load is reversed, the shear stiffness restarts at the initial small strain stiffness G_0 and then as the load reversal is continued, the stiffness decreases again (Brinkgreve, 2019a).

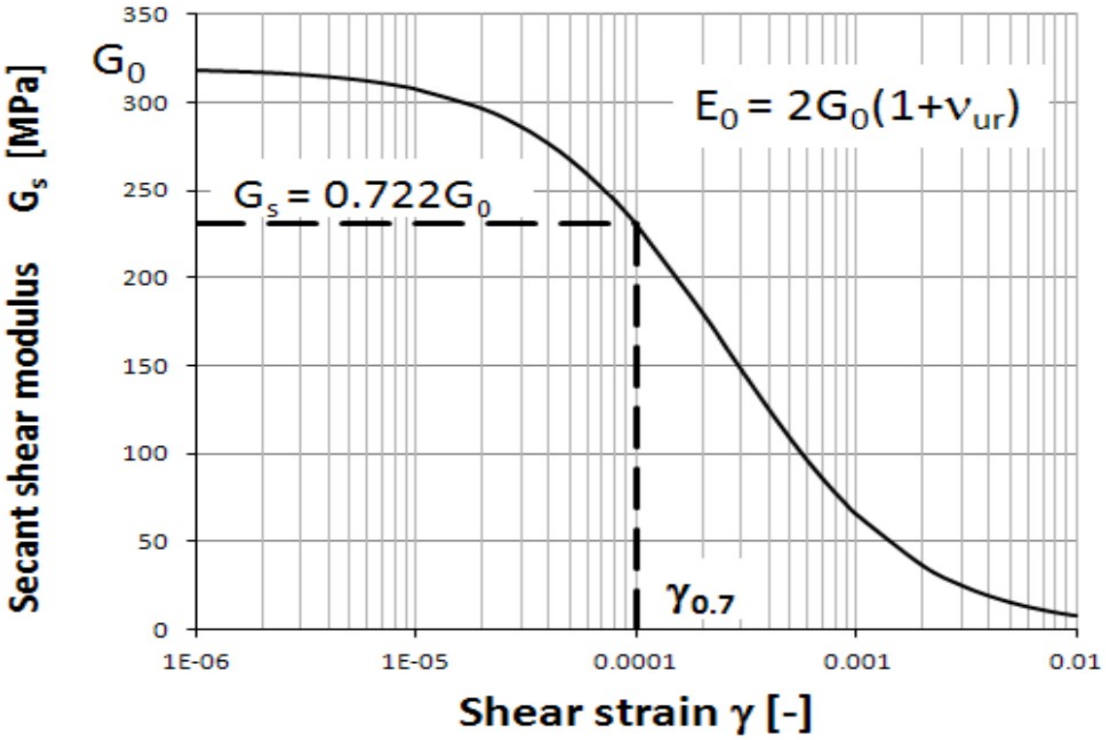

Figure 2.15: Shear modulus reduction curve adopted in the HSsmall model (Obrzud & Truty, 2018)

2.3. Loads acting on the quay

To understand the working of a quay wall under loads, it is necessary to begin with the functional requirements of a quay wall. There are four primary functions of a quay wall, namely, the retaining function, bearing function, navigation function and safety function (De Gijt & Broeken, 2013). The retaining and bearing functions impose loads on the quay wall and are discussed below.

Retaining function- The first and foremost function of a quay wall is to safely retain earth pressure. In many cases, both earth and water are retained by a quay wall. The first load imposed on a quay wall is the permanent load of earth pressure due to dredging of the soil. The required depth of dredging depends on the ship with the deepest loaded draught.

Bearing Function- The quay is required to safely bear the loads imposed by operational activities such as loads due to storage of liquid or dry bulk and loads due to vehicular traffic and cranes. The layout of a quay wall is designed to accommodate the storage zones and transshipment zones. The storage zones impose loads such as bulk load and container load. The transhipment zone includes the crane loads and mooring or bollard loads on the quay wall.

The quay wall experiences a diverse lot of variable and permanent loads throughout its lifespan. The loads are both horizontal as well as vertical. Horizontal loads include primarily the lateral earth pressure due to dredging of the soil in front of the wall, the water pressure on the quay structure, the loads due to cranes and finally the mooring and berthing loads from the ships. The tension piles also exact a horizontal load on the quay wall whereas the horizontal component of the compressive forces in the compression piles have a relaxing effect on the horizontal loads experienced by the quay wall (De Gijt & Broeken, 2013). Vertical loads include the weight of the soil backfill on the relieving platform, the vertical component of the anchor forces, and dominantly the surface loads on top and behind the relieving platform such as bulk storage or tank loads as well as crane loads and traffic loads.

For quay walls, most of the external loads arises due to surcharge load from the storage of containers or bulk

storage placed on top of the wall or behind the wall, which leads to development of additional stresses in the soil, both vertical and horizontal.

Container Loads: Containers at a quay deck in The Netherlands are usually of two sizes, 40 ft (12.20*2.44*2.62m) and 20 ft (6.10*2.44*2.62 m). The maximum weight allowed for either sized container is 350 kN. The most common load of a loaded container is 270 kN. The load calculations on the stack area are based on uniformly distributed load as 17.5 kN/m^2 for 1 layer of containers, 35 kN/m^2 for 2 layers, 45 kN/m^2 for 3 layers and so on, regardless of the size of the containers (De Gijt & Broeken, 2013).

Bulk Goods: For bulk goods storage, it is necessary to load the goods behind the quay wall at a design distance and up to a design height. In case of liquid storage in a tank, the load is calculated as uniformly distributed vertical load. In case of dry bulk storage such as iron ore, the material is placed in a heap which leads to development of shear load on the ground surface as shown in Figure 2.16 . The horizontal forces generated may lead to additional loads on the quay wall and generation of extra anchor forces compared to dead load with no horizontal component. In such cases, the heap of the material is modelled with soil elements with the parameters adjusted to suit the material stored (De Gijt & Broeken, 2013).

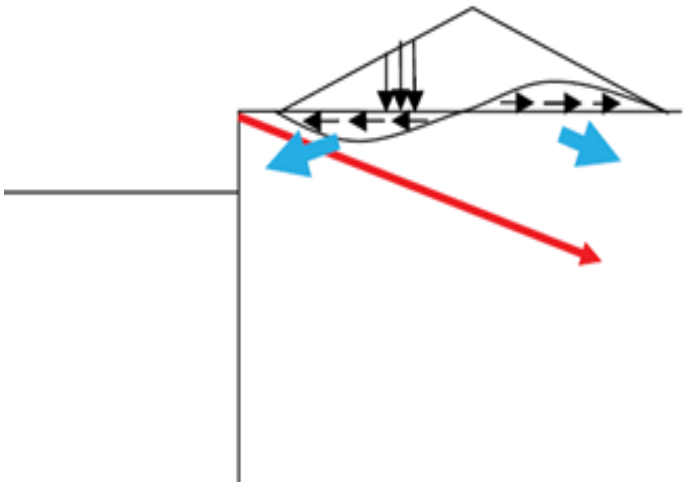

Figure 2.16: Shear loading on the ground caused by heaped bulk storage (De Gijt & Broeken, 2013)

Often, the soil profile is dominated by fine grained soils with a low permeability. If the quay wall in such soil conditions is loaded in a short span, the soil will not be able to drain and the excess pore pressures will lead to higher loads on the quay wall (De Gijt & Broeken, 2013). In case of uncertainty about the operational surcharge loads on the quay wall, a minimum of 20 kPa is assumed as a uniformly distributed load in the design phase (CUR 166: Part-2, 2008).

Bollard Loads- Bollards are installed at the deck of the quay wall to safely moor the ships using hawsers. Due to the tension in the hawsers, a seaward load is applied on top of the quay wall. The capacity of a bollard depends on the size of the ship, the wind force, and the action of waves and currents (De Gijt & Broeken, 2013). The hawser direction is generally between 0º and 180 º in the horizontal plane and up to 60 º in the vertical plane. In the case of marine quays where large vessels are berthed, a double bollard set-up is installed for safe mooring. Depending on the size of the ship and the water that it displaces, the hawser tensile forces are depicted in the Table 2.1.

Crane Loads- For quay walls with a relieving platform, the crane rails on the waterside are integrated with the superstructure directly on top of the sheet pile wall, while the landside crane rails are founded on separate foundation with a hinged leg which do not affect the quay wall structure (De Gijt & Broeken, 2013). The crane rails are installed only after the deformations due to dredging have already occurred. The representative vertical loads imposed by cranes is between 300 and 1800 kN/m, with the horizontal load

Loaded Displacement in ton	Representative Hawser Force in kN
<10,000	300
<20,000	600
<50,000	800
<100,000	1,000
<200,000	1,500
<250,000	2,500
>250,000	>2,500

Table 2.1: Representative hawser force for different ships (De Gijt & Broeken, 2013)

being between 10 to 15% of the vertical load. Crane loads consist of the weight of the crane along with the hoisting load, wind load and loads due to movement and braking of the crane.

At the APM terminal at the Port of Rotterdam, container cranes with 35m rail gauge and a maximum wheel load of 910 kN, with eight wheels, are installed. At the Euromax and Brammenkade quay walls, the crane rail has a 30.48m gauge and a wheel load of 1,230 kN, with 10 wheels. Table 2.2 can be used as a guideline for crane loads as per the rail gauges and lifting capacities of cranes.

Rail gauge (m)	Lifting capacity on the water side with an outreach of	Lifting capacity on the land side with a backreach of	Self weight (kN)	Max. wheel load water side (kN)	Max. wheel load land side (kN)	Distance between wheels (m)
15.24	410 kN – 36 m	410 kN – 13 m	5,150	293	274	1.75
15.24	500 kN – 38 m	500 kN – 12 m	8,100	474	433	1.20
20.00	500 kN – 43 m	500 kN – 16 m	9,770	568	542	1.00
30.48	500 kN – 40 m	500 kN – 18 m	8,970	408	609	1.24
35.00	670 kN – 52 m	670 kN – 25 m	12,122	691	691	1.05
48.00	450 kN – 30 m	450 kN – 20 m	7,350	420	383	1.50
61.00	450 kN – 30 m	450 kN – 28 m	18,000	700	700	1.00
30.48	700 kN – 64 m	700 kN – 25 m	28,000	1,200	1,200	1.05

Table 2.2: Container Crane loads for existing cranes at the Port of Rotterdam (De Gijt & Broeken, 2013)

Anchor Loads- When using prestressed anchors, the load is considered as an independent load. Moreover, in the case of anchors installed at an angle, even in absence of prestressing, the vertical component of the anchor force is considered as an additional vertical load on the quay wall (CUR 166: Part-2, 2008; Schouten, 2020). The tensile load generated in the anchors leads to an increase in the axial load of the combined wall (De Gijt & Broeken, 2013).

The loads that are not deemed significant in this study due to their low magnitude of force and effects are the traffic loads, accidental collision loads, ice loads and fender loads. The study of environmental loads such as wind loads, wave loads, and temperature induced loads are beyond the scope of this thesis

Long-term Effect of Cyclic Surcharge Loads

Plenty of literature is available on the behaviour of the Quay walls during the construction phases as well as operational phases. However, for the operational phases, the design calculations are performed only with a single application of the surcharge loads with various load combinations and different design approaches. Not much research has been done to assess the long-term effects of loading and unloading of surface loads on the quay system.

Several quay walls at the Port of Rotterdam have been showing continuously increasing displacements of the combined wall, for instance, the quay wall at the Brittanie Harbour in the Port of Rotterdam. To ascertain the causes of these continuously increasing wall displacements, two major studies were carried out on different quay walls at the Port of Rotterdam, using analytical and numerical methods.

De Gijt et al. (2011) studied the possible causes of the continuous displacement of a quay wall in the Port of Rotterdam in its 7 years of operational phase under design loads. After studying the time dependent soil behaviour including consolidation and creep in the clay dominated soil profile, it was observed that the negative top displacement (landward) due to consolidation was cancelled out against the positive top displacement (seaward) due to creep as presented in Figure 2.17. Hence, the time dependent soil behaviour was ruled out as a possible cause of the continuous displacements of the wall.

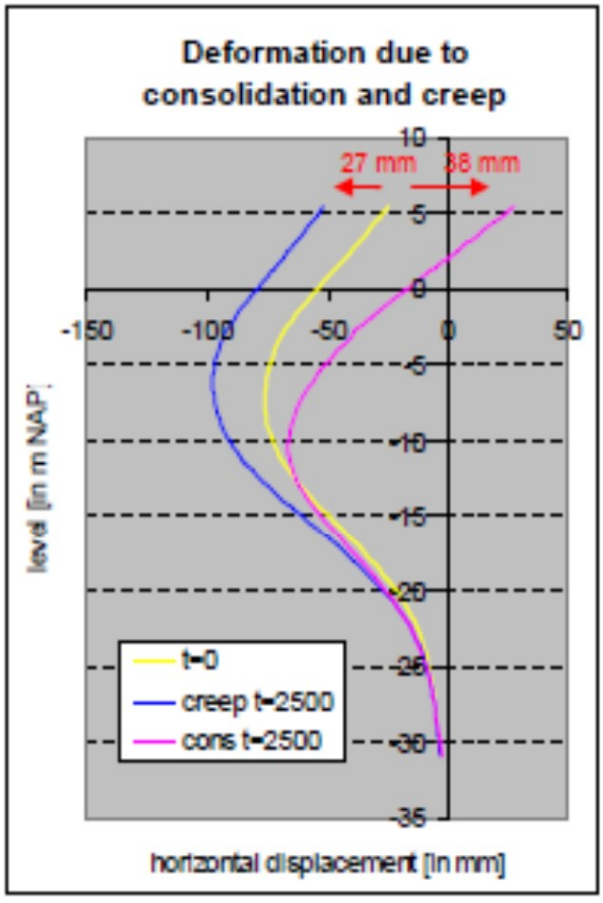

Figure 2.17: Time-dependent deformation of the wall (De Gijt et al., 2011)

It was found that the most probable reason of the continuously increasing wall displacements was the cyclic application of surcharge loads. Various magnitudes of surcharge loads were simulated in the FE model of the quay wall, and it was observed that with each new cycle of loading, new plastic points were generated in the soil in the active zone, along with redistribution of stresses in the soil, which ultimately led to progressive development of plastic strains in the soil. Figure 2.18 presents the results of the cyclic loading simulations performed during the study.

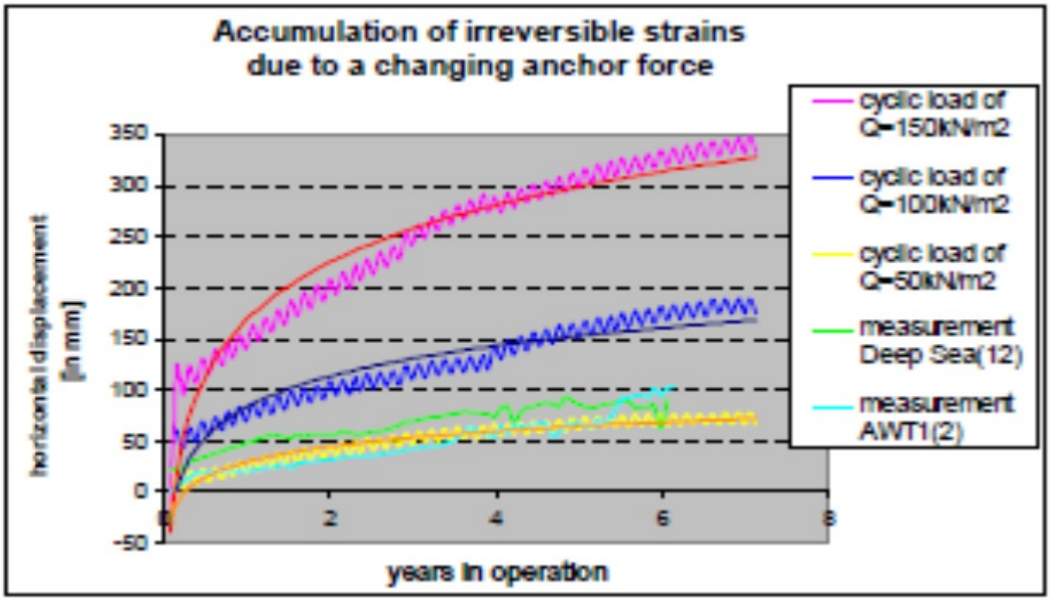

Figure 2.18: Development of wall displacement in time due to cyclic surcharge loads (De Gijt et al., 2011)

The rate of generation of new plastic points and the rate of stress redistribution reduces after the initial load cycles due to densification of the soil structure. Hence, the rate of accumulation of wall displacement also reduces with increasing load cycles, but the accumulation rate does not converge to zero.

Another similar study was carried out by Tolba et al. (2020) to investigate the progressively increasing wall displacements over a period of 5 years of operational phase of a quay wall at the Brittanie Harbour in the Port of Rotterdam. A three-dimensional finite element model was created to simulate the unload-reload behaviour of the quay wall under surcharge loads. The research showed that on unloading the surcharge, the wall did not return to previous displacement values due to the irreversible strains developed in the soil behind the wall. These irreversible strains kept continuously generating and consequently the wall kept on accumulating the horizontal displacement with increasing unload-reload cycles. The research concluded that the reason for the continuously increasing horizontal displacement of the wall was the accumulation of plastic strains in the soil due to repeated unloading and reloading of the surcharge loads.

2.4. Influence of thin clay layer presence on SI piles

Dutch method to predict pile base capacity based on CPT

The axial capacity of a pile loaded under compression consists of the pile base capacity and the shaft capacity. In the Netherlands, the base capacity of the pile is calculated using the Koppejan Method (Gavin et al., 2019) which correlates the base capacity with the design or average value of q_c, which is the weighted average of the tip resistance in the zone of influence around the pile tip, using a reduction factor α_p. The zone of influence is defined as the vertical range of space in which the characteristics of soil have an influence on the end bearing capacity of the compression pile (Rica & Van Baars, 2018). This zone is considered from 8D above the pile tip to up to 4D below the pile tip in the Dutch (Koppejan) method. The design q_c value is limited between 12 MPa and 15 MPa depending on the thickness of the bearing layers, the lower value of q_c is used for a bearing layer which is less than a meter thick (Gavin et al., 2019). To determine

the total axial capacity of the pile, both the shaft and the base capacities are calculated using the Equation 2.3 and Equation 2.4. Constant reduction factors α_s and α_p are used to calculate the unit shaft resistance T_f and the unit base resistance q_b respectively.

$$T_f = \alpha_s \cdot q_c \tag{2.3}$$

$$q_b = \alpha_p \cdot q_c \tag{2.4}$$

As the objective is to analyse the influence of clay layer on the end bearing capacity of the SI piles, only the Equation 2.4 will be elaborated in this thesis.

Factors affecting pile end bearing resistance

Reduction Factor α_p

The current Dutch standard (NEN 1997-1: EC 7, 2016) considers screw injection piles as partial displacement piles (Gavin et al., 2019) and presents the value of α_p = 0.63 for closed-ended displacing piles, which was used in the design of bearing capacity for the screw injection piles at the HTT quay wall as shown in the design report by Imbrechts et al. (2017b). However, the CPT method to determine the pile axial capacity is widely debated upon due to many uncertainties in the calculation methods (White & Bolton, 2005). In the CPT based method of calculating the pile end bearing capacity, many uncertainties lie in the averaging of the q_c value or the design q_c value (Gavin et al., 2019), and in the estimation of the zone of influence over which the q_c values are averaged (Chai et al., 2022), especially in the case of inhomogeneous soil profile around the pile base (White & Bolton, 2005). Additionally, there are also conflicting experimental results about the correct site-specific and installation method specific value of α_p to be used for the bearing capacity calculations.

In research on the influence of the installation methods of closed ended driven piles in dense sand, several load tests were performed on the screw injection piles by Duffy et al. (2024a). The α_p value for screw injection piles was shown to be in the range of 0.30 to 0.50, which is similar to that of a bored pile or a non-displacement pile (Bustamante & Gianeselli, 1982). However, in this thesis, the α_p value of 0.63 is used to stay consistent with the Dutch standard design method of SI piles which was adopted for the HTT quay wall design. Other factors relevant to the end bearing capacity of piles loaded under compression are partial embedment, residual stress, and local inhomogeneity around the pile base (White & Bolton, 2005).

Partial embedment (L/D)

Partial embedment of a pile occurs when the pile is not sufficiently embedded into the bearing stratum to mobilise its full bearing capacity from the given layer. As the length over diameter ratio (L/D) of a CPT is higher than that of a pile, the required embedment length for a CPT is lesser than that required for a pile, resulting in a lower value of q_b than q_c. This phenomenon is incorporated in the reduction factor α_p already. White and Bolton (2005) present the effect of partial embedment on reduction factor for base resistance over a vertical range of -2D depth to +8D depth around the pile base. The Figure 2.19 below explains the effect of partial embedment on the reduction factor α_p. In the case of HTT quay wall, the embedment length of the SI piles is sufficient according to the partial embedment criterion. The equivalent diameter of the pile is 850 mm and the embedded length of the pile in the Pleistocene sand is 11 meters.

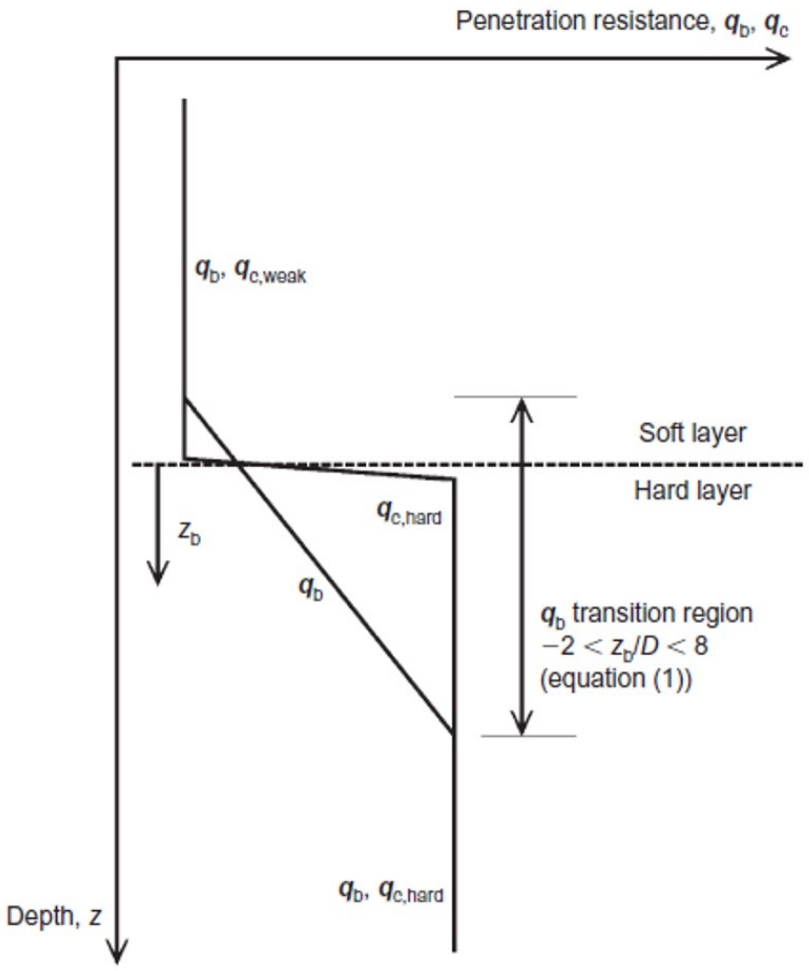

Figure 2.19: Effect of partial embedment on the base resistance of a pile (White & Bolton, 2005)

Residual stresses

Residual stresses arise when the compressive stress is locked in at the pile base due to pile installation. It is a phenomenon which occurs in driven piles due to driving force, which stores the compressive force in the lower part of the piles and may result in an underestimation of the end bearing resistance during load tests (Duffy et al., 2024a; Gavin et al., 2019; Matic et al., 2019). In the case of screw injection piles installed using a grout, residual stresses do not arise as the unhardened grout cannot lock in any stress development during installation (Duffy et al., 2024a). As explained earlier, the screw injection piles behave as bored or non-displacement piles. The absence of residual stress in non-displacement piles was shown to be the case by the load tests performed on the continuous flight auger piles (non-displacement) by Gavin et al. (2009). Along with no residual stresses present at the base of the non-displacement piles, there was also no friction fatigue observed along the shaft as there is no cyclic load experienced by the pile during installation (Gavin et al., 2009).

Having already discounted the possibility of any concerns related to partial embedment and residual stress development at the base of the piles, the effect of **local inhomogeneity** around the pile base is considered next. The influence of this local inhomogeneity is the main objective of this chapter, and it will be studied for the case of HTT quay wall where locally embedded clay layers are shown to be present around the zone of influence of the compression pile tips (Imbrechts et al., 2017b).

Local Inhomogeneity

Much research has been conducted on the influence of a thin weak soil layer on the pile end resistance and on the tip resistance of a CPT. The pile end bearing resistance as well as the tip resistance from CPT are significantly affected by the presence of weak soil layers around the zone of influence of the pile tips or CPT

cone tips. Młynarek et al. (2012) studied the effect of interbedded weak soil layer on the recorded tip resistance of a CPT in an around the weak layer. It was shown that the effect of weak layer interbedded in a stiff layer was seen as a reduction in the tip resistance recorded in the stiff layer near the two interfaces of stiff and weak layers. This reduction was seen when the tip of the CPT cone was 3 to 12 diameters of cone above and below the weak layer, depending on the stiffness of the weak layer. The lower the relative stiffness of the weak layer, the larger the zone over which the reduction in tip resistance is observed. The analysis of the effect of stiffness of a weak layer on the cone resistance in and around the weak layer has shown that the stiffness of the weaker layer needs to be considered, and the cone resistance is to be corrected for that layer and in the surrounding soil layers up to 12 cone diameters above and below the weak layer using a correction factor K_c which depends on the thickness of the stiff and weak layers and the stiffness moduli of the same layers (Młynarek et al., 2012). The CPT tip resistance correction is beyond the scope of this study. This study will solely focus on the effect of weak soil layers on the pile base resistance.

White and Bolton (2005) and Xu and Lehane (2008) compared the differences in the extent to which a weak soil layer affects the tip resistance of a CPT and the pile base resistance. In the presence of a weak soil layer around the tip of the CPT or around the tip of a compression pile, the reduction in pile base resistance is greater than the reduction in the tip resistance of a CPT. Due to the larger volume of soil around a pile base compared to the cone of a CPT, the reduction of base resistance of a pile is greater than that of a CPT, in a region of weak soil embedded inside the bearing soil layer (White & Bolton, 2005).

The region over which the presence of weak soil layers affects the end bearing resistance of a compression pile overlap with the zone of influence of the pile tips. When the soil layer is present in the zone of influence, the reduction in the end bearing capacity can be as large as 40% depending on the position of the weak layer with respect to the pile tip (Chai et al., 2022). The zone of influence is widely debated upon in different literature depending on the pile geometry and structural properties and depending on the bearing soil layer parameters. The zone of influence is estimated to different ranges in different literature according to the soil conditions and the loading/ settlement criteria considered in the study. For instance, for piles in clean sand, the analytically calculated influence zone above the pile tip is between 1.5D to 2.5D, and below the tip it ranges from 3.5D to 5.5D, where D is pile diameter (Yang, 2006). The Dutch Method (Koppejan) estimates the zone of influence from 0.7D to 4D below and 8D above the pile tip, while the French Method (Bustamante & Gianeselli, 1982) estimates it ±1.5D around the pile tip.

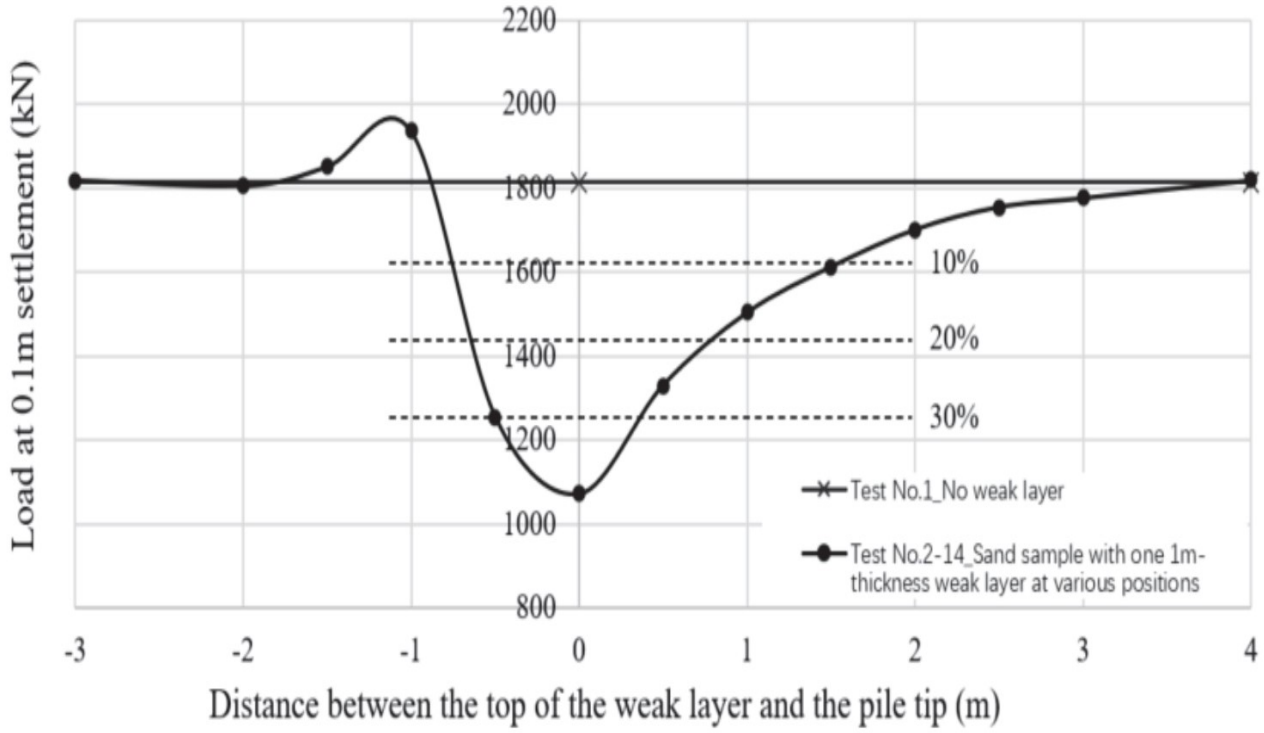

Figure 2.20: Influence of weak clay layer on the bearing capacity of a pile in sand (Chai et al., 2022)

Figure 2.20 illustrates the effect of a clay layer on the end bearing capacity of a pile, as shown by Chai et al. (2022). In a 3D finite element analysis of closed ended piles loaded under axial compression, the effect of

weak layer on the end bearing capacity of the pile was studied by simulating load tests in Plaxis-3D. The zone of influence in clean sand with deep interbedded weak layers, for a settlement criterion of 0.1D settlement of the pile tip, was found to be 1D above the pile tip and 4D below the pile tip. For the load test, a pile of diameter 1 m was chosen with a settlement criterion for the pile head at 0.1D, i.e., 100 mm. A thin clay layer of the thickness 1D was modelled at different locations with respect to the pile tip. It was found that when the weak layer is just below the tip of the pile at 1D, the bearing capacity of the pile could reduce by 40% in 0.1D settlement criterion. When the weak layer is just above the pile tip, i.e., the top of the weak layer is 1D above the pile tip, the bearing capacity could increase by 10% (Chai et al., 2022).

The Figure 2.20 presents the reliability analysis of the pile end bearing capacity with respect to various positions of the thin weak layer from the pile tip. A positive value of the distance signifies that the layer is below the pile tip. The distance is measured from the weak layer's top surface to the pile tip. When the distance is -2D, given the thickness of the layer to be 1m, the bottom of the clay layer is 1m, i.e., 1D above the pile tip. Chai et al. (2022) concluded that the zone of influence for the pile end bearing capacity in sands, in the presence of a thin weak layer, is from 1D above the pile tip to 4D below the pile tip with a 0.1D settlement criterion of the pile base.

Chapter 3

Case Study

3.1. Case Description

The Hartel Tank Terminal project is a maritime infrastructural project for the shipment and storage of petrochemical freight including oil products and bio fuels. The design life of this Quay is 100 years as per the agreement with the Port of Rotterdam (Putteman et al., 2017).

Figure 3.1: HTT Quay wall after the construction of storage tanks enclosed within bund walls

The project Hartel Tank Terminal consists of 1230 meter of a deep-sea quay wall with additional 980 meters of quay wall for inland vessels which only require a Nautical Guaranteed Depth of -7.0 m. In total, the length of the HTT quay wall is around 2200 meter. It also consists of a jetty of length 255 meters accommodating 4 berths in Hudson harbour. This quay wall was connected to the preexisting Brammenkade quay wall (Putteman et al., 2017). The zone B of the quay wall at Maasvlakte is designed to be used by VLCC ships. These ships require a Nautical Guaranteed Depth of -23.60 m NAP. To accommodate these ships at the port, the design depth of -25.60 m NAP was achieved at the end of dredging.

They quay wall construction started in early 2018 and was finished in October 2019 with the preparation of a

27-hectare site adjacent to the quay behind the bund wall at 40 meters from the quay. This site contains 54 oil tanks with total storage capacity of 1.3 million m^3. The tank terminal has been operational since 2021. The terminal at Maasvlakte is designed for multiple types of ships to be berthed and is accordingly divided into different zones based on the nautical Guaranteed Depth required by each ship. These zones are Zone A to D, Zone UB and Zone TK. The quay wall at this terminal connects with the Brammenkade terminal in zone UB and zone TK is where the quay wall merges with the natural seabed slope at the shore.

Zone	**A**	**B**	**C**	**D**
	Suezmax	VLCC	Suezmax	MR2
Ground level	+4.5 m NAP			
NGD	19	-23.6	-19	-14.6
Design depth	-20.5	-25.6	-20.5	-16.1
Retaining height	25	30.1	25	20.6
Relieving platform	yes	yes	yes	no
Number of sections in zone	11 (A1 to A11)	20 (B1 to B20)	11 (C1 to C11)	8 (D1 to D8)

Table 3.1: Zones A to D at HHTT quay and their specifications (Schouten, 2020)

Currently, this terminal is used a tank terminal for the shipment and storage of oil products and biofuels, where ships like VLCC, Suezmax, LR2 and MR2 can berth. However, it is planned for this terminal, zone A, B and C, to be converted to a container crane terminal in the future where a crane load will be added to it without changing the bottom depth in front of the quay (Imbrechts et al., 2017a)

3.2. Elements of quay wall

All zones in the HHTT terminal are constructed with a combined wall of alternating tubular piles and sheet pile walls. The zone A, B and C have a relieving platform founded on SI piles and the combined wall, whereas the zone D does not have a relieving platform. In this thesis, we will consider only zone B with a relieving platform. This zone is composed of the combined wall, relieving platform, MV piles or tension piles, and SI piles or compression piles.

Combined Wall

As the quay wall at HHTT is designed for a large retaining height of 30.10m and high surface loads, the retaining structure chosen for the quay wall must have adequate bending stiffness and must be economically viable. A combined wall, consisting of heavy X70 steel tubular piles of diameter 1420 mm and thickness 24 mm as primary members and triple PU28 sheet piles as secondary members, meets both these needs. The primary members take most of the horizontal load from active zone in the soil and transfer it partly to the tension piles. The secondary members have a negligible bending stiffness compared to the primary members and act mostly as a seal (De Gijt & Broeken, 2013). The sheet piles are shorter than the tubular piles and the load from the soil is transferred to the tubular piles through arch action in the soil.

The secondary members of the combination wall consist of 3 PU28 sheet piles each of 600 mm width. The bending stiffness of these planks is negligible compared to tubular piles (Imbrechts et al., 2017a). The interlock used in the combination wall is C9 of width 74 mm. The centre-to-centre distance of tubular piles is 3.294 m.

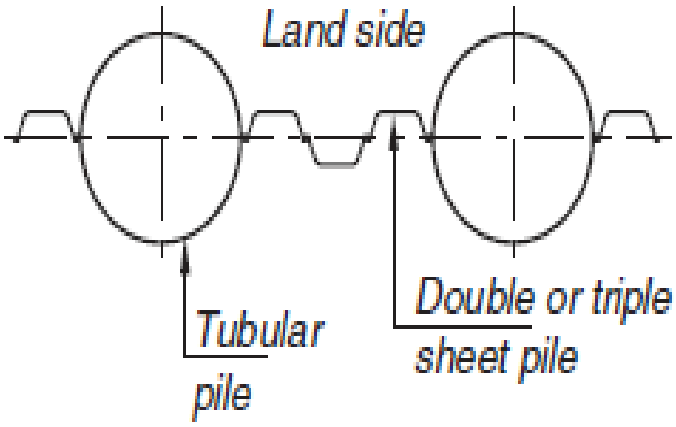

Figure 3.2: Combined wall with steel tubular piles and triple PU28 sheet piles (De Gijt & Broeken, 2013)

The combined wall, through the tubular piles, also provides a vertical load bearing capacity to the loads imposed from the relieving platform on top of it. The connection of the combined wall with the relieving platform is an eccentric hinged support, with a steel saddle, to reduce bending moment in the wall. The use of a hinged support also reduces the anchor forces in the tension piles (De Gijt & Broeken, 2013). This hinge support is made by use of a cast iron saddle which is positioned eccentrically on top of the tubular piles. This eccentricity transfers the normal force from the relief floor to the tubular piles in such a way that it leads to reduction in the field moment in the combined wall (De Gijt & Broeken, 2013; Schouten, 2020).

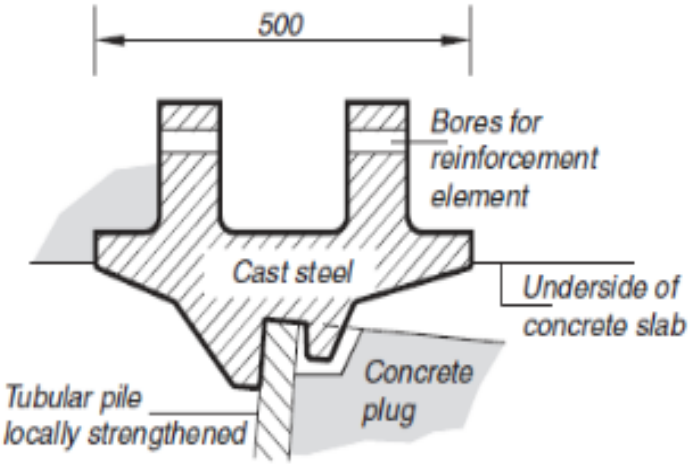

Figure 3.3: Cast iron saddle eccentrically placed on tubular pile (De Gijt & Broeken, 2013)

MV Piles

Muller Verpress piles offer large tension capacity for anchorage in a retaining wall with a large retaining height, leading to high horizontal loads, and/or high surface loads. MV piles are being used at Maasvlakte quay walls since 1984 (De Gijt & Broeken, 2013). The structure of this steel pile is an H profile HEB 600 steel beam of quality S420 with a layer of grout body around the pile. 6 MV piles at this site are driven per section at an angle of 45 degrees with the horizontal and can be driven up to 70 meters into the ground with the aid of grout. The tension piles generate anchor forces to absorb the horizontal earth pressure behind the retaining structure. The connection of MV piles with the relieving structure is hinged as it is safer than a fixed connection. A representative value for the maximum tensile capacity of these piles is 6000 kN (De Gijt & Broeken, 2013).

Figure 3.4: MV pile tip with grout pipe (Spruit et al., 2019)

SI Piles

The SI piles are installed for the purpose of supporting the quay wall vertically and horizontally. These are compression piles designed to transfer the vertical loads on top of the relieving platform to deeper Pleistocene sand layers. All the bearing capacity of these piles is derived from the Pleistocene sand layers (Imbrechts et al., 2017b). The piles are installed by screwing hollow steel casings at an angle of 9-16 degrees with the vertical, with screw diameter of 850 mm and the diameter of the tube 609 mm, into the soil with the aid of grout injection around the tip of the pile (Spruit et al., 2019). The grout makes the driving process easier, especially in the deep sand layers, and stiffens the interface between the pile and the surrounding soil after hardening (Schouten, 2020). The casing is then filled with reinforcement and concrete. The steel casing significantly increases the bending stiffness of the piles. The SI piles are placed in rows of two at a center-to-center distance of 3.294 m. There are 7 piles in each section of the quay (Imbrechts et al., 2017a).

Due to the horizontal effective stress present in the soil behind the quay, the soil tends to move towards the quay, perpendicular to the rows of bearing piles, in the active zone. Since the SI piles are stiffer than soil, they tend to absorb the movement of the soil and take up part of the horizontal stress imposed by the soil. This reduces the horizontal stress on the quay wall and is called Shielding Effect. Multiple studies have been conducted to show the shielding effect of the rows of bearing piles on the horizontal load borne by the quay wall. In research by Galema (2013), it was shown that the maximum field bending in the combined wall was reduced by up to 13% due to the Shielding effect of the bearing piles. This shielding effect can be explained further by the arching effect which takes place around the rows of bearing piles. The stiff piles react to the horizontally moving soil and lead to development of soil arches around the pile which are wider than the piles. In this way, the rows of bearing piles act like an additional retaining wall with the help of arching effect in the soil.

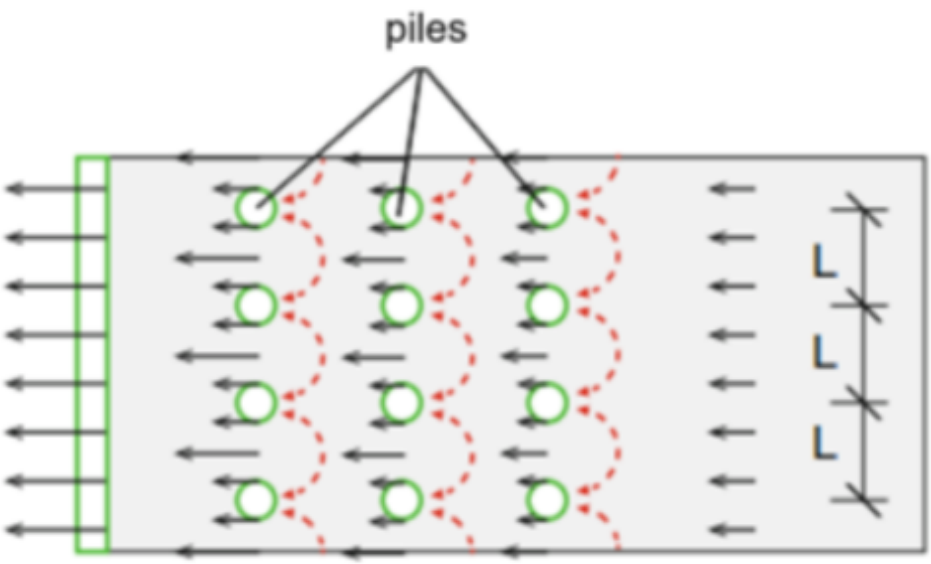

Figure 3.5: Soil arches around the bearing piles (Qiu & Grabe, 2012)

Relieving Platform

The quay wall at the Hartel Tank Terminal has a deep lying relieving platform in zones A to C. The zone D does not have a relieving platform. The relief floor is made of reinforced concrete and is supported by the bearing and retaining combi-wall, vertically, on the waterside, and by the compression and tension piles on the landside. This relieving structure reduces the horizontal load experienced by the top of the quay wall, which arises from the active earth pressure behind the wall. The figure below explains the relieving action of this superstructure. For a deep lying relief floor, the maximum relieving action on the combined wall is equal to the weight of the soil above the relief floor and the surcharge acting on top of it (Schouten, 2020).

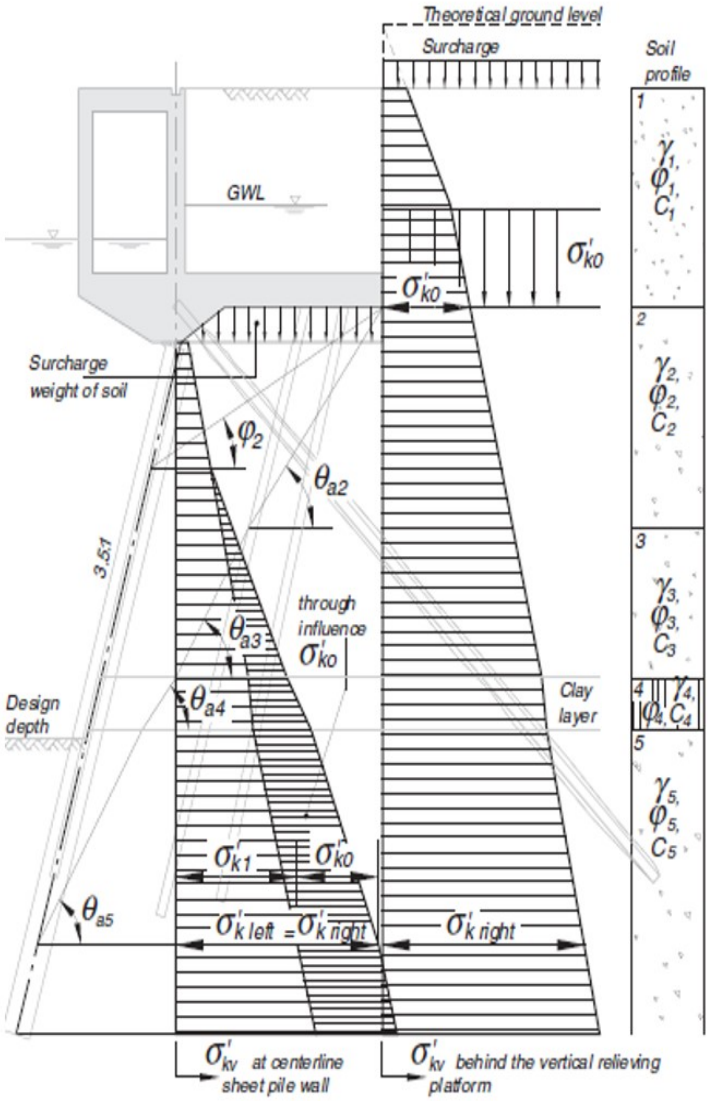

Figure 3.6: Principle of a deep relief floor (De Gijt & Broeken, 2013)

In the figure, σ'_{k0} is the effective stress due to the weight of the soil on the relief floor and the surcharge on top of the floor. The zone of influence of relieving action on the combi-wall starts from the intersection of the line starting from the far corner of the floor at the angle of internal friction of the soil layer on which the floor rests, with the axis of combi-wall. This zone extends to the point where the active sliding surface θ_{a5}, in the layer of soil where the toe of the combi wall is embedded, intersects with the combi wall. The relieving action is maximum at the uppermost region of the combi-wall and reduces with depth (De Gijt & Broeken, 2013).

In this way, the relief floor makes it possible to reduce the length of the combined wall by reducing the horizontal load and consequently the field moment generated in the wall.

Smart Quay Wall

The quay is equipped with smart sensors such as Fiber Bragg Grating sensors, Inclinometers, and piezometers. In addition, measurement bolts are also placed on the top of the concrete relieving floor or the front wall to measure the absolute deformation in X, Y and Z direction. The details of how these sensors operate are not deemed crucial for this thesis. A brief description of the sensors is however provided.

Fiber Bragg Grating sensors

These sensore employ fiber optics to measure deformations in structures based on the changes in the

reflected wavelength compared to the input wavelength. The wavelength is affected by changes in strain and temperature. Hence, the changes in wavelength evaluate the changes in the strain for a constant temperature.

These FBG sensors are deployed in the HTT quay wall to measure the anchor strains in the MV piles and the strains in the connection between the bearing piles and the relief floor. The figures below depict where the sensors are placed in the tension and bearing piles. There is one MV pile in zone B4 installed with this sensor. In the MV piles, 6 sensors are placed right below the connection with the relief floor as the maximum anchor forces are present right at the connection. There is no bearing pile equipped with this sensor in zone B4. In bearing piles, the sensor is fixed to the reinforcement of the pile.

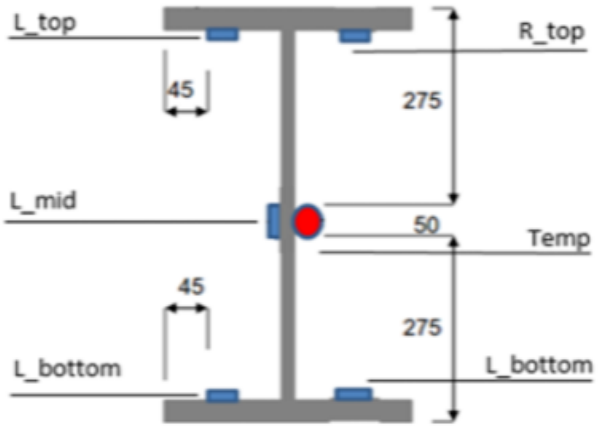

Figure 3.7: Placement of FBG sensors in the H-profile MV Piles

Inclinometers

The inclinometers are installed in a steel casing attached to the tubular piles of the combi-wall and the front wall of the relief floor. This sensor measures the titling in the structure and quantifies the total lateral deformation in the structure perpendicular to the plane of the quay.

XYZ Measurements

There are four measurement bolts on the top of the front wall of the relief floor in section B4. The reference measurement is taken with respect to the RD-coordinates of bund wall which is at a distance of 40 m from the front wall. The deformations in X, Y and Z directions are measured with the help of a total station.

Chapter 4

Numerical Model

For simulating the construction phases of the quay wall as accurately as possible, it is necessary to use a finite element software like Plaxis to be able to analyse the behaviour of the quay wall during installation of the structural elements as well as during the dredging process. For this thesis, section B4 of the quay wall is analysed as the measurement data from this section has been shown by Schouten (2020) to be the most useful for validating the finite element model. The design reports provide the important structural geometry and dimension details. The Figure 4.1 shows the cross-section of the quay wall at zone B of the Hartel Tank Terminal. This drawing is used to acquire all the geometrical data related to the quay wall such as dimensions and angles of installation of the pile trestle and the combined wall.

The quay is modeled with Plaxis-2D with 15-noded elements for the medium finite element mesh. The modeling type is plane strain condition. The model has a width of 240 meters, extending 160 metres into the water side and 80 meters into the land side. The height of the model is 55 meters ranging from y= +5.0 NAP to y= -50.0 NAP. This chapter will further elaborate the soil and structural input parameters used for the FE model.

The soil survey data is available from the in-situ tests such as CPT, for both sand and clay layers that are encountered in the soil profile. This Plaxis model based on the construction phases of the quay wall will be validated with the measurement data from the site of zone B4. This will later serve as the basis for testing the behaviour of the quay wall under load-unload conditions and for the effect of the presence of clay layers in the deeper sand layers on the quay wall behaviour.

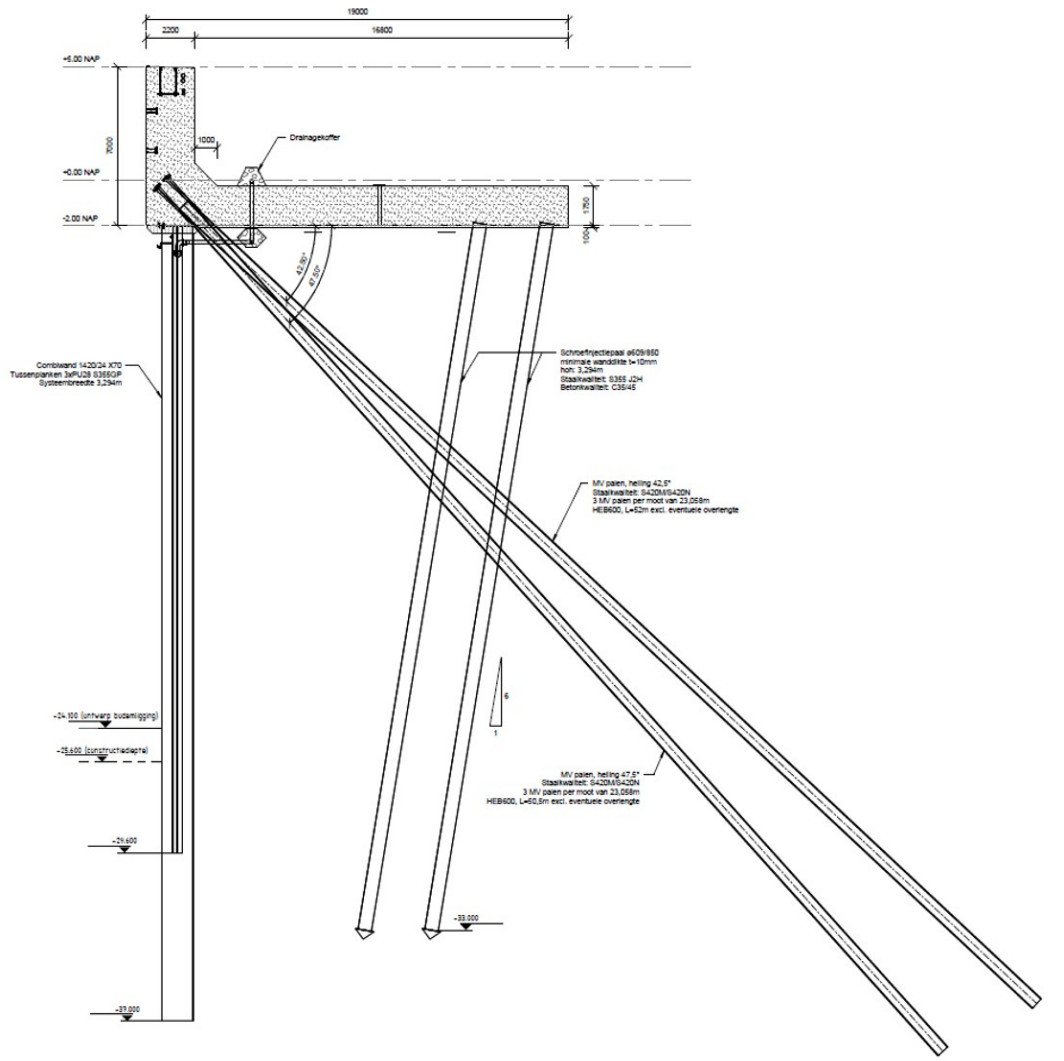

Figure 4.1: Drawing of the cross-section at zone B4 of HTT quay wall (Putteman et al., 2017)

4.1. Soil Profile

The soil profile was determined based on the soil survey performed by Wiertsema & Partners Dijkstra in 2016 until 2017, and Fugro Weijst in 2010. The soil investigation data consists of in-situ tests such as cone penetration tests, borehole data and laboratory tests such as triaxial tests. The CPTs performed around HTT quay wall are presented in the report Geotechnisch Onderzoek VN-66080-1 by Dijkstra (2016).

The CPTs around the site were carried out in three axes with Axis 1 being 25 m from the wall in the passive zone and Axis 3 being 25 m into the active zone. Axis 2 coincides with the axis of the combined wall. DKM032B to DKM036B are conducted closest to the quay wall in zone B4 and hence these will be the most appropriate tests to be considered for this zone (Imbrechts et al., 2017a). The mean readings of q_c value, sleeve friction (f_s) and friction ratio (R_f) from CPTs on axis 2, were selected for estimating the soil stratigraphy in this thesis. Other relevant CPTs for zone B4 are DKM132 and DKMP133 on axis 1 on the passive side, and DKM327 and DKM0328 on axis 3 on the active side of the quay wall. Figure 4.2 is taken from the Design Report HHTT-DZK-RAP-DO-0303 of the HTT project by Imbrechts et al. (2017a) and it shows the locations of various CPTs conducted around zone B4. The CPTs that are marked in red frames are the ones available in the report by Dijkstra (2016).

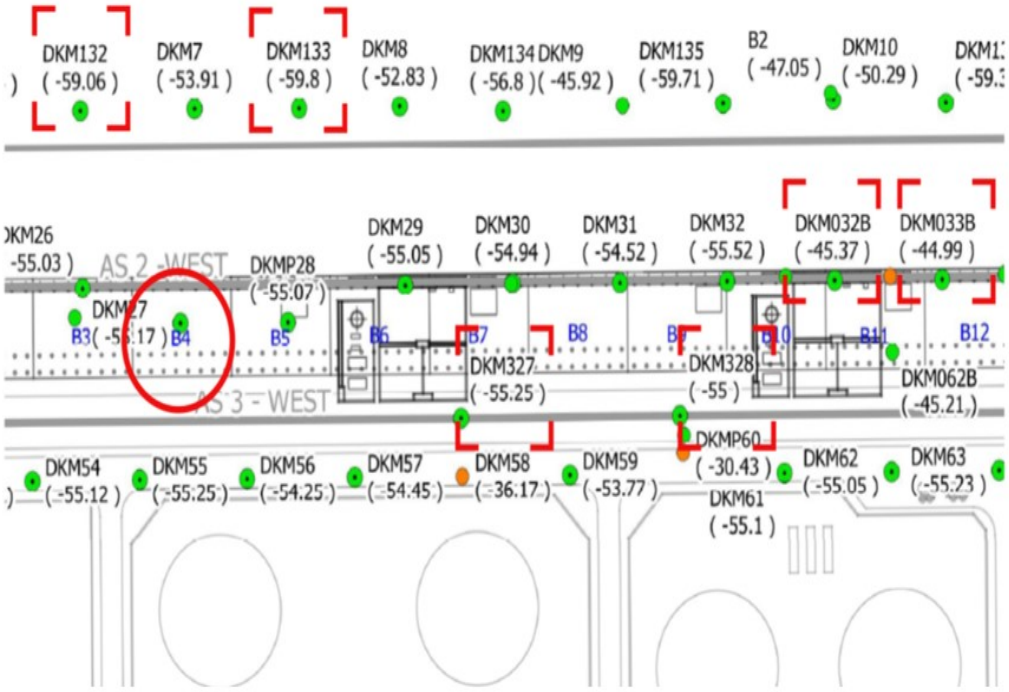

Figure 4.2: Locations of CPTs around zone B4 (Imbrechts et al., 2017a)

The soil parameters from the design report are presented in the Table 4.1. It can be seen that layer b, which is a clay layer, is merely 30 cm in thickness and so its effect is not considered significant in the deformations of the wall. E1 and E2 are also very similar in their properties and will be represented with one layer. The reason for this simplification of soil profile is that the quay wall is a stiff structural system which redistributes the stresses into other structural members such as MV piles, over a large volume of soil. This means that small variations in the soil properties average out over a larger volume of soil which governs the global behaviour of the quay system (Schouten, 2020).

Parameter	**a**	**b**	**C.1**	**D**	**E.1**	**E.2**	**F**
γ_d - unsaturated weight [kN/m³]	17	14	19	18	18	18	18.5
γ_n - saturated weight [kN/m³]	19	14	20	18	18	18	20
ϕ' - shear resistance [°]	30	25	35	27.5	25	25	36
ψ - dilatancy angle [°]	0	0	5	0	0	0	6
c' - drained cohesion [kPa]	0	0	0	0	0	0	0
Drainage modeling	Drained	Drained / Undrained A	Drained	Drained	Drained / Undrained A	Drained	Drained
c_u - undrained cohesion [kPa]	-	-	-	-	-	-	-
$E_{oed,100}$ [kPa]	30,000	3,000	50,000	15,000	10,000	10,000	50,000
$E_{50,100}$ [kPa]	30,000	3,000	50,000	15,000	5,000	5,000	50,000
$E_{ur,ref}$ [kPa]	90,000	12,000	200,000	45,000	40,000	40,000	200,000
m	0.500	1.000	0.500	0.500	1.000	1.000	0.500
ν - poisson	0.200	0.200	0.200	0.200	0.200	0.200	0.200

Table 4.1: Soil parameters as per design report (Imbrechts et al., 2017a)

The soil profile considered in this thesis is a simplified stratigraphy to study the global behaviour of the quay wall. One of the CPTs namely DKM032B from axis X-2 used for interpreting the soil stratigraphy and soil parameters is presented in Figure 4.3 below. The rest of the CPTs used in this thesis are presented in Appendix B.

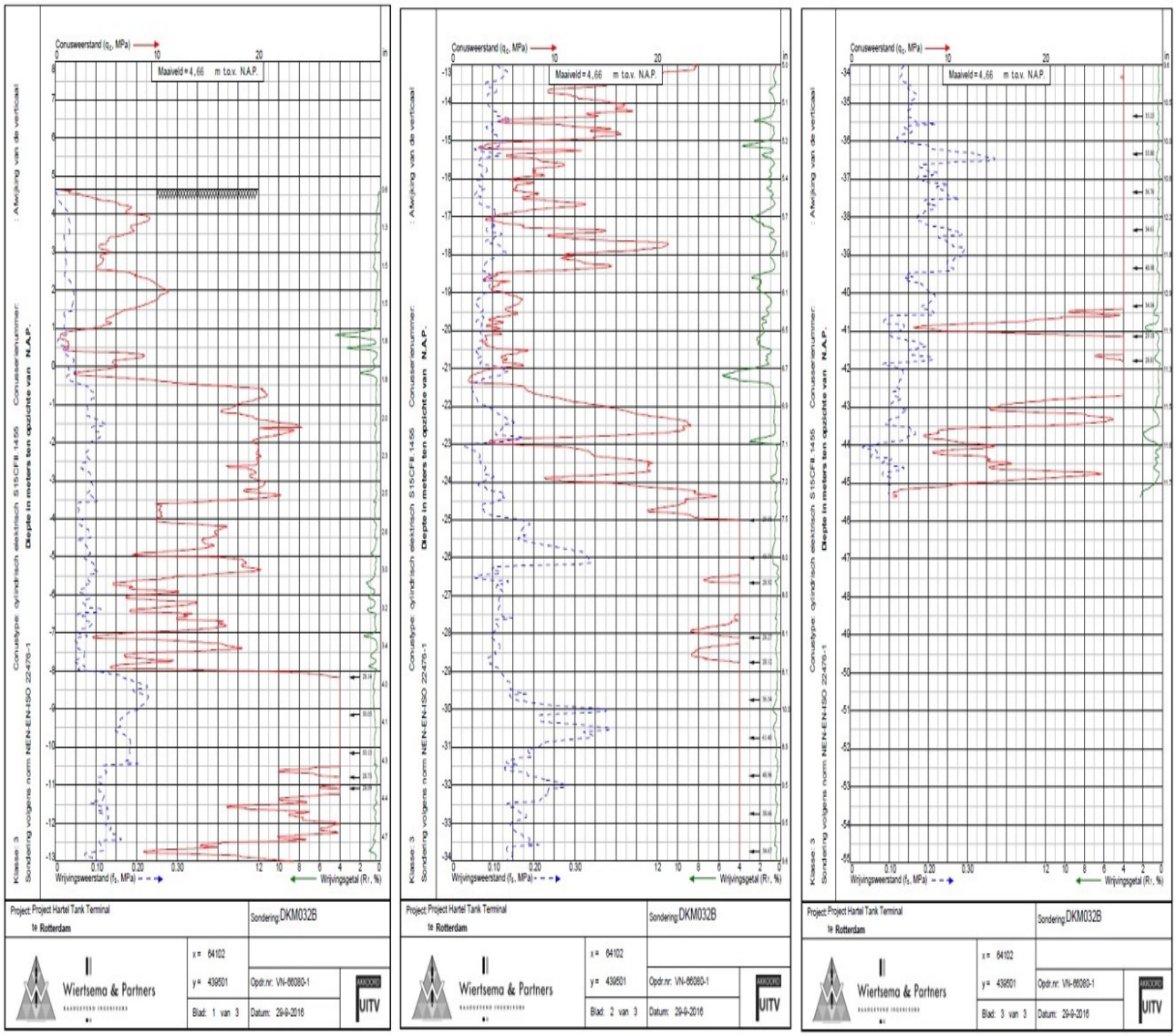

Figure 4.3: CPT DKM032B from axis X-2 taken from the report Geotechnisch Onderzoek VN-66080-1 by Dijkstra (2016)

The simplified soil profile extracted from the CPTs around zone B4 is shown in the Table 4.2 below. This soil profile is considered in this thesis.

Layer no.	Soil type	Top Level [m NAP]	Description
1	Sand Fill	+5.0	Fine sand for raising the surface level of Maasvlakte
2	Sand	0.0	Fine to moderately coarse sand
3	Sand	-13.0	Fine and loosely dense, silty sand
4	Clay	-19.0	Wijchen clay layer, moderately stiff, weakly sandy
5	Sand	-22.0	Pleistocene deposit, dense, moderately coarse with bands of silt and clay.

Table 4.2: Soil layer description

4.2. Soil Parameters

The cone penetration test is the most popular soil testing method in the Netherlands due to the availability of soft penetrable soil. CPT is used to quantify the mechanical parameters and the stratigraphy of the subsoil. The CPT records mechanical parameters of the subsoil continuously throughout the depth (z) in terms of the cone tip resistance q_c, sleeve friction f_s and excess pore pressure u_2. The soil parameters used in the FE model are determined from empirical relationships with the parameters obtained from CPT. These relationships are then extended to suit a wide range of soil types. The parameters calculated from the CPT method are good estimations of the actual ground conditions. Few basic equations used for parameter determination in CPT are:

$$q_t = q_c + u_2(1 - \alpha) \tag{4.1}$$

$$R_f = \frac{f_s}{q_c} \text{ or } \frac{f_s}{q_t} \tag{4.2}$$

In the equations above, q_t is the corrected tip resistance with the pore pressure reading, u_2 is the pore pressure recorded behind the cone, α is the cone area ratio, R_f is the friction ratio. The first equation is used to correct the tip resistance with the pore pressure present at the depth.

Volumetric Unit Weight

The saturated unit weight of soil was correlated to corrected tip resistance by Robertson and Cabal (2010). In Equation 4.3, γ is the saturated unit weight of soil $[kN/m^3]$, γ_w is the unit weight of water $[kN/m^3]$, R_f is the friction ratio, q_t is the corrected cone tip resistance and p_a is the atmospheric pressure in the same units as q_t.

$$\frac{\gamma}{\gamma_w} = 0.27 \log R_f + 0.36 \log\left(\frac{q_t}{p_a}\right) + 1.236 \tag{4.3}$$

Relative Density The in-situ density of the sand governs its stiffness and shear strength properties. The relative density represents the state of the sand compared to maximum and minimum possible densities of the sand. The relative density is defined as the ratio of the difference of maximum and the in-situ void ratio with the difference of maximum and minimum void ratio.

$$RD = \frac{e_{\text{max}} - e}{e_{\text{max}} - e_{\text{min}}} \tag{4.4}$$

The correlation between the cone tip resistance and relative density of sand is given by Murphy et al. (2018), is presented below

$$D_r^2 = \frac{(q_c/p_a)}{350\left(\sigma'_{v0}/p_a\right)^{0.5}} \tag{4.5}$$

In this equation, q_c is the cone tip resistance, σ'_{v0} is the initial vertical effective stress, and P_a is the atmospheric pressure.

Strength and Dilatancy Parameters

The correlation between peak friction angle ϕ'_p and q_c value normalised with effective vertical stress was

given by Mayne and Kulhawy (1990), along with the effective cohesion for cohesive and cohesionless soils. The dilatancy angle ψ was correlated with RD of sand by Brinkgreve et al. (2010) and with the peak friction angle of clay by Bolton (1986) . All these equations are shown below.

$$\phi' = 17.6 + 11\log\left(\frac{(q_c/p_a)}{(p_a/\sigma_{v0})^{0.5}}\right) \quad \text{(Sand)} \tag{4.6}$$

$$\phi' = 29.5 \cdot B_q^{0.121}\left[0.256 + 0.336 \cdot B_q + \log Q\right] \quad \text{(Clay)} \tag{4.7}$$

$$B_q = \frac{u_2 - u_0}{q_t - \sigma_{v0}} \tag{4.8}$$

$$Q = \frac{q_t - \sigma_{v0}}{\sigma'_{v0}} \tag{4.9}$$

$$\Psi' = -2 + \frac{12.5D_r}{100} \quad \text{(Sand)} \tag{4.10}$$

$$\Psi' = \phi' - 30 \quad \text{(Clay)} \tag{4.11}$$

$$c' = 0.1 \text{ kPa} \quad \text{(Sand)} \tag{4.12}$$

$$c' = 0.03\sigma'_{v0} \quad \text{(OC Clay)} \tag{4.13}$$

Stiffness Parameters

Liao and Mayne (2007) provided a correlation between the reference oedometer stiffness Eoedref of soil with the corrected cone resistance and initial vertical stress in the soil. Schmudderich et al. (2020) provided relationships between E_{oed}^{ref} and other reference stiffness moduli as shown in the equations below.

$$E_{\text{oed}}^{\text{ref}} = 5(q_t - \sigma_{v0}) \tag{4.14}$$

$$E_{50}^{\text{ref}} = E_{\text{oed}}^{\text{ref}} \quad \text{(Sand)} \tag{4.15}$$

$$E_{50}^{\text{ref}} = 2 \cdot E_{\text{oed}}^{\text{ref}} \quad \text{(Clay)} \tag{4.16}$$

$$E_{\text{ur}}^{\text{ref}} = 3 \cdot E_{\text{oed}}^{\text{ref}} \quad \text{(Medium to Dense Sand)} \tag{4.17}$$

$$E_{\text{ur}}^{\text{ref}} = 4 \cdot E_{\text{oed}}^{\text{ref}} \quad \text{(Loose Sand)} \tag{4.18}$$

$$E_{\text{ur}}^{\text{ref}} = 5 \cdot E_{\text{oed}}^{\text{ref}} \quad \text{(Clay)} \tag{4.19}$$

The power parameter m, correlated to relative density accounts for the rate of stress dependency of soil stiffness and is negatively related to the RD. For sands, m is given by Equation 4.20. For clays, m = 1.0

$$m = 0.7 - \frac{D_r}{320} \tag{4.20}$$

Other small strain parameters such as the reference small strain shear modulus G_0^{ref} and the threshold shear strain level $\gamma_{0.7}$, where the secant shear modulus reduces to 72% of initial small strain stiffness G_0 are calculated from the CPT correlations stated in Benz (2007).

$$G_0 = \alpha \cdot q_t \tag{4.21}$$

$$Y_{0.7} = 0.107 G_0 \left[2c'(1 + \cos 2\phi') + \sigma'_{v0}(1 + K_0) \sin 2\phi'\right] \tag{4.22}$$

The soil parameters calculated from the CPT are presented in Table 4.3. These parameters are used as input parameters for the soil materials in the finite element model.

Soil Layer	**GU 1**	**GU 2**	**GU 3**	**GU 4**	**GU 5**
γ_{unsat} [kN/m^3]	17.00	18.00	18.00	17.00	19.00
γ_{sat} [kN/m^3]	18.30	20.00	19.60	18.10	20.70
ϕ'_p [°]	39.50	40.80	36.70	30.00	40.30
ψ [°]	4.60	6.30	3.60	0	6.30
c' [kPa]	0	0	0	8.70	0
E_{oed}^{ref} [MPa]	49.80	76.00	32.00	2.80	76.30
E_{50}^{ref} [MPa]	49.80	76.00	32.00	2.20	76.30
E_{ur}^{ref} [MPa]	149.4	228.00	96.00	11.20	228.80
m [-]	0.5	0.5	0.5	1.0	0.5
G_0^{ref} [MPa]	80.90	168.80	130.90	33.90	130.90
$Y_{0.7}$ [-]	2.1×10^{-4}	1.8×10^{-4}	2.7×10^{-4}	7×10^{-4}	3.66×10^{-4}

Table 4.3: Soil input parameters for the Plaxis model

Additional model input parameters were taken from the HTT quay wall design reports by Putteman et al. (2017) and Imbrechts et al. (2017a) as shown in Table 4.4 below.

Parameter (symbol)	**Value**	**Unit**
Coefficient of earth pressure K_0, NC	$1 - \sin\phi'$	[-]
Poisson ratio (ν)	0.2	[-]
Reference stress (p_{ref})	100	[kPa]
Failure ratio (R_f)	0.9	[-]
Interface stiffness ratio (R_{inter})	0.8	[-]

Table 4.4: Additional soil material parameters for the model

4.3. Structural Elements Model Input Paramenters

The structural elements input data is taken from the design report by Imbrechts et al. (2017a). The finite element model properties in this thesis are also inspired by the work of Schouten (2020). The summarized structural elements model input is presented in the Table 4.5.

Structure	Tubex Piles Combi-wall	PU28 sheet pile	MV-Piles HEB600	SI-Piles	Floor (relieving platform)	Front wall (relieving platform)
Dimensions [mm]	D_{outer}: 1420 Thickness: 24	Width: 1800 Height: 454	Width: 300 Height: 600	D_{tube}:609 D_{screw}:850 D_{eqv}:850	Width: 16800 Height: 1750	Width: 2200 Height: 7000
Centre-to-centre distance [mm]	3294	3294	3845	3294	-	-
Material	X70 steel	S355GP steel	S420 steel	C35/45 (concrete) S355 (steel)	C35/45 concrete	C35/45 concrete
Young's Modulus [kN/m^2]	200×10^6	200×10^6	200×10^6	Steel: see left Concrete: see right	20×10^6	20×10^6
C/s area [mm^2/m]	31955	120	7025	Steel: 5715 Concrete: 82715	175×10^4	220×10^4
Moment of Inertia [mm^4/m]	7786×10^6	323×10^6	445×10^6	Steel: 256×10^6 Concrete: 1794×10^6	446615×10^6	87333×10^6

Table 4.5: Model input parameters of structural elements

Plate Elements- Combined Wall and Relieving Platform

The plate elements in Plaxis-2D are used to model the continuous out-of-plane slender elements that have significant flexural rigidity or bending stiffness (EI) and normal/axial stiffness (EA). This makes the plate elements an ideal choice for structures such as sheet pile walls, diaphragm walls and quay walls which extend in the z-direction, as stated in the Plaxis Reference Manual (Brinkgreve, 2019c). Due to the significant flexural and axial stiffness of the combined wall and the relieving platform, the plate element is an ideal choice for modelling these structural elements. The plate elements are connected to the surrounding soil with interface elements which model the soil-structure interactions such as relative displacements between the structure and the surrounding soil using an interface stiffness input. The interface stiffness is a reduction factor applied to the strength parameters of the soil (c and ϕ) surrounding the structure. For smooth structures such as a sheet pile wall or a quay wall, the interface stiffness value of 0.8 is used (Brinkgreve, 2019c).

The combined wall consists of tubular piles interlocked with sheet pile wall elements. The intermediate sheet piles consist of triple PU28 planks with a width of each plank being 600 mm. The interlock used is of type C9 with total width of 64 mm and with an additional 10 mm tolerance for installation. The tubular piles have the outer diameter of 1420 mm. Therefore, the centre-to-centre distance of the tubular piles is $3 * 600 + 74 + 1420 = 3.294m$. The stiffness of the sheet piles is negligible compared to the tubular piles (De Gijt & Broeken, 2013) and so it is not considered in the model calculations. Due to the inexistent end bearing capacity of the plate elements, the 'prevent punching' option is enabled. However, it still resulted in unrealistic vertical settlement of the plate element (Schouten, 2020). Applying a fixed-end anchor under the

plate element resolved the issue of unrealistic punching through the soil.

The relieving platform is also modelled as a plate element including the cast iron saddle. In the case of relieving platform, the out of plane stiffness is accounted for by using a poisson's ratio of 0.2. The Table 4.6 shows the bending and axial stiffness of the plate elements along with the poisson's ratio and the weight.

Plate	EA [kN/m]	EI [kNm^2/m]	V [-]	W [kN/m/m]
Combined wall	6.41×10^6	1.622×10^6	0	0
Floor RP	35×10^6	8.932×10^6	0.2	17.5
Front wall RP	44×10^6	17.75×10^6	0.2	35.2
Cast iron saddle	210×10^9	210×10^9	0	0

Table 4.6: Additional model input for plate elements

Embedded Beam Elements- SI piles and MV piles

The SI piles and the MV piles are modelled as embedded beam elements to better simulate the structural behaviour as well as three-dimensional soil-structure interactions. The embedded beam elements are used to model long, slender structural elements such as piles, anchors and rock bolts in a plane-strain model (Brinkgreve, 2019c). It simulates the skin resistance as well as the base resistance in piles. The embedded beam element simulates the 3D soil-structure interactions using in-built out of plane interface elements consisting of line-to-line interface along the shaft and point-to-point interface at the base. The interface elements are made up of springs in the longitudinal and transverse directions along with a slider in the longitudinal direction.

For the calculations of axial and shaft capacity of SI and MV piles, the effect of grout is not considered significant. The grout, however, is considered for determining the equivalent diameter of the SI piles as reported by Duffy et al. (2024b).

For the SI Piles, the bearing capacity (F_{max}) and friction capacity (τ_{max}) are calculated with the Dutch method to predict pile capacity, presented in the design document by Imbrechts et al. (2017b).

$$F_{\text{max}} = \alpha_p \cdot q_b \cdot A_{\text{tip}} \tag{4.23}$$

$$T_{\text{max}} = \alpha_s \cdot q_s \cdot A_{\text{circumference}} \tag{4.24}$$

In the Equation 4.23 and Equation 4.24, α_p and α_s are pile factors equal to 0.63 and 0.09 respectively taken from NEN 9997-1+C1:2016. q_b is the base tip resistance set at 10 MPa and q_s the shaft tip resistance set at 15 MPa. A_{tip} is 0.56 m^2 and Acircumference per meter length of pile is 0.567 m^2. The skin friction is calculated per meter length of the pile as the maximum friction capacity input parameter in PLaxis-2D is defined per meter length of pile. The positive skin friction, which adds to the load bearing capacity of the SI piles, is generated only in the Pleistocene sand. Due to the presence of active wedge above the Wijchen clay layer, there is no positive shaft friction generated in the SI piles (Imbrechts et al., 2017b).

For MV piles, It can be assumed that the MV piles can not generate any shaft resistance above the Wijchen clay layer due to the presence of active region which relaxes the soil around the pile shaft. So, the anchors derive 100% of their shaft friction capacity from the Pleistocene layer (Imbrechts et al., 2017c), as is shown in the Figure 4.4.

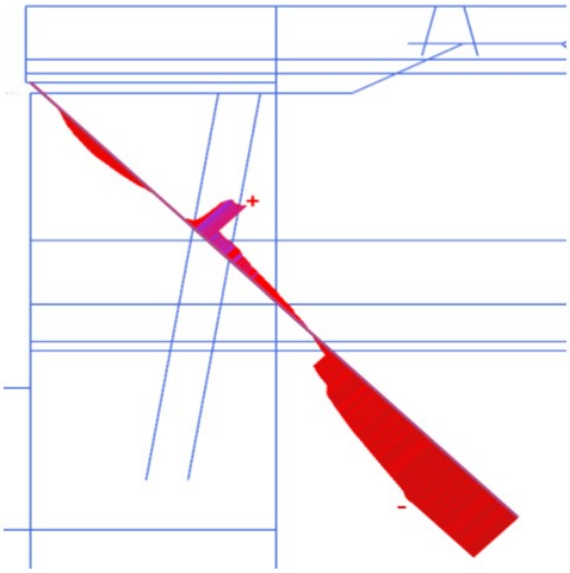

Figure 4.4: Shaft friction around MV pile mobilised in the Pleistocene sand (Imbrechts et al., 2017c)

The characteristic shaft friction q_s is derived from the relation given by De Gijt and Brassinga (1990) using the CPT based method, as shown in Equation 4.25. The total shaft resistance is calculated by integrating the characteristic shaft resistance over the length of pile embedded in the Pleistocene sand as shown in Equation 4.26.

$$q_s = \alpha_t \cdot \min(q_c, 18 \text{ MPa}) \tag{4.25}$$

$$R_s = c \cdot \int_0^L q_s \, dz \tag{4.26}$$

In the equations above, q_s (kPa) is the characteristic skin friction, α_t is the shaft friction factor (α_t for Maasvlakte sand = 0.014), R_s is the characteristic shaft resistance, c (m) is the circumference of the pile including the grout and L is the embedded length. As the q_c value for the Pleistocene sand is greater than 50 MPa, the max characteristic skin friction is given by Equation 4.27.

$$q_{s,\max} = 0.014 \times 18 \text{ MPa} = 252 \text{ kPa}. \tag{4.27}$$

Characteristic shaft resistance R_s per unit meter of the MV pile with a circumference (c) of 2.2 m per meter of pile is 554 kN per meter of pile. The group effect in case of MV piles is non-existent as the center-to-center distance of the piles is greater than 6 times the equivalent diameter of the piles (CUR 2001-4, 2003).

As per De Gijt and Broeken (2013), the maximum representative tensile force that MV piles With HEB600 profile can bear is 6,000 kN. As per the load tests on MV piles at Hartel Tank Terminal conducted by Spruit et al. (2019), the maximum tensile force recorded at the top of the MV piles was between 8000 kN and 10770 kN for piles with an approximate length of 60 m. The maximum shaft friction mobilised at failure was 250 kPa at the top of Pleistocene sand layer and 600 kPa at the toe of the pile. van Paassen and van Dalen (2009) conducted load tests on MV piles at Euromax quay wall which were designed to bear a tensile load of 7200 kN/pile. The length of the piles was 56 m. The ultimate tensile force that the HEB 600B piles were able to withstand was around 9000 kN / pile before failure according to creep criterion of > 2mm was reached.

In the case of skin friction capacity of the tension piles, it is calculated with the CPT based method (CUR 2001-4, 2003; Imbrechts et al., 2017c). The maximum skin friction per meter of the pile at the top of the Pleistocene sand is around 244 kN per meter of pile. At the toe of the pile, skin friction capacity is 554 kN per meter of the pile.

In this thesis, 6399 kN is considered the ultimate anchor capacity of MV piles (Imbrechts et al., 2017c) and 244 kN/m and 554 kN/m as the maximum skin friction at the top of Pleistocene layer and at the toe of the pile respectively. Since the MV pile is loaded in tension, a small value of 200 kN is set for the base capacity F_{max}. The following table presents the input strength parameters of the embedded beam elements.

Embedded Beam	EA [kN]	EI [kNm^2]	$A_{circumference}$ [m^2]	Spacing [m]	F_{max} [kN]	T_{max} [kN/m]
SI-Pile	9.2×10^6	2.87×10^5	2.67	3.295	3572	765
MV-Pile	5.4×10^6	3.42×10^5	2.20	3.845	200	554

Table 4.7: Embedded beam elements strength properties

4.4. Simulating Construction Phases

The construction of the quay is simulated in various phases to match the actual construction process. In the description of the phases, the height (m) is in reference to the NAP.

Phase 0: Initial Phase

The soil profile is modeled using soil boreholes. The global water level is set at 0 m NAP. The seabed gradient of 1:4 is drawn from the ground level of +5.0 m NAP to the seabed level of -24.5 m NAP. Only the soil material is activated along with the global water level.

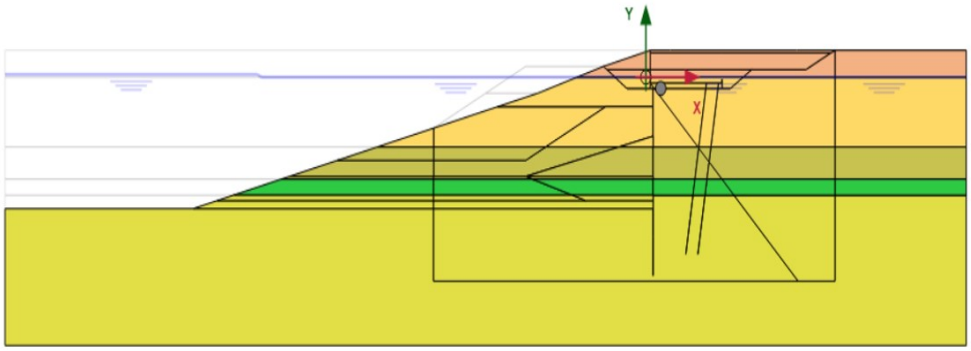

Phase 1: Construction of MV Platform

MV platform raised on waterside up to +2.0 m NAP and excavation of soil up to +1.40 m NAP on the landside.

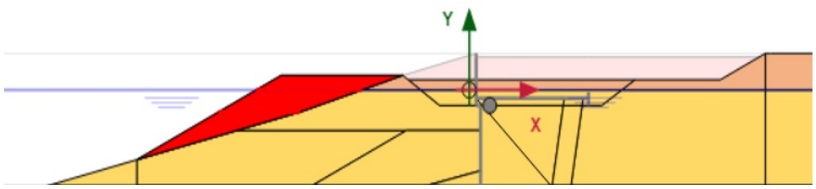

Phase 2: Ground water drainage activated

The ground water is lowered to -3.0 m NAP using vertical drains for enabling dry pit construction. A new global water level is activated in the plaxis model after creating new user water level segments.

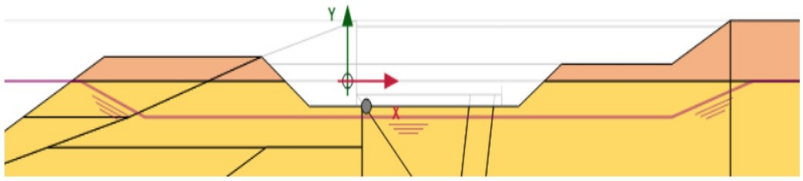

Phase 3: Excavation on landside to -2.10 m NAP

The excavation is done to facilitate the installation of structural members of the quay wall.

Phase 4: Installation of SI piles

The SI piles with shaft diameter of 609 mm and base/screw diamter of 850 mm are modelled with embedded beam element of equivalent diameter of 850 mm, due to the presence of grout (Duffy et al., 2024b). The inclination of 5:1 is simulated with a centre-to-centre distance of 3.294 m.

Phase 5: Installation of Combi-wall

Combined wall is activated with the top at - 2.85 m NAP. the centre-to-centre of the tubular piles is 3.294 m.

Phase 6: Installation of MV piles The MV pile is also modelled with an embedded beam element at an inclination of 45 degrees with the horizontal.

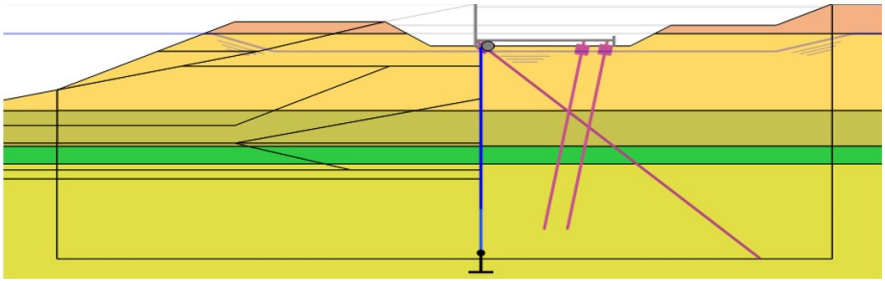

The SI Piles and MV Piles are modeled using embedded beam elements. The Combi-wall, Relieving platform, and the cast iron saddle are modeled as plate elements, as explained in section 4.3.

Phase 7: Construction of Relieving Platform

The relieving platform is built at -2.35 m NAP with the front wall up to a height of +5.00 m NAP. The relieving platform is connected to the combined wall with a cast iron saddle, which is also modeled as a plate element.

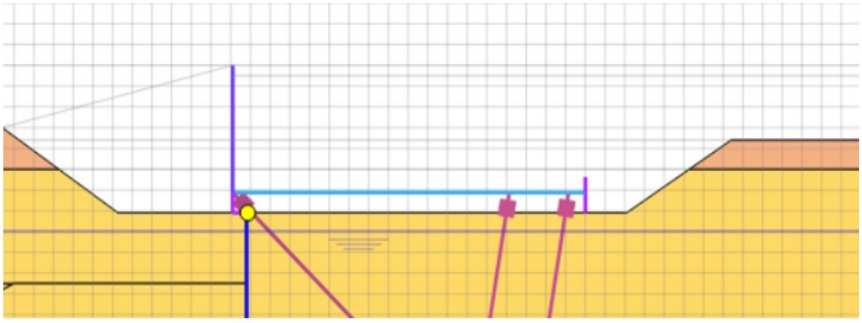

Phase 8: Sand filling on top of the relief floor up to +4.5 m NAP followed by compaction.

Phase 9: Stoppage of drainage system to restore the natural ground water level modelled as global water level.

Phase 10: Excavation of soil in front of the wall to -5.5 m NAP followed by installation of fenders and bollards.

Phase 11a to Phase 11f: Excavation in front of the wall in multiple steps

The phases 11a to 11f simulate the incremental increase of the permanent dredging load through increasing retaining height. The Figure 4.5 below the dredging steps that were followed during construction.

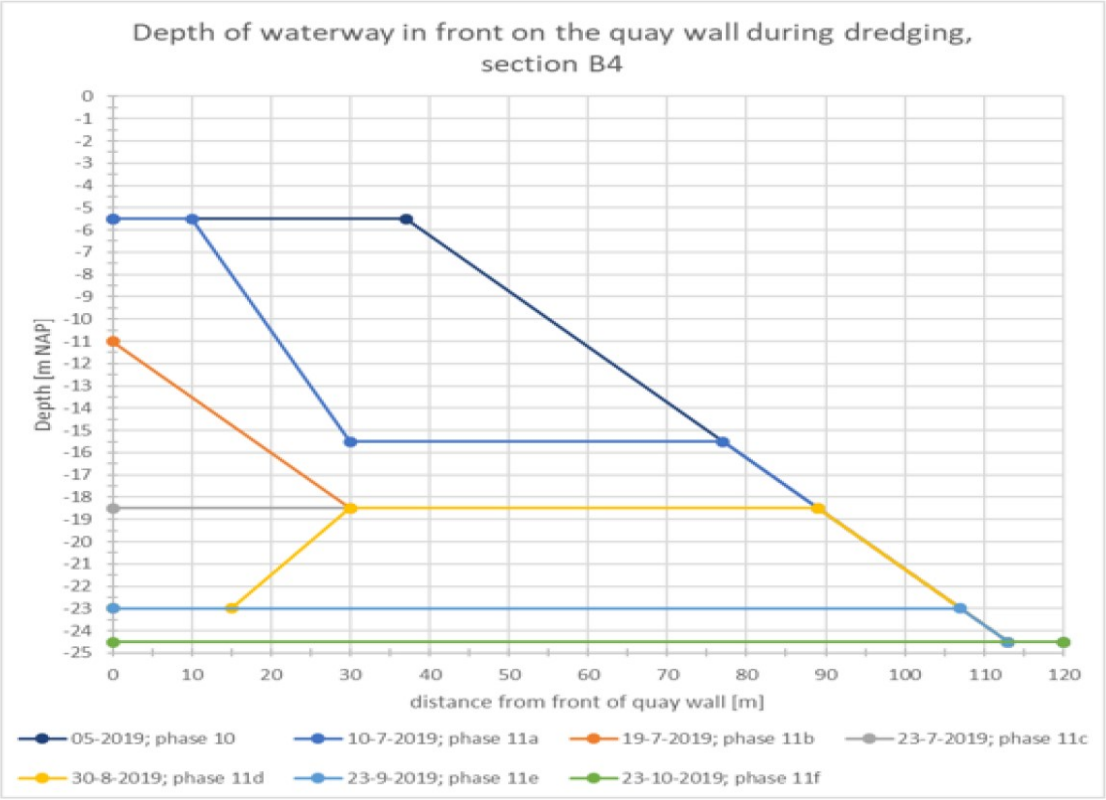

Figure 4.5: Dredging steps at zone B4 of HTT quay wall (Schouten, 2020)

Water Level input

As presented in the design reports by Imbrechts et al. (2017a) and Putteman et al. (2017), the water level in the harbour and the ground water level shows a difference of 0.5 m in the head before the dredging away of Wijchen clay layer. This is due to the overpressure present in the Pleistocene sand layers because of the presence of the Wijchen clay layer which acts as an impermeable boundary, as shown in Figure 4.6. The effect of this clay layer on the water level is shown in the figure. The water level is set to 0 m NAP in all the phases except the ones with active drainage with water level at -3.0 m NAP (Imbrechts et al., 2017a).

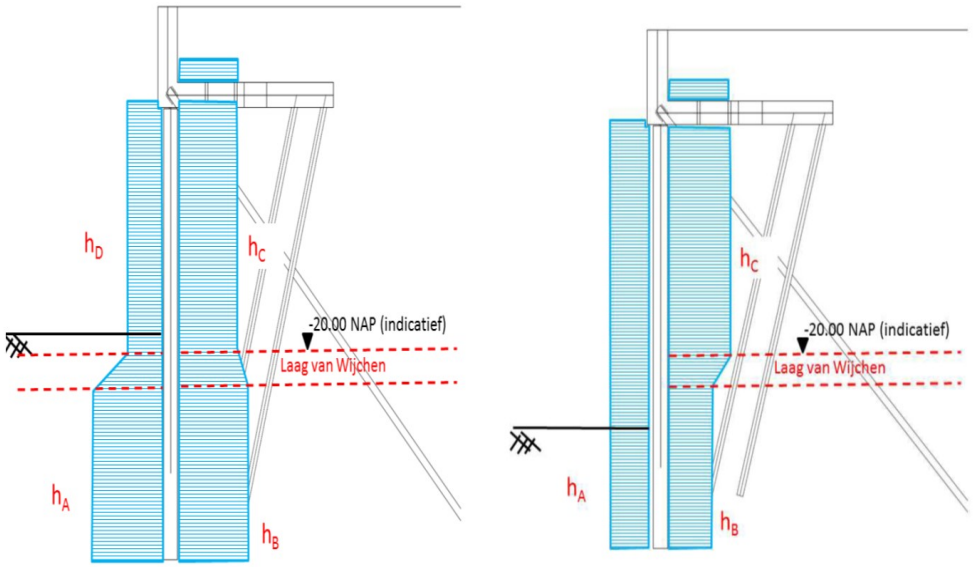

Figure 4.6: Water levels before and after the dredging of Wijchen layer (Putteman et al., 2017)

Since the soil profile is dominated by coarse grained soils, the consolidation calculations are not performed. Instead, the first phase is calculated with Gravity Loading to generate in-situ soil stresses, and the rest of the phases are calculated with Plastic calculations. The drainage type of the material is set to Drained in the sand layers and Undrained Scheme A for clay layer. Due to the soil profile being dominated by coarse grained soil, plastic calculations are preferred over consolidation calculations and the time intervals are set to zero.

4.5. Validation of the Plaxis Model with Measurement Data

For this thesis, section B4 was chosen to be studied as the Inclinometer measurements of the wall and the anchor forces in MV piles are most accurate in this zone (Schouten, 2020). The Plaxis model of the construction phases is validated using the Inclinometer data from the DZK-B04 sensor installed along the front wall at zone B4, and the Anchor force data acquired from the B04-L-mid sensor installed along the MV pile.

Inclinometer Data and Plaxis Output

The inclinometer used at the HTT quay wall has a systemic accuracy of around ±6.8 mm/ 25 m. At zone B4, inclinometer DZK-B04 has been used over a height of 39 m leading to a maximum measurement error of ±10.6 mm. As the wall starts deforming only at the onset of dredging, the initial dredging phases do not cause significant wall displacement to be accurately captured by the inclinometer. Therefore, only the measurement data of later construction phases 11C, 11D and 11F are compared with the finite element results.

The DZK-B04 inclinometer data presents the real time values of inclinometer readings along with the reference measurement values. However, the measurement data shows a zero value for the toe displacement as the inclinometer value is calibrated with a refence zero initial value for the toe. A slight toe displacement of 3 to 5 mm towards seaside is a common occurrence (Schouten, 2020). The finite element model shows a toe displacement in the same range of 3 to 5 mm which has been inculcated in the measurement data as a correction.

The Figure 4.7 presents the comparison of the FE-model wall horizontal displacements with the measurement data from the site.

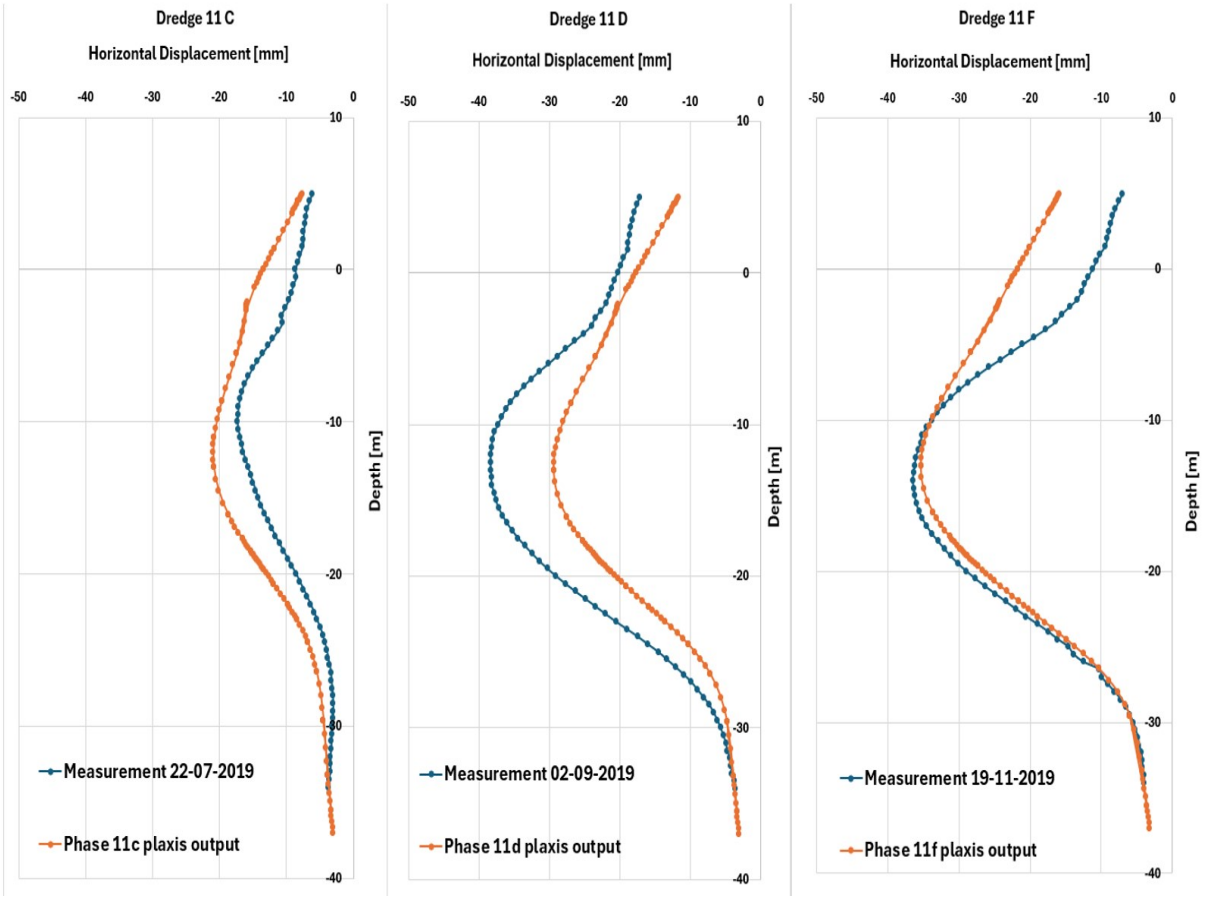

Figure 4.7: Validation of FE model with inclinometer measurement data

In both the measurement data of the dredging phases and the corresponding FE model results, the displacement of the wall increases as the dredging progresses. The FE model results follow the measurement data quite closely on the conservative side, meaning, the FE model mostly shows slightly larger displacements than the measurement data. In the case of 11 D, the measurement was taken 3 days after the dredging phase was complete and therefore the wall had more time to deform which shows in the delayed measurement as larger displacements than in FE model. The complexity of the whole quay structure due to the presence of the relieving platform could also have added to this slight deviation in the calculation results from the measurement data in phase 11 D.

It is concluded that overall, the calculation results from the FE model match very well with the inclinometer measurement data from the site and the FE model is quite representative of the actual site conditions.

Anchor Forces data and Plaxis output

The anchor forces in the measurement data from the sensor B04-l-mid match very well with the anchor forces calculated from the FE model suggesting that the axial stiffness input parameter of the HEB600 profile of steel as well as the shaft friction reduction factor ($\alpha_t = 0.014$) are representative of the actual site conditions. Towards the end of the dredging phases, the anchor forces from the plaxis output are slightly more conservative compared to the measurement data as can be seen in Figure 4.8

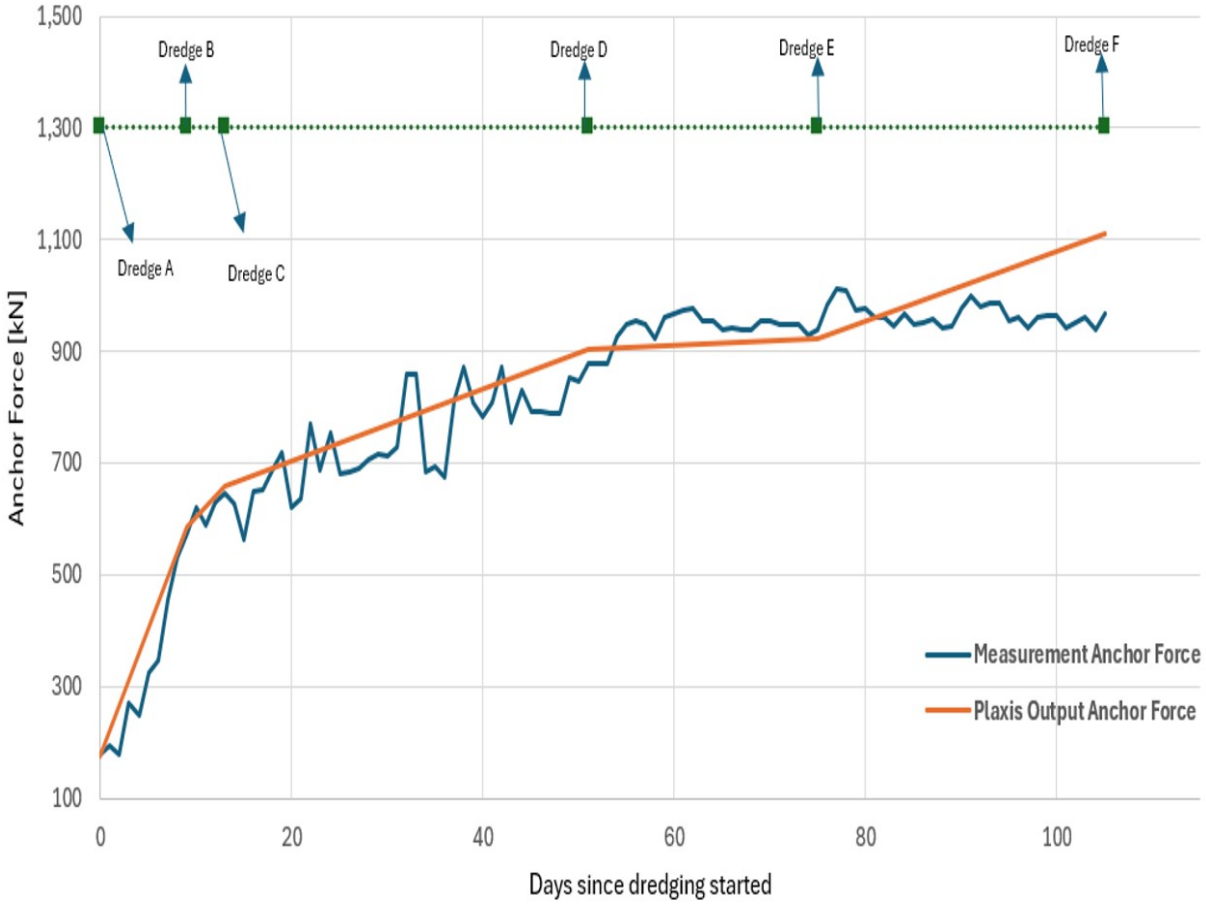

Figure 4.8: Validation of FE Model with anchor force data

It can be concluded that overall, the calculation results from the construction phases simulated with the FE model match very well with the inclinometer measurement data of the combined wall and the anchor force sensor data of the tension piles. The FE model is a good representation of the actual site conditions. This validated model will be used to simulate cyclic loading of surcharge and for the simulation of subsurface weaknesses.

Chapter 5

Modeling the Cyclic Loading Behaviour

5.1. Introduction

The analysis of the deformation behaviour of the quay wall due to unload-reload processes is critical for holistic long term geotechnical evaluation of the quay wall. Quay walls, throughout their lifespan, experience diverse loading conditions due to operational activities and environmental conditions. Analysing the long-term performance of quay walls under repeated unload-reload cycles is important for the long-term safety, stability and maintenance of these structures. This chapter focuses on such analysis of the quay wall at the zone B4 of Hartel Tank Terminal, which was also designed for a future modification into a container crane terminal instead of a liquid bulk storage terminal. The two critical loading conditions considered in this thesis are cyclic unload-reload of surcharge loads and cyclic variations in the water load due to fluctuating water levels.

This chapter attempts to answer the first sub question of the research objective, which is based on the deformation behaviour of the front wall as well as the anchor force mobilisation in the tension piles. It starts with background information on the design load combinations inspired from the HTT project design report by Mariteam and Port of Rotterdam (Imbrechts et al., 2017a). After validating the design load combinations from the design reports with the FE model, the surcharge unload-reload simulations are executed, and the results are elaborated for wall horizontal displacements and anchor forces in the MV piles. Similar simulations are carried out for the effect of changing water levels, where the water level fluctuations are taken from the piezometers installed at zone B4.

5.2. Unload-Reload Behaviour of the Quay wall

The dredging of the soil in front of the wall mobilises very prominent horizontal earth pressures on the wall. This permanent horizontal load is one of the major loads experienced by the quay wall throughout its lifespan and is a major component of the total load applied to the quay wall. In addition to this permanent load, several external surcharges also act on the quay wall. These surcharges are grouped in two main load combinations as per the design report of the project (Imbrechts et al., 2017a). The quay wall experiences a diverse lot of variable and permanent loads throughout its lifespan.

The section of quay wall that is studied in this thesis is the section B4 in zone B of the Hartel Tank Terminal in

the Maasvlakte area of the Port of Rotterdam. It has a deep relieving floor to comply with the high surcharge load bearing requirement. The loads are both horizontal as well as vertical. Horizontal loads include primarily the lateral earth pressure due to dredging of the soil in front of the wall, the water pressure on the quay structure, the loads due to cranes in the future modification plans and finally the mooring and berthing loads. The tension piles also exact a horizontal load on the quay wall whereas the horizontal component of the compressive forces in the compression piles have a relaxing effect on the horizontal loads experienced by the quay wall (De Gijt & Broeken, 2013). Vertical loads include the weight of the soil backfill on the relieving platform, the vertical component of the anchor forces, and dominantly the surface loads on top and behind the relieving platform such as bulk storage or tank loads as well as crane loads and traffic loads.

The loads used in this thesis for the loading and unloading behaviour of the quay wall in the long term are taken directly from the design reports by Putteman et al. (2017) and Imbrechts et al. (2017a) published by Mariteam and Port Authority of Rotterdam. A detailed analysis of the applications of load combinations and their effects on different structural parts of the quay system has been done by the Port Authority and the designer Mariteam and published in the design report HHTT-DZK-RAP-DO-0301 (Putteman et al., 2017). For the first part of this thesis, the same load combinations and the design cases from the above design report are used to analyze the loading and unloading behavior of the quay wall over a long term.

The loads are categorised in two scenarios, namely, **current scenario** and the **future modification scenario**. In the current scenario the loads that are currently being applied on the quay wall are analysed. These loads primarily include the Uniform Surface Load, Tank Load and the Bollard Load. In the future scenario, the quay wall terminal is modified from a liquid bulk storage terminal to a container terminal with the introduction of crane load. According to the design reports authorised by the Port Authority, the substructure was found to be of sufficient capacity to tolerate the application of crane load, meaning that the combined wall, the tension piles and the compression piles are already dimensioned adequately for this new purpose (Imbrechts et al., 2017a). The construction depth of the zone B was also found sufficient for the modification of the terminal to a container terminal (Imbrechts et al., 2017a). This modification, however, introduces a crane load to be modelled and studied based on experiences from the previous container terminal projects. This crane load replaces the tank load in the future scenario (Putteman et al., 2017).

Below are described the loads to be studied in this thesis and their characteristic values to be applied on the quay wall in the FE model.

Surcharge Loads

1 Uniform Surface Load (OB)

In this thesis the abbreviation for Uniform Surface Load will be OB, as it is presented in the design reports. A uniformly distributed top load of $40kN/m^2$ extending from the front wall of the relieving platform to the length of 46 m landside. 30% of this load is permanent causing no excess pore pressures in the clay layers. 70% of it is instantaneous load leading to overpressures in the clay layers (Putteman et al., 2017). Since this load is not significant to cause huge overpressures in clay layers and for simplicity of the model, whole of this load will be modelled using drained calculation conditions.

2 Uniform Tank Load (TB)

As presented in the design reports, the abbreviation for tank load in this thesis will be TB. The characteristic three-dimensional tank load is $320kN/m^2$ over the contour of the tank (Putteman et al., 2017). This 3D tank load is translated into a 2D load which can be modelled in our two-dimensional Plaxis model. The two-dimensional value of this uniformly distributed tank load is presented as a characteristic load of $168kN/m^2$. This load extends from 48 m landside to 80 m landside. The tank load also considers the load due to filling of the area around the tank within the bund walls. The bund walls are designed to retain liquid up to a height of 4 m within the contours leading to a load with an upper limit of $40kN/m^2$ (Imbrechts et al., 2017a). This load is also accommodated in the total tank load.

It can be predicted in advance that the uniform surface load will prove to be more significant than the tank load, as it is applied directly on top of the relief floor. The tank load is applied at a large distance from the front wall.

3 Bollard Force (BB)

Abbreviated as BB in the design reports (Putteman et al., 2017) and (Imbrechts et al., 2017a), and in this

thesis. The bollard force arises from the mooring of the ships to the quay deck. The mooring force can act in the horizontal plane within -45 degrees to +45 degrees. In this thesis, the mooring force is considered at a direction of 0 degrees with respect to the horizontal, same as it is considered in the design reports. There are three bollard pairs in two adjacent sections. One bollard pair results in a force of $2400kN$, with one of the bollards working at full capacity and the other at 70% capacity. The horizontal characteristic bollard force to be used as a line load out of plane of the 2D FE model is calculated as $3 * 2400kN * (1 + 0.7)/2 * 7 * 3.294m = 265.4kN/m$ (Imbrechts et al., 2017a).

The point at which the load acts on the quay wall in 500 mm above the top of the front wall, at NAP +5.50m, and hence, a moment of $132.5kNm/m$ is also considered.

4 Crane Load

The crane load is abbreviated as KB, same as mentioned in the design reports. Modeled in the future modification scenario, this load is applied directly at the kesp of the quay with both horizontal and vertical components. Based on other similar terminals with crane rails such as the North Sea Terminal in the Port of Antwerp, the container crane with a maximum vertical reaction line load of $1500kN/m$ is assumed. Since the crane load is not currently present at the quay, estimates of the magnitude and nature of this crane load have been made by the Port Authority based on the following principles as explained in the design report (Putteman et al., 2017):

- The center-to-center distance of the landside and waterside crane tracks is 30 meters.
- The landside crane track is assumed to be founded on separate piles which will not exert any load on the quay. Therefore, only the waterside crane track on the kesp of the quay will be analysed.
- As explained in the previous point, the center line of the waterside crane track coincides with the kesp of the quay section. The kesp spreads the line load from the corners of the crane to the whole 23 m wide section of the quay. Hence, the assumption is made that each section of the quay fully absorbs the load from the crane on top of it.
- The uniform surface load OB is maintained throughout the future scenario between the crane tracks on the land side and the waterside.

The crane load can work in 6 different load cases based on the storm conditions, meaning direction of the wind which affects the horizontal component of the crane load, and based on the mode of operation, meaning whether the boom of the crane is folding out or dropping down (Imbrechts et al., 2017a). The Table 5.1 describes these 6 load cases for the waterside crane load derived from the design report (Imbrechts et al., 2017a).

Abbreviation	Load Case Description	Vertical [kN/m]	Horizontal [kN/m]
KB(a)	Boom up during storm	875	171
KB(b)	Boom down, in operation	1002	61
KB(c)	Boom up, out of operation	620	61
KB(d)	Boom up during storm, reversed	75	-171
KB(e)	Boom down, in operation, reversed	0	-61
KB(f)	Boom up, out of operation, reversed	329	-61

Table 5.1: Description of crane load cases (Imbrechts et al., 2017a)

The positive value of horizontal force refers to the case where the wind blows from the land towards the waterside. That is, force directed towards the waterside is positive. Figure 5.1 illustrates the surcharge loads in the current loading scenario and future modification scenario, using Plaxis-2D.

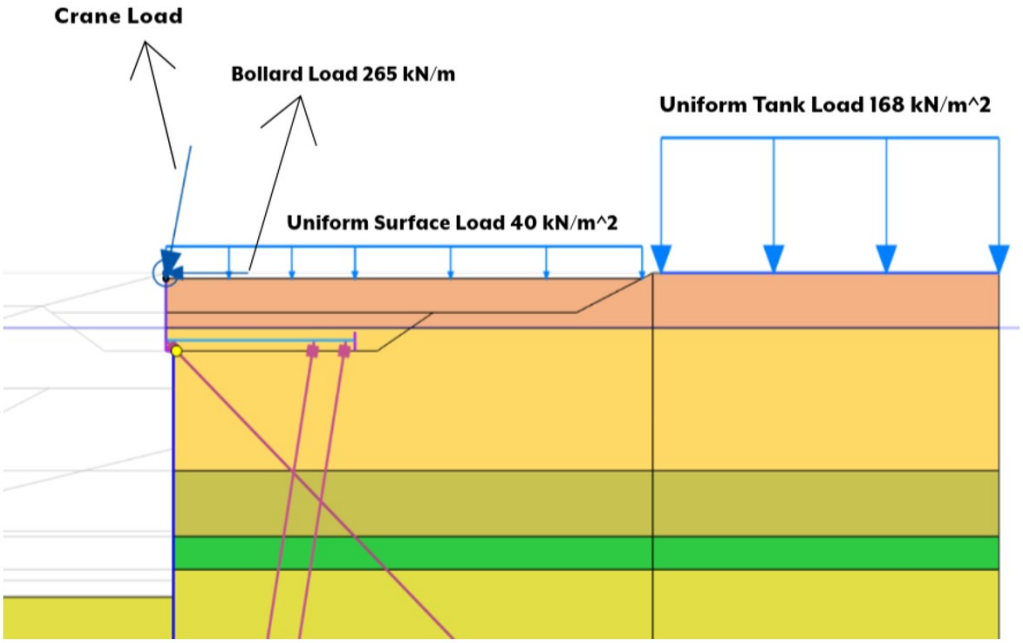

Figure 5.1: : Loads acting on the quay wall in current loading scenario (Tank load) and future loading scenario (Crane load)

The loads that are not deemed significant in this study due to their low magnitude of force and effects are the traffic loads, accidental collision loads and fender loads (Putteman et al., 2017). The study of environmental loads such as wind loads, wave loads, and temperature induced loads are beyond the scope of this thesis.

5.2.1. Design Load Cases

As explained in Section 2.3, the quay wall is subjected to surcharge loads both in the current scenario, where the quay serves as a liquid storage and transshipment terminal, and in the future scenario where it serves as a container terminal with the application of crane load. In both these scenarios, the load combinations are grouped into two design cases.

For the consideration of the loads, two design cases were formulated by the Port Authority and the designer Mariteam to study the effects of the loads on the combined wall and the tension piles separately. The two design cases are considered according to their effects on different structural parts of the quay system. These are targeted at studying the horizontal deflections in the wall along with the maximum bending moment generated in the wall, and the maximum anchor forces generated in the MV piles (Putteman et al., 2017) and (Imbrechts et al., 2017a).

Design Case 1: (OG1) Mobilisation of the maximum lateral earth pressure on the combined wall

The combination of loads in this design case is formulated in such a way that the resultant of the forces generates the largest possible lateral earth pressure behind the quay wall and the maximum load on the relieving platform (Imbrechts et al., 2017a).

This design case has the following effects on the quay wall:

- Mobilisation of the maximum field moment in the combined wall.
- Maximum head moment and field moment in the compression piles.

The bending moment and the normal forces in the combined wall are maximised due to the maximum lateral earth pressure generated behind the wall and the maximum value of the vertical top load on the relieving

platform. Maximum bending moment arises as most of the vertical top load in this design case is taken up by the pressure piles and the normal reaction forces of the combined wall.

Design Case 2: (OG2) Mobilisation of maximum Anchor Forces

This is the design case that mobilises the maximum tension in the MV piles, i.e. maximum anchor forces. In this case, the vertical load directly on top of the relief floor is omitted to prevent the generation of extra compressive forces in the SI piles, the horizontal component of which would cause a relaxing effect on anchor forces. Therefore, the uniform surface load is considered only behind the relieving platform. This load combination includes horizontal loads on top of the front wall which directly increase the generated anchor forces.

Loads activated as per the Design case

Uniform Surface Load

In design case 1, the vertical uniformly distributed surface load is activated both on top of the relief floor and behind it. The part of the line load directly on top of the relief floor increases the normal forces in the combined wall and the compression piles, hence being useful to enhance the axial forces and bending moment generated in the quay wall and the bending moment generated in the compression piles.

In design case 2, the part of the line load on top of relief floor is deactivated. This reduces the normal force, or the compression, generated in the compression piles. The reduction of compressive forces in the compression piles also reduces the relaxing effect it has on the lateral earth pressure experienced by the combined wall. The reduction of the Shielding effect on the combined wall leads to greater anchor forces in the tension piles

Tank Load

Tank load is activated in both the design cases as it has a negative effect for all structural parts of the quay wall. The effect of this load on the responses of structural elements is however not comparable with the effect of loads such as Uniform Surface load or the Bollard load (Imbrechts et al., 2017a). This is because it is applied at a large distance of 48 m from the quay wall compared to the uniform surface load which is applied starting from the waterside edge.

Bollard Load

In design case 1, the bollard force is deactivated. This load reduces the bending moment in the combined wall as well as the compression piles. This is because the bollard force tends to translate the superstructure towards the water with respect to the sub structure. The connection between the combined wall and the relieving platform is close to a hinged connection, so when a horizontal force is applied on top of the relief floor towards the water, it tends to rotate the superstructure in an anticlockwise direction leading to the reduction of the head bending moment in the combined wall and the compression piles.

Crane Load

As explained above, it is activated in the future modification scenario and operates in 6 different conditions. The conditions are governed by the direction of wind during a storm and the mode of operation of the crane. Based on the magnitude of the horizontal components of loads in each case, it is determined which case of crane loading is suitable for the given design case. For reference, the Table 5.1 describing the various crane loading conditions can be consulted again to categorize each crane load in the two design cases.

- **KB(a)** – As this load case has the largest horizontal component of the crane load directed towards the waterside on the top of quay, it is only activated in design case 2. This will maximise the anchor forces directly. For further explanation, consider the effect of bollard force on the quay superstructure and the

tension piles. This crane load has a similar effect on the relieving platform, i.e. it pushes the superstructure forwards towards the water side reducing the compression in the SI piles, therefore deactivated in design case 1, and increasing the tension in the MV piles.

- **KB(b)** – This load is activated in design case 1 as it has the largest vertical load directly on top of the quay wall. This load directly increases the axial reaction in the combination wall and the compressive reaction in the SI piles. Hence it is suitable for design case 1. This load is not considered in design case 2 as it has a much smaller horizontal component compared to KB(a).
- **KB(c)** - It is omitted from both design cases as it has smaller vertical as well as horizontal components compared to both KB(a) and KB(b). Only one type of crane load is activated in a loading phase in the FE model. Since KB(a) and KB(b) entail much more significant horizontal and vertical components of the load respectively, KB(c) is not considered in the loading phases.
- **KB(d)** - This load is activated only in design case 1. The negative value of the horizontal component signifies that the force is directed towards the landside. This force has a favourable effect on the bending moment generated in the combined wall and the compressive reactions in the compression piles, and a relaxing effect on the anchor forces. For these reasons, it is only suitable for design case 1.
- **KB(e)** - This load is not significant enough for either of the two design cases, KB(d) and KB(f) are more significant loads for design case 1. This load is not significant enough for design case 2 either.
- **KB(f)** - This load is again activated in design case 1 due to its significant vertical force and the landwards directed horizontal force. For the last three cases in which the wind blows from the waterside towards the landside, this has the largest vertical force. Also, because of the relaxing effect of landwards directed horizontal force on the anchor forces, it is not considered in design case 2.

The crane load KB(b) is chosen as the primary crane load for the future scenario in design case-1. Due to the large vertical component of KB(b), it is predicted that the bending moment generated in the combi-wall will be highest. In the case of the future scenario of design case-2, KB(a) is chosen as the primary crane load as its largest horizontal component will directly increase the generated anchor forces in the MV piles.

Validating the effects of the two design cases

To validate the effects of the design cases, the load combinations from both the design cases are applied on the wall in the current loading scenario i.e. excluding the crane load. Describe the effects of load directions etc.

The Table 5.2 below describes the loads applied in both design cases.

Load	Design Case 1	Design Case 2
Uniform Surface Load	40 kN/m/m	40 kN/m/m (Not applied on top of relief floor)
Uniform Tank Load	168 kN/m/m	168 kN/m/m
Bollard Load	0	$F_x = -265$ kN/m $M = 132.5$ kNm/m

Table 5.2: Loads applied to validate design cases with the FE model

The formulation of the two design cases OG1 and OG2 is verified by comparing the resulting lateral earth pressure, the field moment in the combined wall, the head and field moment in the pressure piles, and the maximum anchor forces.

• Horizontal Earth Pressure behind the quay wall

To check the differences in the horizontal earth pressure behind the quay wall for the two design cases, a cross section was chosen right behind the wall. In the top part of the soil behind the wall, it was observed that

the horizontal earth pressure is greater in design case 1 (OG1) than design case 2 (OG2). The horizontal earth pressure behind the top part of the wall, at a depth of 5 m, in design case 1 approximately 10.5 kPa and in design case 2 is around 7.5 kPa. As the depth increases, the two pressures come close in value. The difference in the horizontal pressures is only visible to the depth where the soil is directly experiencing the effects of the surcharge. The earth pressure distribution for the whole cross-section is presented in the Appendix C.

• Maximum Field Moment in the Combined Wall

Once the lateral earth pressure was proven to be greater for design case 1, the effects of greater lateral earth pressure was analyzed on the quay wall in terms of the bending moment generated. The maximum field moment in the quay wall was verified to be the largest in design case 1 (OG1). The bending moment throughout the structural cross-section of the quay wall is presented in the Appendix C. The difference in the maximum field moment generated in the two design cases is not very significant.

Model Phase	Max. Field Bending Moment in Combi-wall [kNm/m]
End of Dredging 11F	620
1st Load-OG1	695
1st Load-OG2	660

Table 5.3: Comparison between the maximum field moment in the combi-wall in design cases OG1 and OG2

• Maximum Head and Field Moment in SI Piles

Next, the maximum head moment and field moment in the compression piles are compared for the two design cases. Plaxis output in figure 5.2 shows clearly that both the head moment and the field moment are greater in the design case 1. The maximum head moment in the pile in design case 1 is 261 kN/m, approximately 10 times the head moment in design case 2 which is -23 kN/m. The maximum field moment in design case 1 is -45 kN/m, around 1.5 times more than in design case 2 which is -29 kN/m.

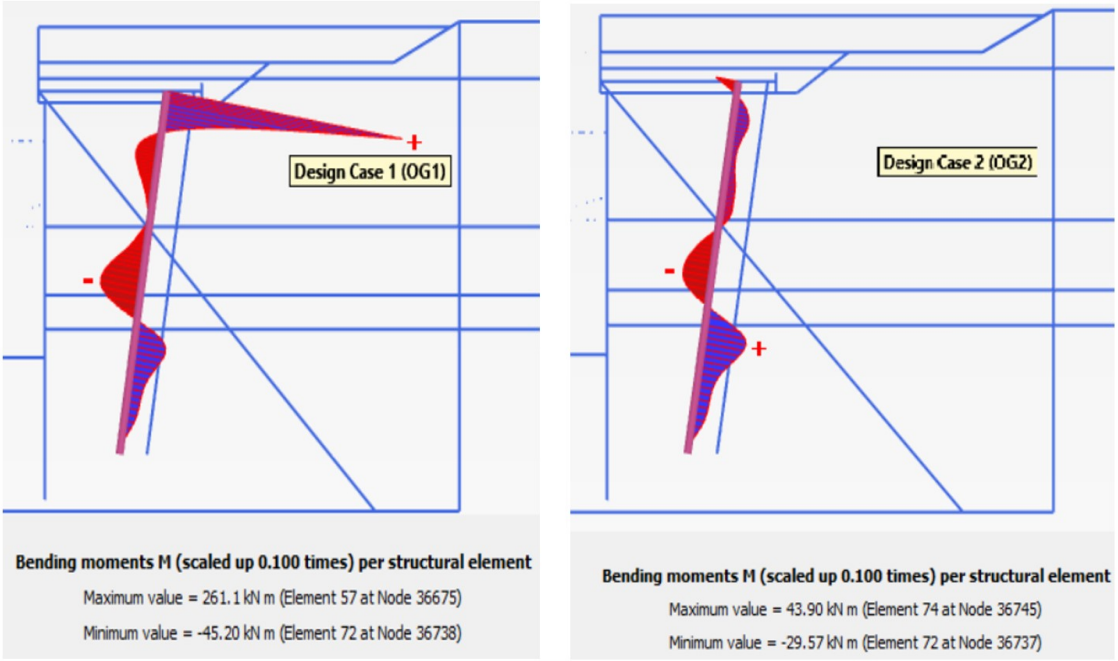

Figure 5.2: The bending moment in the compression pile for design case 1 (left) and design case 2 (right)

• Maximum Anchor Forces in Tension Pile

The maximum anchor force is generated at the connection with the relieving platform front wall. The biggest difference is observed in the anchor forces for the two design cases. The maximum anchor force mobilised in design case 2 is approximately 2613 kN which is twice the maximum anchor force of 1340 kN mobilised in design case 1. The anchor forces are presented in figure 5.3.

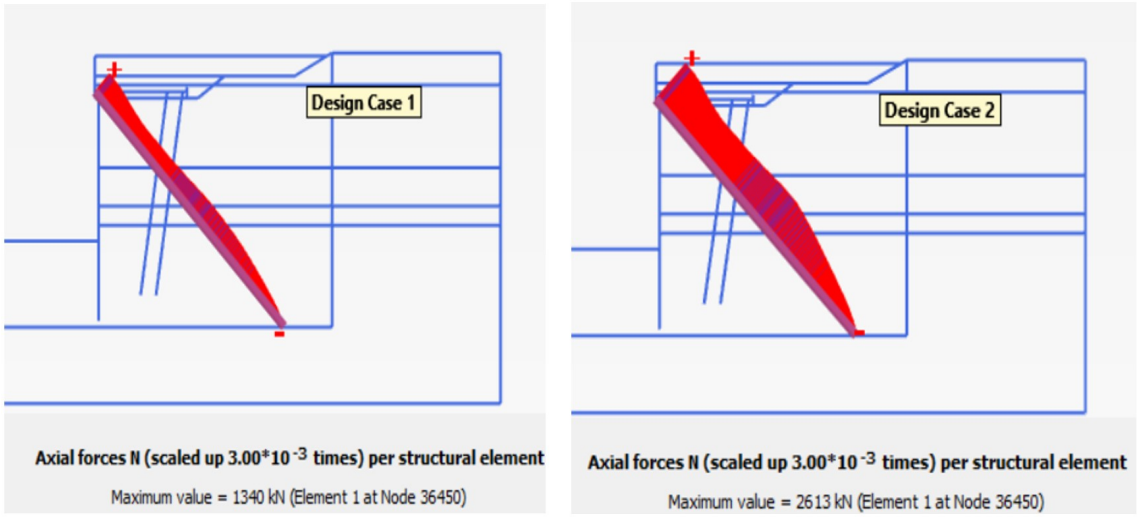

Figure 5.3: Anchor Forces mobilised in the two design cases OG1 and OG2

Since the difference in the anchor forces was so large, the wall displacements were also necessary to be checked for the two design cases. It can be predicted in advance that design case 2 leads to greater wall displacements than design case 1 as the larger anchor forces must have been caused by larger horizontal displacement of the wall.

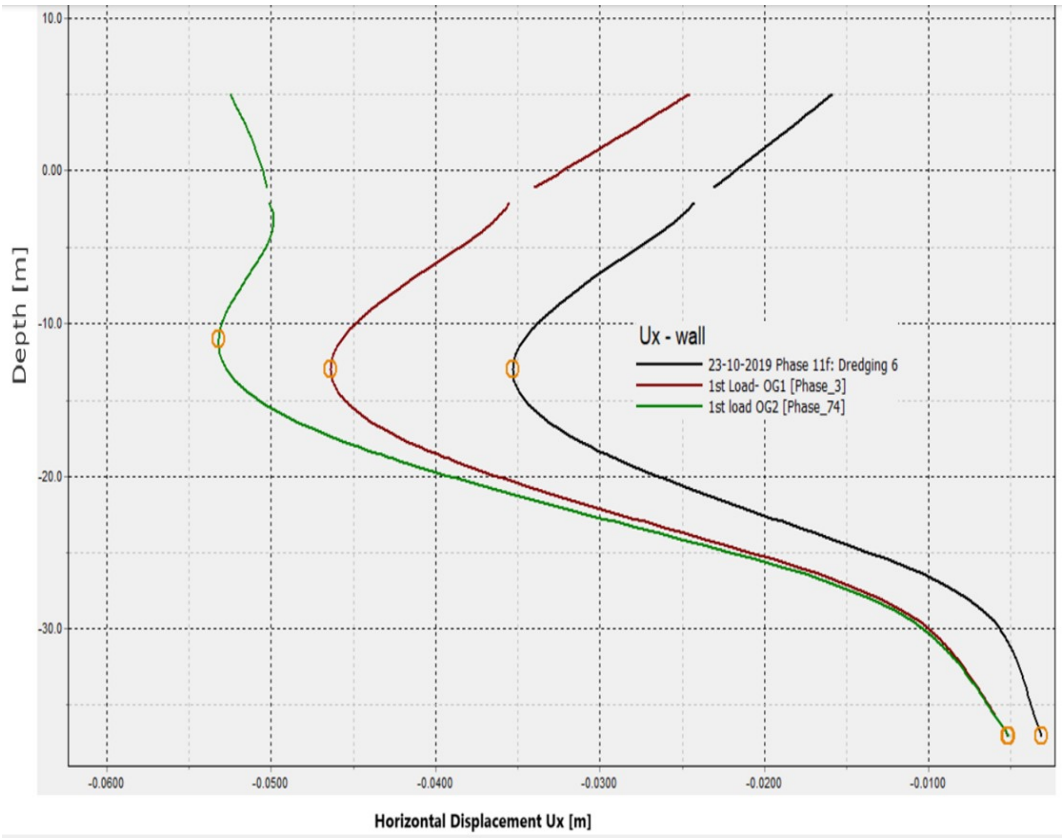

Figure 5.4: Combi-wall displacement at the end of dredging and in design cases OG1 and OG2

Figure 5.4 shows that the maximum horizontal displacement of the wall at the end of dredging is 35 mm at

depth of around 13 m and 16 mm at the top of the wall. Due to the loading as per design case 1, the maximum horizontal displacement reaches a value of 46 mm at the same location and 25 mm at the top of the wall. In design case 2, the maximum displacement reaches 53 mm while the top of the wall also displaces significantly up to a value of 52 mm. The large displacement of the top of the wall in design case 2 is due to the application of the horizontal bollard load of 265 kN in the seaward direction. The application of this bollard load also explains the large anchor forces mobilised in design case 2.

The formulation of the design cases and their effects in the structural members is now validated with the Plaxis results. Since design case 2 leads to greater wall displacements and anchor forces, the rest of the section will explore the load combinations as per design case 2 to check the long -term effects of unloading-reloading of the quay wall with multiple cycles of unloading and reloading.

5.2.2. Unload-Reload Simulation Method

For analyzing the long-term behavior of the quay wall under multiple cycles of unloading and reloading, the load combination from design case 2 is applied on the quay wall as it mobilises larger wall displacement and anchor forces compared to design case 1. The phases are calculated with plastic-type calculation.

In the first attempt at simulating the unload-reload behavior of the quay wall, 10 cycles of loading were used for both the current and future scenario. However, the incremental deformations in the wall and the incremental mobilisation of anchor forces in the MV pile per loading cycle still showed an increasing trend. Hence, more load cycles were simulated to reach a converged and stable value of increments in the wall displacements and anchor forces with more loading cycles.

As cyclic loading is not considered in the design reports of the project HTT Quay wall, no information on the frequency and duration of unloading and reloading of surcharge loads is available. In addition, the quay wall at HTT has not been in use for a few years, so there is no available information about the loads currently experienced by the quay wall. To decide how many cycles of unload-reload must me simulated, similar cases of cyclic surcharge loading on quay walls were referred to, such as, the quay wall at the Port of Rotterdam studied by De Gijt et al. (2011) for its behavior under cyclic surcharge loading. At the studied quay wall, the cyclic loading of surcharge had a frequency of 28 days. Although it was not made clear in the research done by De Gijt et al. (2011) how the surcharge originated, whether it was due to container load or tank load, the same frequency of cyclic surcharge loading has been assumed for the HTT quay wall and is adopted in this chapter. Over a period of 4 operational years of the HTT quay wall, from the year 2020 to year 2023, assuming a frequency of loading to be 28 days or one month, this would lead to around 48 cycles. For simplicity, 40 cycles of design case-2 loading are considered for this study.

There are 40 cycles of unload-reload of surcharge in the current scenario followed by 40 cycles in the future scenario. In the Plaxis model, the cyclic loading phases of future scenario, where the crane load replaces tank load, are modelled successive to the current scenario without resetting any displacements. The table 5.4 below represents the loads that are activated in the loading phases and deactivated in the unloading phases to simulate the cyclic surcharge loading behaviour of the quay wall.

Load	Design Case 2			
	Current Scenario		Future Scenario	
	Load	**Unload**	**Load**	**Unload**
Uniform Surface Load	40 kN/m/m (Not applied on top of relief floor)	12 kN/m/m (Not applied on top of relief floor)	40 kN/m/m (Not applied on top of relief floor)	12 kN/m/m (Not applied on top of relief floor)
Uniform Tank Load	168 kN/m/m	0	0	0
Bollard Load	$F_x = -265$ kN/m $M = 132.5$ kNm/m	0	$F_x = -265$ kN/m $M = 132.5$ kNm/m	0
Crane Load	0	0	**Kb(a)** $F_x = -171$ kN/m $F_y = -875$ kN/m	0

Table 5.4: Summary of loads activated to simulate the cyclic surcharge loading behaviour of quay wall

5.2.3. Wall Horizontal Displacement Results

Horizontal Displacement Design Value- As per the design report by Imbrechts et al. (2017a), the maximum allowed horizontal displacement of the combined wall is 1% of its retaining height. The retaining height of the quay wall extends from +5 m on the ground surface to -25.60 m below the ground surface, which is the final dredged level. The total retaining height being 30.60 m and the maximum allowable horizontal displacement is therefore 306 mm (Imbrechts et al., 2017a).

Cyclic Loading Results

To understand the development of the wall displacement during loading cycles, the figure 5.5 illustrates the curve that plots the points of maximum horizontal displacement of the wall (Ux) with each unload-reload cycle in the current loading scenario followed by the future loading scenario.

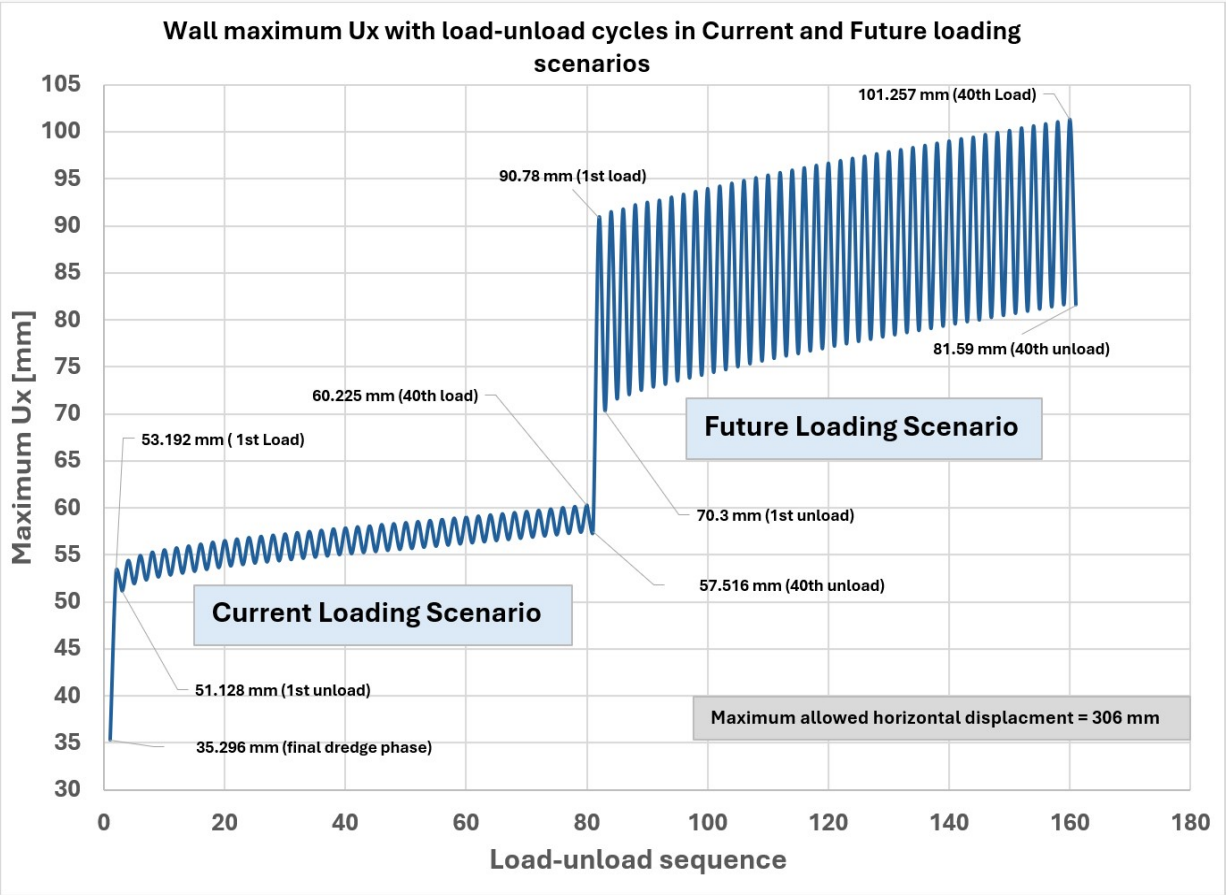

Figure 5.5: Maximum horizontal displacement in the combi-wall with unload-reload cycles in the current and future loading scenarios

The figure 5.5 shows progressively increasing maximum wall displacements for both the current and future scenarios with each cycle of surcharge loading. The maximum displacement of the wall occurs after the first application of load in both the scenarios as was shown by De Gijt et al. (2011).

At the end of dredging phase, which is the end of construction of the quay wall, the maximum horizontal wall displacement is 35.296 mm at the depth of 13 m. On applying the current scenario load combination for the first time, the maximum wall displacement increases to 53.192 mm at the depth of 11 m. However, on unloading the load combination, the wall does not return to the original position but goes back to a horizontal displacement value of 51.128 mm. The first load cycle therefore leads to the initial wall displacement accumulation of 51.128 mm - 35.296 mm = 15.8 mm. The rate of accumulation of wall displacement drops exponentially after the first load cycle. The rest of the load cycles in the current loading scenario led to an extra accumulation of 6.4 mm. In total, after 40 load cycles in the current loading scenario, the accumulation in maximum wall displacement is 15.8 + 6.4 = 22.2 mm. Throughout the current loading scenario load cycles, the maximum horizontal displacement of the wall occurs at depth of 11 m.

After the 40 load cycles from the current loading scenario of the wall, the load cycles of the future loading scenario are simulated. The displacements for the future scenario are not reset to zero in the Plaxis model, and the calculations are carried forward from the last unload phase of current scenario. The load combinations in the future loading scenario replace the tank load with the crane load. The crane load applied on top of the wall has a large horizontal component of 171 kN in the seaward direction, applied directly on top of the front wall, in addition to the already activated seaward horizontal bollard load of 265 kN. Together, the two horizontal loads on top of the front wall led to larger wall displacements. De Gijt et al. (2011) showed that there is a non-linear relationship between the additional displacements and the magnitude of loading. Higher loads generate more new plastic points and cause more redistribution of stresses in the soil, and hence more accumulation of wall displacements is seen when the future loading scenario is simulated. After the last load cycle from the current scenario, the wall displacement is 57.516 mm. On applying the first loading from the future scenario, the wall displacement increases to 90.78 mm, the point of maximum displacement being the top of the front wall. On unloading the first load, the wall does not return to the original position but instead to a displacement value of 70.3 mm. Therefore, an initial accumulation of 70.3 mm – 57.516 mm = 12.784 mm

is observed in the wall displacement, at the top of the front wall. After the first load cycle, the rate of accumulation of wall displacement drops exponentially again. In total, after 40 cycles of loading from the future scenario, an extra wall displacement of 24 mm is observed at the top of the front wall.

The difference in wall horizontal displacement values between the unloading and reloading in current scenario is about 3 mm whereas in the future scenario it is around 20 mm, due to larger horizontal loads activated in future loading scenario. This also suggests more elastic deformation in the soil behind the wall in case of larger horizontal loads. These observations prove that future loading scenario is more crucial in the geotechnical assessment of the quay wall.

It is observed that the wall displacements in the Future loading scenario (with a crane load) are much more critical than the displacements in the Current loading scenario. The crane load adds a large horizontal load directly on top of the front wall which results in the maximum horizontal displacements being observed at the top of the front wall as opposed to the current scenario where the maximum horizontal displacement is observed at a depth of 11 m. To better understand the whole picture of the maximum wall displacements and at what locations in the wall those displacements occur, figure 5.6 along with table 5.5 show the maximum wall displacement points in the wall.

In figure 5.6, the Plaxis output cross-sectional curves of the quay wall representing horizontal wall displacements plotted against depth of the wall are shown for selected phases. These phases include the end of dredging (construction) phase 11F, the phases of first and the last load applications from the current scenario, and the phases of first and the last load applications from the future loading scenario. The curves depict the progressively increasing wall displacements with increasing load cycles for both the current load scenario and the future load scenario. The points of maximum wall displacement vary as per the load combinations. The direction of the loads and the points (location) of application of the loads affect the position where the maximum wall displacement is observed in the combi-wall.

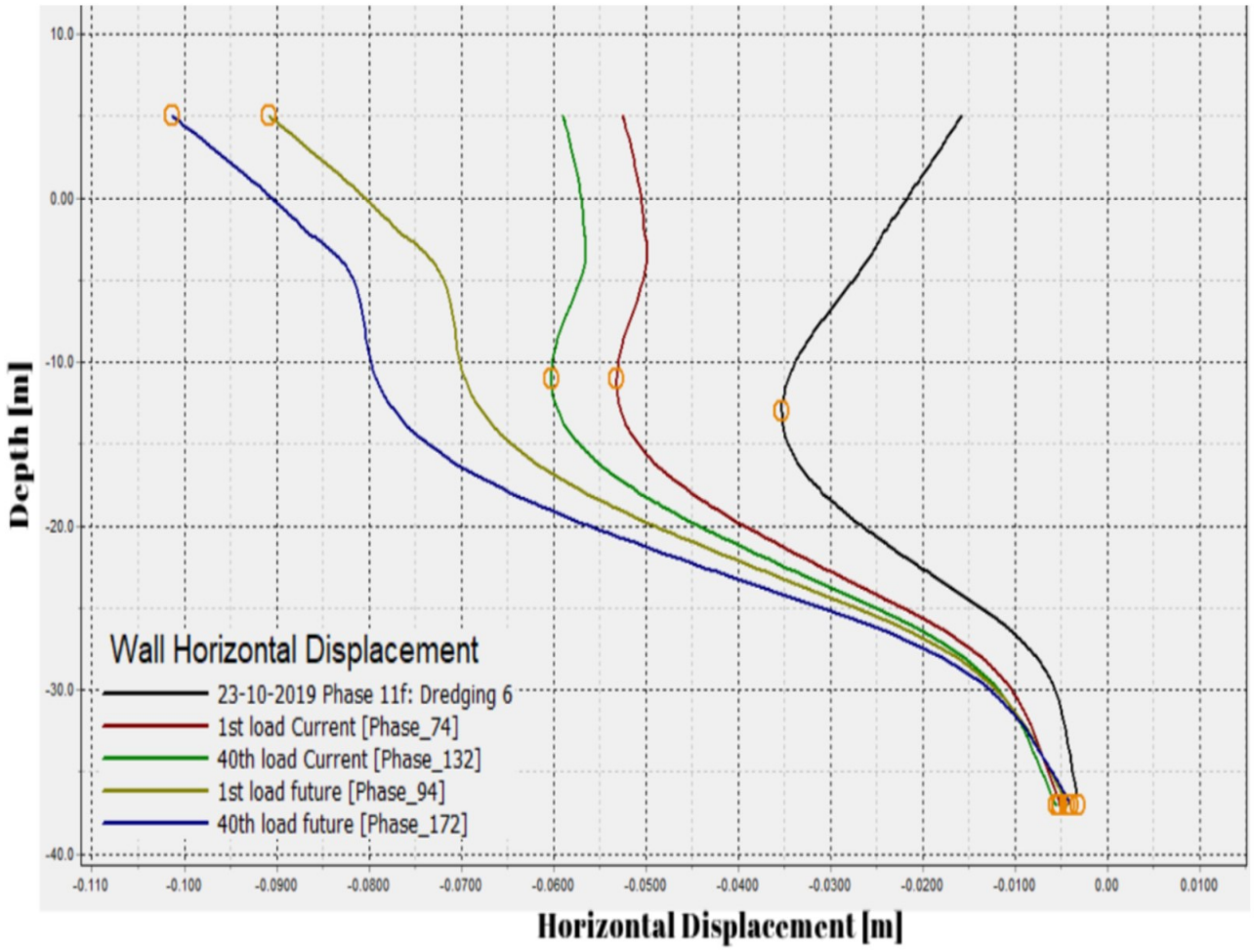

Figure 5.6: Horizontal Displacement of the wall with load cycles in current and future scenario

Table 5.5 summarizes the maximum wall displacements observed in the wall due to the loading cycles from current and future scenario, along with their locations (depths) along the wall.

Phase	End of Construction	1st Load Current Scenario	40th Load Current Scenario	1st Load Future Scenario	40th Load Future Scenario
Maximum Horizontal Displacement [mm]	35.296	53.192	60.225	90.78	101.257
Depth [m]	-13	-11	-11	+5	+5
Percentage of Design Value Reached	11.5%	17%	20%	30%	33%

Table 5.5: Summary of maximum horizontal wall displacements with load cycles

In figure 5.6, the curve in black on the right shows the horizontal wall displacement at the end of construction when no surcharge is applied on or behind the wall. The maximum wall displacement reached by the end of dredging is 35 mm at a depth of 13 m. At this stage, the displacement of the wall compared to the maximum allowed displacement of 306 mm is merely 11.5%. The two curves in the middle show the displacement for the 1st load application and the 40th load application in current loading scenario. The maximum values being 53 mm and 60 mm at the depth of 11 m at the end of 1st load application and 40th load application respectively. On first application of surcharge load in current scenario, the wall displacement reaches a value which is around 17% of the design value. After the last loading cycle in the current scenario, around 20% of the maximum allowed displacement is reached. Around 22 mm of displacement was accumulated after 40 load cycles in current loading scenario.

The two curves at the left most present the displacement for the future scenario with a crane load activated. The maximum displacement in the wall occurs at the top due to the large horizontal components of the Bollard force (265 kN/m) and the Crane load (171 kN/m) applied directly on top of the front wall. The maximum displacement of the wall for the first loading cycle in future scenario is 90 mm and in the last cycle (20th) is 101 mm. The first load application in future scenario leads to a displacement which is around 30% of the maximum allowed displacement. The final loading in future scenario leads to a displacement of around 33% of the maximum allowed value. A total of 24 mm of wall displacement gets accumulated due to repeated unloading and reloading in future loading scenario.

Rate of Accumulation of Wall Displacement

It was shown by De Gijt et al. (2011) and Tolba et al. (2020) that when the surcharge is removed during unload-reload cycles, the quay wall does not return to the original position due to plastic strains generated in the soil. New plastic points are generated in the soil and the stress is redistributed with each cycle of unload-reload, which leads to the accumulation of displacements in the retaining wall.

The rate of new plastic strain generation and stress redistribution reduces after initial cycles as the soil undergoes densification due to initial load cycles (De Gijt et al., 2011). Over numerous early cycles of loading, the densification increases, and the soil fabric is then in a more stable arrangement after which redistribution of stresses and generation of new plastic points is minimal. The cyclic loading of surcharge loads leads to an accumulation of plastic strains in the soil and to the accumulation of quay wall displacement. However, as the soil densifies with increasing load cycles, the rate of accumulation of wall displacements reduces exponentially.

The increments or accumulation in displacement after each load cycle is calculated by subtracting the displacement after an unloading step from the previous unloaded displacement. To assess the accumulation of displacement with each cycle of loading in both scenarios, the incremental displacements of the wall after each unloading step is presented in figure 5.7.

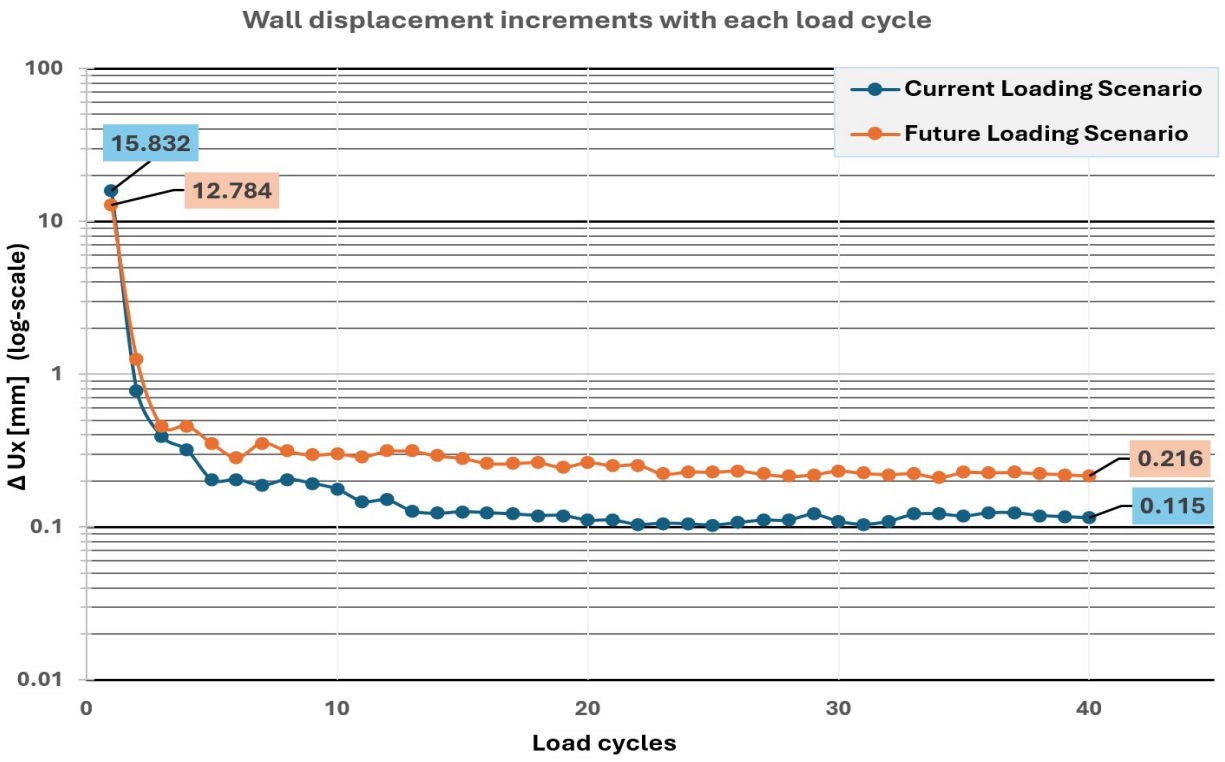

Figure 5.7: Incremental horizontal displacements of combi-wall with reloading steps

The figure 5.7 shows the increments in the displacement of the combi-wall with each loading cycle in the logarithmic scale, recorded after each unloading in both loading scenarios. The increment in current scenario is larger after the initial load cycle with 15.8 mm being the accumulated displacement after 1st loading cycle is complete. The increment in displacement after the second loading cycle is 0.784 mm, which means a 95% reduction in the second increment compared to the first increment. The final value of increment in wall displacement is 0.115 mm which is seen after the 20th loading cycle until the last loading cycle. The final increment in wall displacement per loading cycle shows a 99% reduction compared to the initial increment after the first cycle.

In the future scenario however, the increment initially is smaller than current scenario, around 12 mm, as the soil is already stiffer due to loading in current scenario. However, it drops to a higher fluctuating value of around 0.2 mm after 23 load cycles. The increment in displacement after 2nd load cycle is 1.262 mm, which shows a reduction by 90% compared to the increment in displacement after 1st load cycle of 12 mm. Finally, the displacement increments converge at 0.2 mm per loading cycle, which is double the final increment per load cycle in the current scenario. This signifies that there is more accumulation of displacements over time in the case of future scenario.

The observed correlation between the rate of accumulation of wall displacement and the progression of surcharge load cycles matches well with the analytical findings as reported by De Gijt et al. (2011).

5.2.4. Anchor Force Results

Anchor Force Design Value- As per De Gijt and Broeken (2013), the maximum representative tensile force that MV piles can bear is 6,000 kN. As per the load tests on MV piles at Hartel Tank Terminal conducted by Spruit et al. (2019), the maximum tensile force recorded at the top of the MV piles was between 8000 kN and 10770 kN for piles with an approximate length of 60 m. The maximum shaft friction mobilised at failure was 250 kPa at the top of Pleistocene sand layer and 600 kPa at the toe of the pile. van Paassen and van Dalen (2009) conducted load tests on MV piles at Euromax quay wall which were designed to bear a tensile load of 7200 kN/pile. The length of the piles was 56 m. The ultimate tensile force that the HEB 600B piles were able

to withstand was around 9000 kN/pile before the failure according to creep criterion of > 2mm was reached.

In the case of skin friction capacity of the tension piles, it is calculated with the CPT based method (CUR 2001-4, 2003; Imbrechts et al., 2017c). The maximum skin friction per meter of the pile at the top of the Pleistocene sand is around 244 kN per meter of pile. At the toe of the pile, skin friction capacity is 554 kN per meter of the pile.

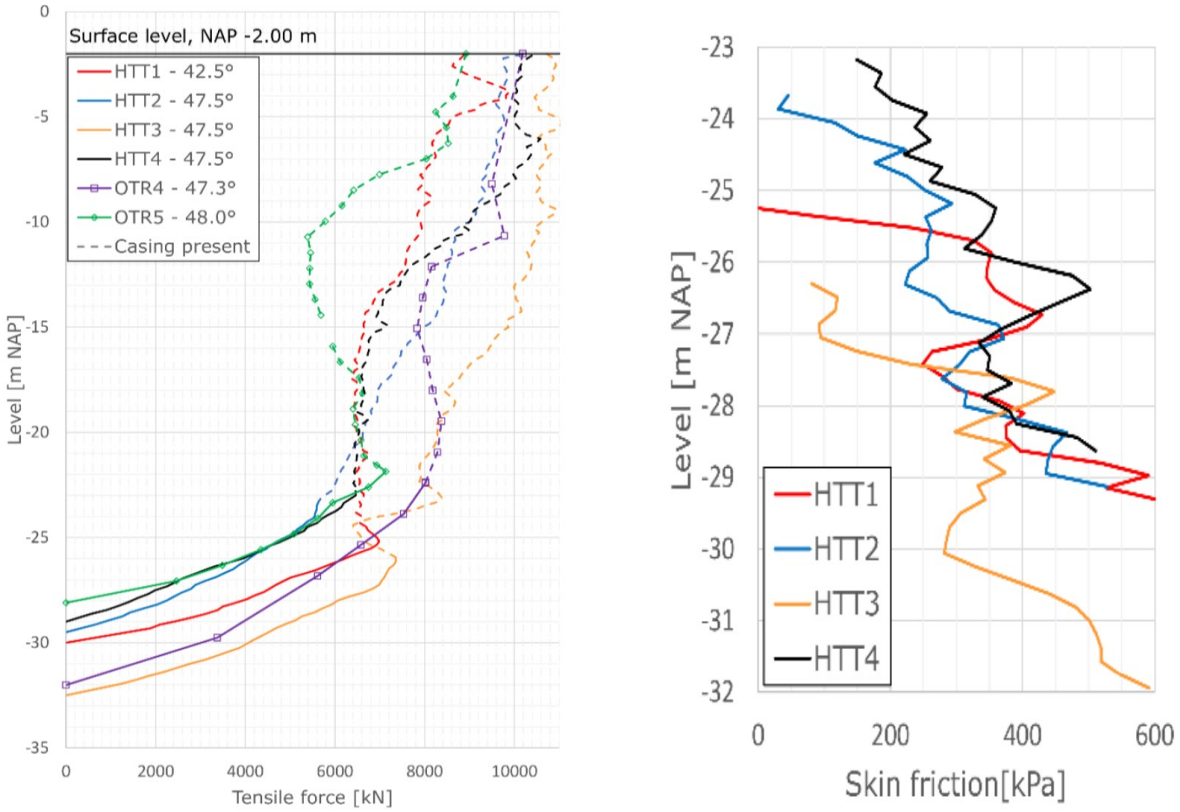

Figure 5.8: Tensile force (left) and skin friction (right, in Pleistocene sand) vs. Depth at the final load step of MV piles load tests at HTT quay wall (Spruit et al., 2019)

In this thesis, 6399 kN is considered the ultimate anchor capacity of MV piles (Imbrechts et al., 2017c) and 244 kN/m and 554 kN/m as the maximum skin friction at the top of Pleistocene layer and at the toe of the pile respectively.

Cyclic Loading Results

Like the horizontal wall displacements, maximum anchor forces in MV pile were also larger in the future loading scenario compared to the current scenario because of the additional horizontal load applied by the crane on top of the wall. Figure 5.9 below illustrates the maximum anchor forces in the current loading scenario followed by the future loading scenario.

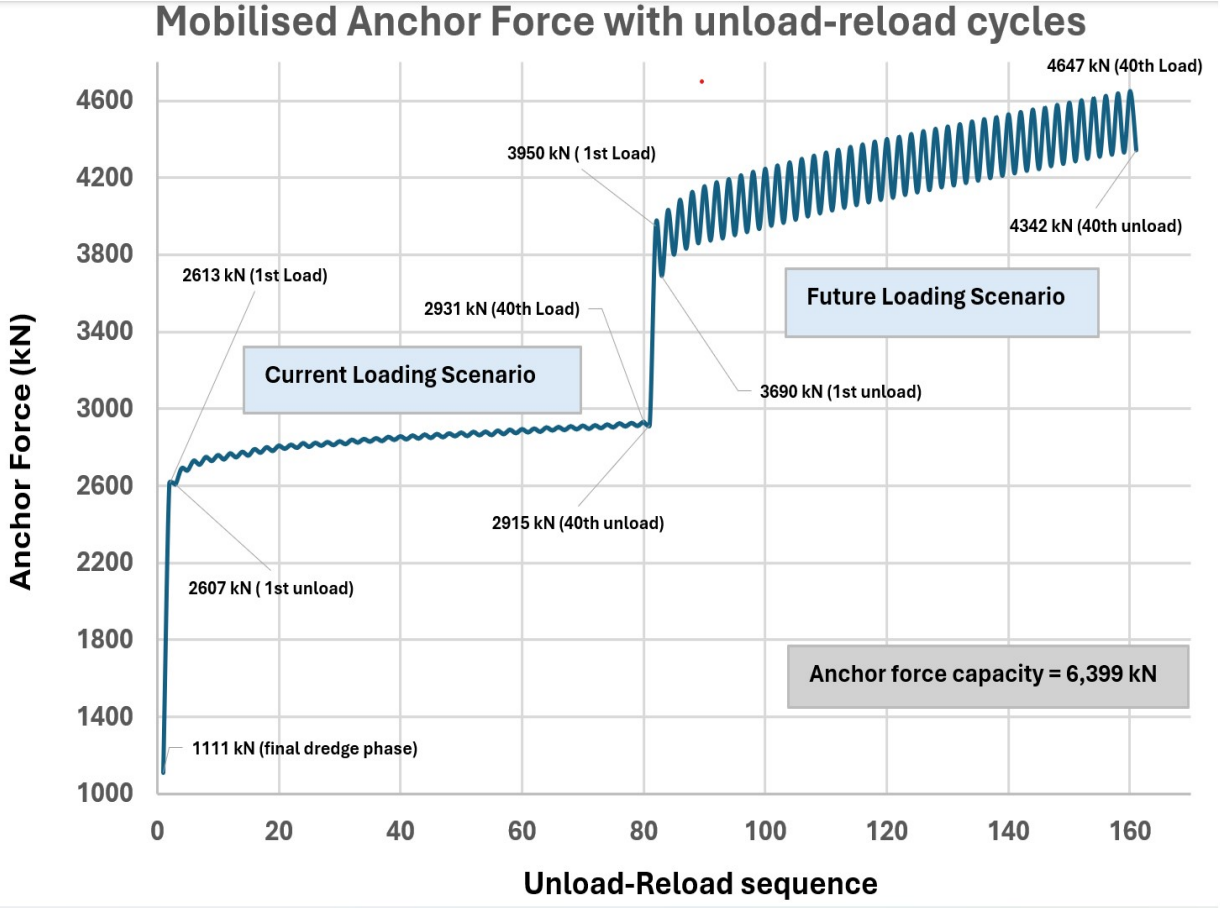

Figure 5.9: Mobilisation of anchor forces with unload-reload cycles in current and future loading scenario

The maximum anchor force in MV pile is generated at the connection between the MV pile and the relief floor (Cast Iron Saddle). The MV pile is analysed in design case 2 with 40 cycles of unload-reload in the current scenario and 40 cycles in the future scenario with a crane load. The maximum anchor force generated at the end of dredging is 1111 kN at the connection with cast iron saddle. This anchor force corresponds to around 17% of the design anchor capacity of 6399 kN. The shaft friction generated at the toe of the pile is 110 kN per meter of the pile. This corresponds to 20% of the shaft friction capacity.

The maximum anchor force due to first load application in current scenario is 2613 kN, which is around 41% of the design capacity. The shaft friction mobilised at the toe of pile is 262 kN per meter of pile, reaching 47% of the shaft friction capacity of 554 kN per meter of pile. After the 40th load cycle in current scenario, the anchor force reaches 2931 kN, which is 46% of the maximum allowable anchor force, with the shaft friction at the toe reaching 310 kN/m i.e. 56% of the shaft friction capacity. An accumulation of 318 kN is observed in anchor forces due to 40 loading cycles in current loading scenario. The increase in anchor force with respect to end of construction is around 135% at the end of 1st loading and 163% at the end of the last loading.

Additional horizontal crane load is applied on the quay wall in future scenario which directly increases the anchor force mobilisation. The maximum anchor force in the MV pile is much larger due to the large horizontal components of the Bollard force (265 kN/m) and the Crane load (171 kN/m) applied directly on top of the front wall. The maximum anchor force for the first load cycle in future scenario is 3950 kN, reaching around 62% of the maximum allowable anchor force, with the mobilised shaft friction of 327 kN/m at the toe (60% of shaft friction capacity). The generated anchor force in the last cycle (40th) is 4647 kN, which is 73% of the maximum allowed anchor force. The mobilised shaft friction is 354 kN/m corresponding to 64% of shaft friction capacity. A total accumulation of around 700 kN is observed in anchor force over 40 load cycles in the future scenario, double the accumulation observed in current scenario.

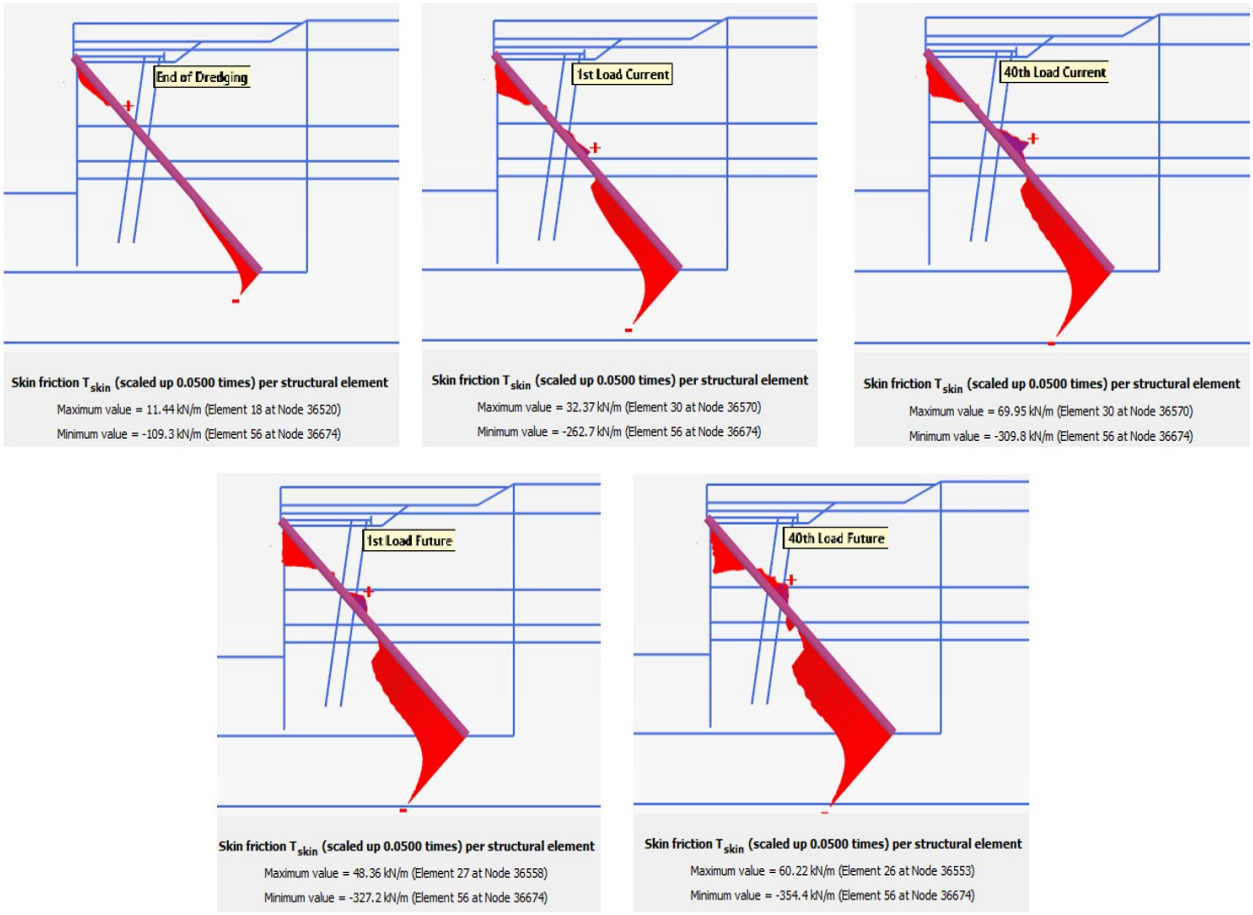

Figure 5.10: Mobilisation of shaft resistance in MV pile with unload-reload cycles in current and future loading scenario

Figure 5.10 exhibits the increase in the mobilised shaft resistance of MV pile with increasing load cycles in the current and future loading scenarios. The shaft friction increases correspondingly with the increase in the anchor forces.

Increments in Anchor force per load cycle

It is observed that the anchor forces in the Future loading scenario (with a crane load) are much more significant than the ones in the Current loading scenario. The crane load adds a large horizontal load directly on top of the wall which results in much larger anchor forces. It is also observed that the difference in the anchor forces between the unloading and reloading phases in the current scenario is much lesser than the one in the future scenario. The difference in anchor forces between the unloading and reloading in current scenario is about 20 kN, whereas, in the future scenario it is 300 kN. There is an accumulation of anchor forces of about 318 kN at the end of the current scenario loading cycles and that of 700 kN at the end of loading cycles in the future scenario. These observations prove that future loading scenario is more crucial in the geotechnical assessment of the MV pile and quay wall.

To assess the accumulation of anchor forces over repeated cycles of loading in both scenarios, the incremental mobilisation of anchor forces with each load cycle in both loading scenarios is presented in figure 5.11.

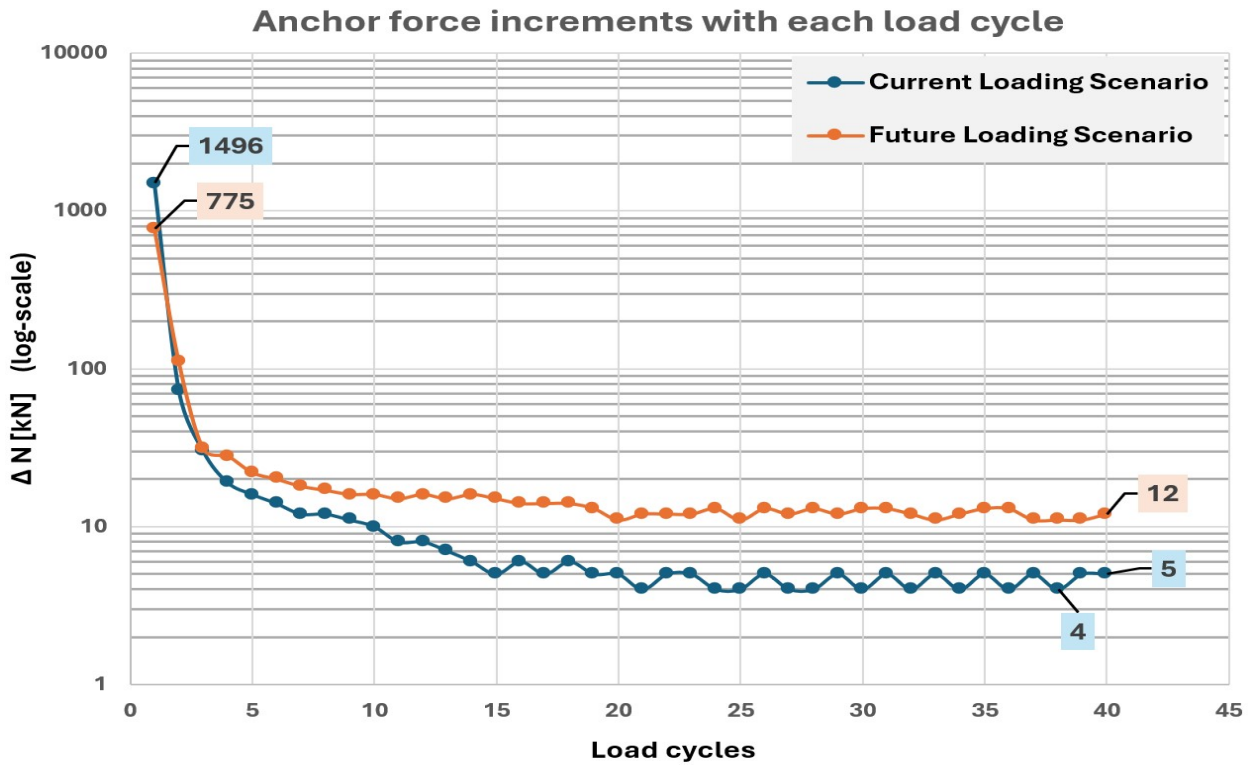

Figure 5.11: Increments in anchor force with load cycles in current and future scenarios

The figure 5.11 shows the increments in the anchor force with each loading cycle, recorded after each unloading in both loading scenarios. The increment in current scenario is larger after the initial load cycle with 1496 kN being the increment after 1st loading cycle is complete. The increment in anchor force after the second loading cycle is 73 kN, which means a 95% reduction in the second increment compared to the first increment. The final value of increment in anchor force is between 4 and 5 kN which is seen after the 20th loading cycle until the last loading cycle. The final increment in anchor force per loading cycle shows a 99% reduction compared to the initial increment after the first cycle.

In the future scenario however, the increment initially is smaller than current scenario, around 775 kN, but it falls to a higher fluctuating value of around 12 kN after 23 load cycles. The increment after 2nd load cycle is 110 kN, which shows a reduction by 85% compared to the increment after 1st load cycle. Finally, the increments converge at 12 kN per loading cycle, which is double the final increment per load cycle in the current scenario. This signifies that there is more accumulation of anchor forces over time in the case of future scenario.

5.3. Behaviour of Quay Wall under Cyclic Water Level Fluctuations

The analysis of the impact of cyclic fluctuations of water level on the deformation behaviour of the quay wall is aimed at acquiring critical insights into the relationship between the hydrostatic conditions in the soil, the distribution of effective stresses or lateral earth pressure experienced by the wall, and the structural response of the wall.

Most of the standards that are followed in The Netherlands such as CUR 211 (De Gijt & Broeken, 2013), Harbours and Waterways EAU 2004 (2005), and Design of Sheet Piles CUR 166: Part-2, 2008, check for hydraulic loads in the design phase of a retaining wall. The hydraulic loads considered in these standards are due to the water level difference between the outer water and the ground water. However, even in cases where there is no water pressure difference between the ground water and free water, the fluctuations in

water levels can change the effective stress condition in the soil and the load imposed on the retaining wall may also change consequently.

The ground water level or the phreatic level along with the pore pressure in the soil are determined using a piezometer (De Gijt & Broeken, 2013). The water level difference between outer water level (harbour water level) and the ground water level creates a pressure difference on the quay wall (De Gijt & Broeken, 2013). This difference is minimized using drainage system in the quay wall, as is the case with most quay walls at the Port of Rotterdam. Along with drainage, the soil profile at HTT is mostly dominated with highly permeable soil layers which eliminate the water pressure differences rapidly. The water pressure difference between the free water and the ground water is negligible at the HTT quay wall site as shown by Schouten (2020). The figure 5.12 compares the water level of the harbour with the groundwater level in the soil behind the quay wall for a period of 10 days. At the time of construction, the water level sensors at the HTT harbour were not installed. Schouten (2020) showed that the water level recordings from the Hartelhaven, which is one kilometer away from the HTT quay wall, are representative of the water level at HTT harbour. The measurement data of the ground water levels were taken from the piezometer installed at HTT quay wall site.

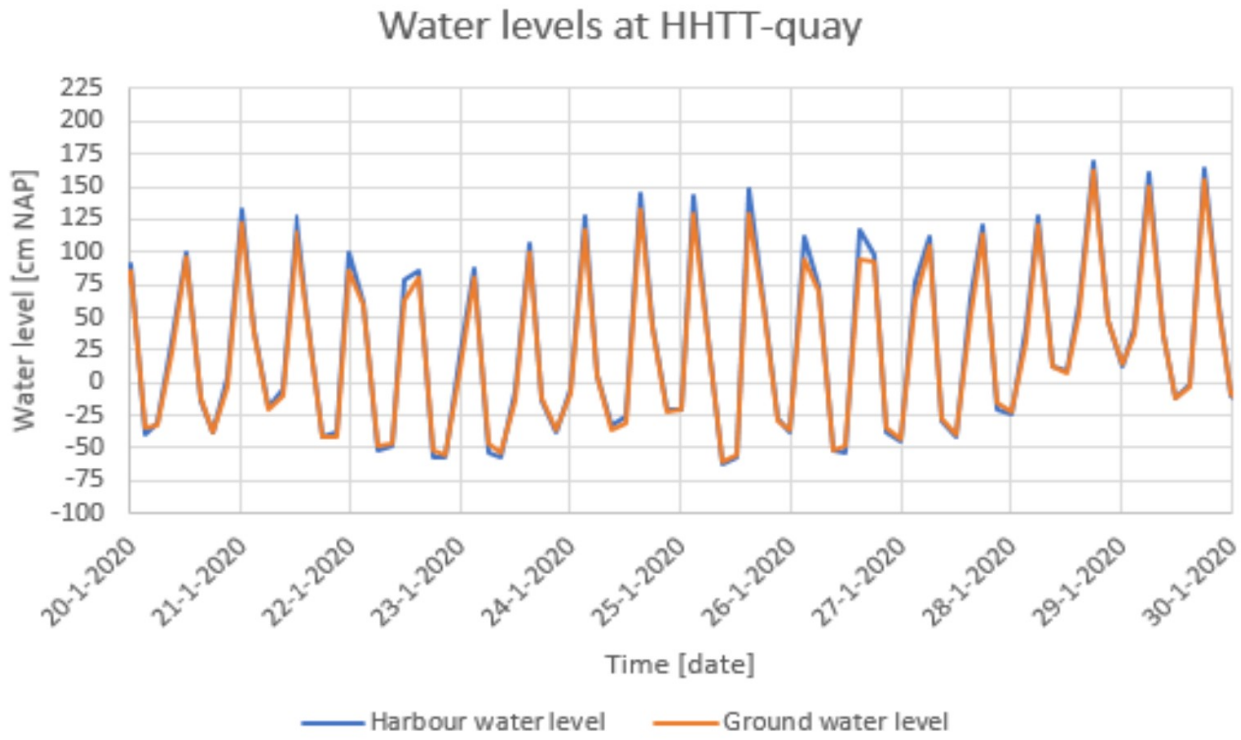

Figure 5.12: Comparison between Harbour water level and Ground water level at HTT quay wall in early operational phase (Schouten, 2020)

It can be concluded that there is no significant water pressure difference between the free water and the ground water. However, even in the case with no water pressure differences, the changing ground water levels directly affect the effective stresses in the soil behind the wall. A lower water level will reduce the pore pressure in the soil hence increasing the effective stress in the soil leading to larger lateral earth pressure exerted by the soil on the quay wall. It can be predicted that a lower water level will increase the horizontal displacement of the wall. Whether the cyclic fluctuations of water level will lead to accumulation of strains in the soil has to be seen in the FE model.

5.3.1. Monitoring Data of Water Level

The figure 5.13 below shows the piezometer readings of current water level fluctuations in the groundwater at zone B4 of the HTT quay wall. The most recent data has been collected over a period of two months to be able to simulate the current water level fluctuations experienced by the quay wall. From the data, the average high-water level experienced by the wall is 1.25 m, and the average low water level is -0.5 m.

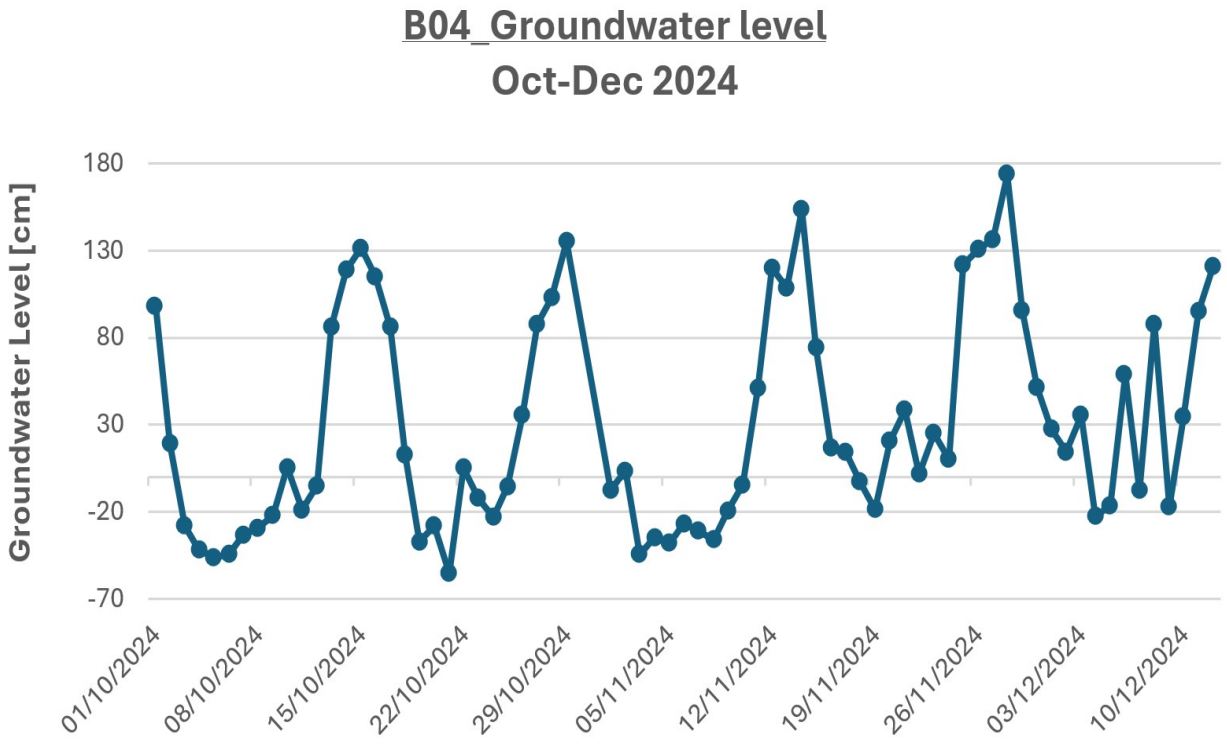

Figure 5.13: Groundwater level fluctuations at zone B4 of HTT quay wall

5.3.2. Water Level Fluctuation Simulation Method

The water level in the construction phases is set at 0 m NAP (Imbrechts et al., 2017b). The average maximum water level is 1.25 m NAP, and the average minimum water level is -0.5 m NAP.

The high and low water levels are modelled as alternate phases and the calculations for the model are plastic type with pore pressures calculated with phreatic type in the FE model. There are 20 cycles of low and high-water levels that are modelled in Plaxis to see the effect on wall displacement and anchor force generation in the MV piles. The alternate phases of high and low water levels are simulated by changing the user water levels in the Flow Conditions of the FE model. For simulating a high water level, a user water level of +1.25 m NAP is chosen as the global water level. Similarly, for a low water level, a user water level of -0.5 m NAP is chosen as the global water level. The calculations of the first model phase simulating a high water level start from the end of dredging phase as its predecessor. The next sub-section exhibits the results seen in the horizontal wall displacements due to fluctuating water levels.

5.3.3. Results of Water Level Fluctuation Simulations

The figure 5.14 below presents the maximum horizontal displacement of the combi-wall with fluctuating water level cycles.

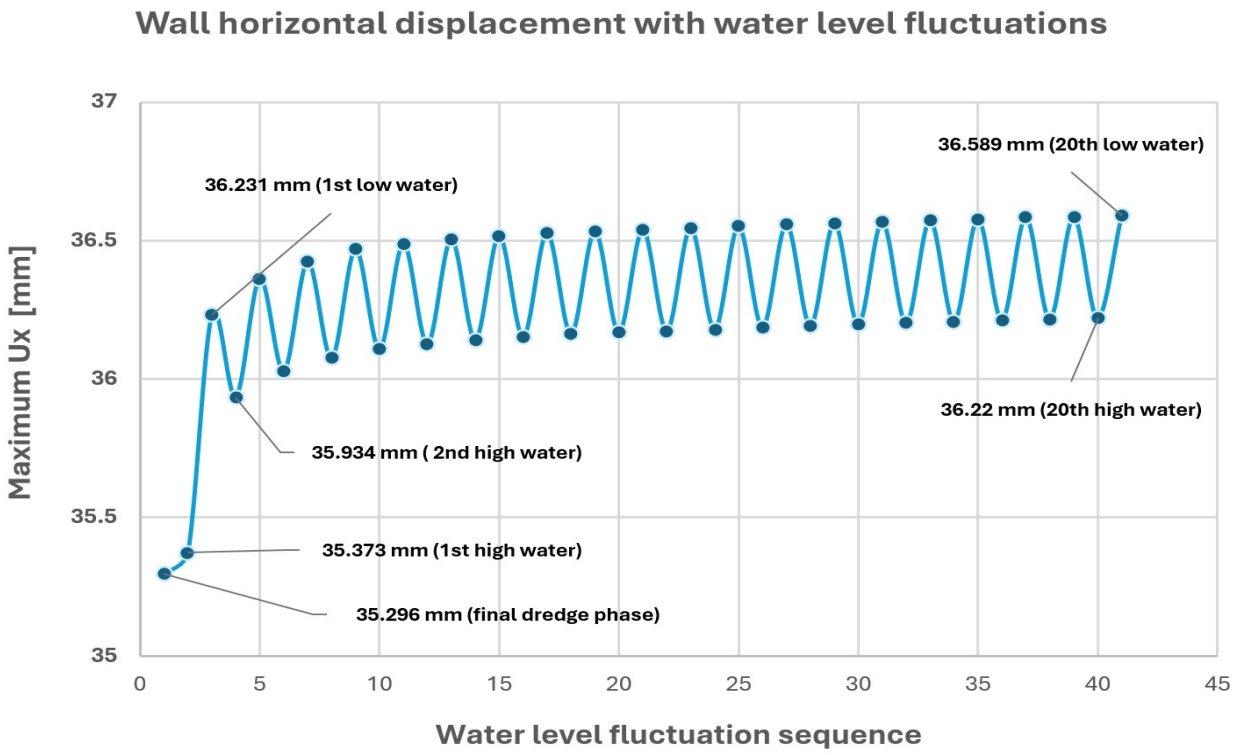

Figure 5.14: Effect of water level fluctuations on the horizontal displacement of combi-wall

The water level cyclic fluctuations did not affect the quay wall displacement significantly and hence cannot be attributed to the accumulation of displacement of the wall. There is only a slight difference in the wall displacement of less than 0.5 mm between the low water phases and high-water phases. The anchor forces also were not affected by the water level changes.

The reason for this could be that the difference between high and low water levels is not very significant. For a higher difference between the high and low water levels, larger difference in wall displacement can be expected as there will be a larger difference in the effective stress distribution in the soil. Another explanation for minimal impact of water level changes on the performance of the quay wall could be the high permeability of the soil behind the quay. Most of the soil profile is dominated by cohesionless highly permeable sands which do not allow excess pore pressure to build up in the soil due to cyclic fluctuations in the water levels.

5.4. Discussion

5.4.1. Cyclic Surcharge Loading

Due to application of surcharge with repeated unloading and reloading, irreversible strains develop in the soil along with reversible strains. The irreversible strains keep on accumulating and showing up as accumulated wall displacement when the loading is repeated. After the first load cycle, maximum accumulation of plastic strains occurs in the soil due to rearrangement of the soil structure into a denser structure. With further loading cycles, there is reduction in further densification of the soil and hence the rate of new plastic points generation and stress redistribution reduce per cycle. This leads to a lesser generation of plastic strains in the succeeding load applications compared to the first load application. However, the soil continues to accumulate plastic strains even if it's a very small fraction of the initial accumulation of strains. The final rate of plastic strain accumulation does not reach zero value, meaning, a minute increment in the wall displacement will keep happening over the lifespan of unloading and reloading the surcharge loads.

Both the wall displacement and anchor forces follow similar trends over long term with more significant increments per load cycle observed in the future scenario. The figures 5.15 and 5.16 present the Plaxis-2D output from various phases to exhibit the evolution of plastic points in the soil with repeated loading.

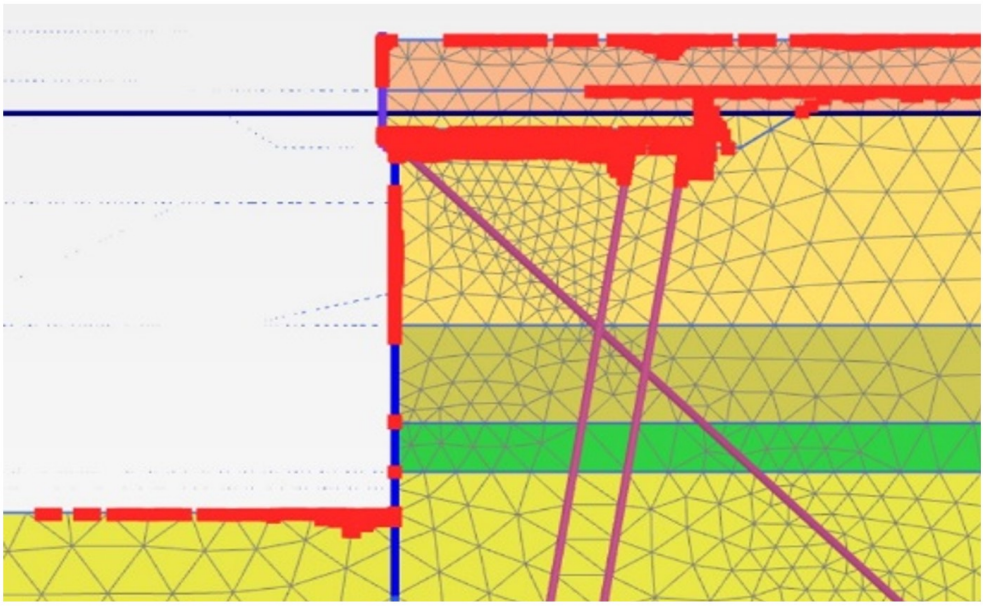

Figure 5.15: Plastic points (red) generated in the soil after final dredging phase

After the final dredging phase, the major load experienced by the quay wall is due to the active earth pressure generated behind the wall and the vertical load imposed by the sand backfill on top of the relieving platform. In the loading phases, the density of these plastic points increases progressively. In all the phases, the plastic points are generated mostly in the soil behind the top part of the wall which experiences maximum distribution of load. The figure 5.16 exhibits the plastic points generated in the soil with repeated loading in the current and future loading scenarios.

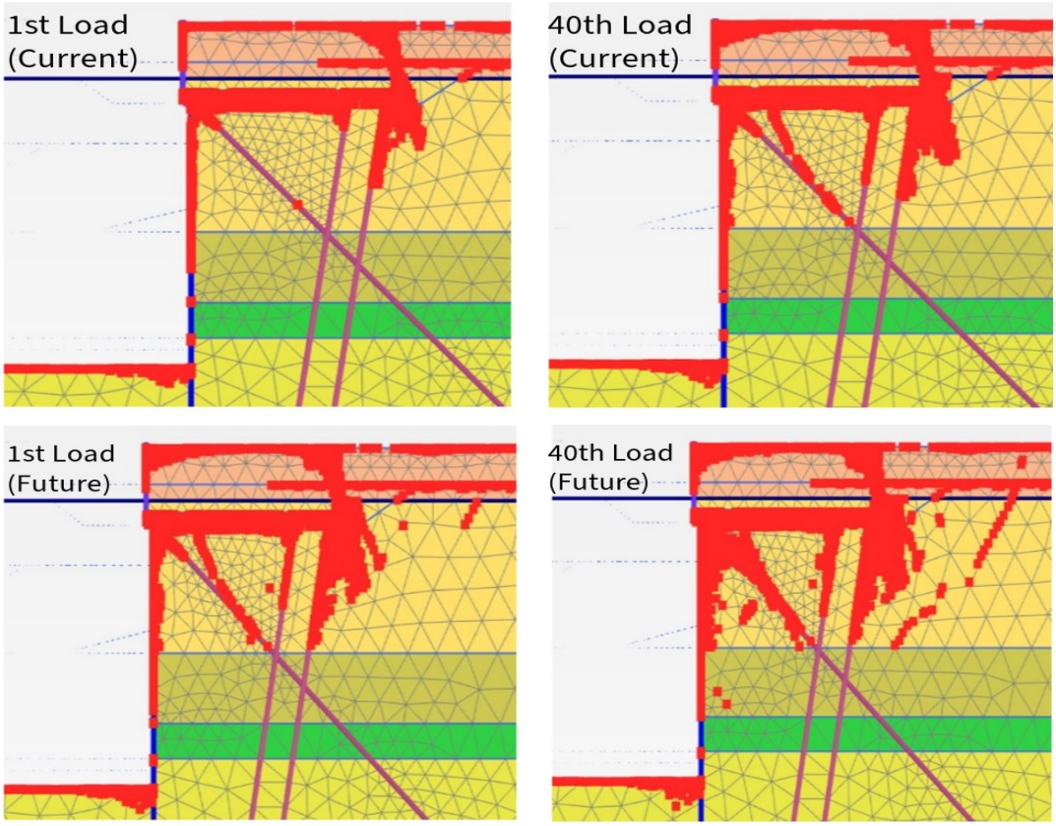

Figure 5.16: Evolution of plastic points in the soil behind the top part of the wall with load cycles in current and future loading scenarios

The evolution of plastic points is evident from the plaxis model. As the loading cycles proceed from current to future scenarios, the density of the plastic points increases significantly indicating accumulation of plastic strains in the soil. From the first load cycle in current scenario to the last loading cycle, new plastic points are generated around the combined wall and the pile trestle due to the progressively increasing relative displacement between the structural elements and the surrounding soil. In the future loading scenario also, the plastic point density increases progressively around the structural elements because of relative displacement between the structures and the surrounding soil. However, a progressive development of a shear band can also be observed in the active region of the soil as the plastic strains in the active region increases. These continuously developing plastic strains in the soil lead to accumulation of the horizontal displacement of the combi-wall with repeated loading and unloading of surcharge load.

Finally, with 40 load cycles in each loading scenario, the accumulation of wall displacement may not seem critical, but the accumulation in mobilisation of anchor forces and shaft friction, close to ultimate capacities, poses a serious concern for the stability of the quay wall under cyclic loading of surcharge over its lifespan.

Another possible factor in the accumulation of plastic strains in the soil due to cyclic loading of surcharge loads is the continuous development of excess pore pressure in the soil skeleton, which in turn would affect the stress state in the soil (De Gijt et al., 2011). As the frequency of loading is low, having considered a time period of around 30 days, as well as the soil profile being dominated by highly permeable non-cohesive soils, this effect is neglected in this study.

5.4.2. Cyclic Water Level Fluctuations

It was theoretically predicted that the changing water levels will influence the lateral earth pressure experienced by the wall and in turn the displacements in the wall. However, in the specific case of HTT quay wall, minimal impact of changing water levels on wall displacement was shown by Plaxis simulations. A minimal displacement difference of < 0.5 mm was observed between high water level phases and low water

level phases, and a negligible accumulation in the wall displacement with the 20 cycles of varying water levels. Anchor forces in the MV piles also showed no significant variation with changing water levels. The two main reasons to justify why the impact of changing water levels was negligible for wall displacements are presented below:

• **Scale of Water Level Variation:** The range of water level fluctuations was not large enough to generate significant changes in the soil effective stresses. The difference in water levels between high and low periods is merely 1.75 m. Although lower water levels did increase the effective stresses by reducing the pore water pressure, the increase in stress was not sufficient to cause sufficient plastic strains in the soil behind the wall or to affect the deformation behaviour of the stiff combined wall. Hence, no significant wall displacement or accumulation thereof was observed.

• **Sand Dominated Soil Profile:** Due to the predominance of highly permeable cohenshionless soils in the soil profile, all the excess pore pressure gets rapidly drained. This intantaneous dissipation of excess pore pressures prevents long term effects on the stress redistribution or strain accumlation in the soil. The findings in this regard also align with De Gijt et al. (2011) who noted that the cyclic loading of water loads on a quay wall in presence of freely draining soils has negligible impact on the accumulation of plastic strains in the soil, leading to negligble accumulation of wall displacements.

5.4.3. Comparing the impact of Cyclic Surcharge Loads and Cyclic Water Loads

The structural response of the quay wall turned out to be significantly different in the case of cyclic water loads, compared to the case of cyclic surcharge loading. To analyse the difference in the quay wall response to the two types of cyclic loads, 20 cycles from the current load scenario are compared with 20 cycles of water loads.

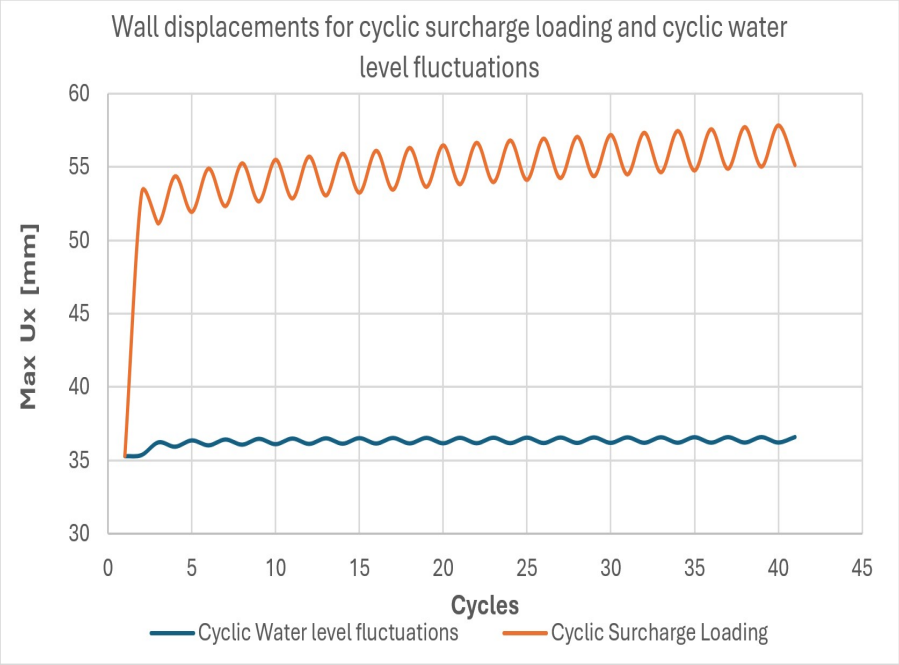

Figure 5.17: Comparison of wall displacement response for cyclic surcharge loading and cyclic water loading

As can be seen in figure 5.17, the cyclic surcharge loads cause significantly larger horizontal displacements compared to cyclic water loads. The wall displacements in the case of cyclic surcharge loads show a progressive trend, leading to accumulation of wall displacement.

Cyclic water loads due to water level fluctuations only lead to small oscillations in the wall displacement. No progressive displacement is observed in the case of cyclic water loads i.e. no accumulation of plastic strains

or continuous wall displacement is seen for this case. There is also no observable difference in the anchor forces mobilised in MV piles during high water or low water level, and no accumulation is observed in anchor forces.

The sensitivity of the quay wall to cyclic surcharge loads causes a concern for the long term analysis of the quay wall structural response to such loads. The cyclic water loads due to water level fluctuations do not exhibit any significant concern for long term deformation analysis of the wall in the case of HTT quay wall, mainly due to the small variations in the water level differences between high water and low water.

Chapter 6

Soil profile with Deep Clay Layer

The Netherlands has a deltaic geological nature, because of which deposits of soft cohesive soils are extensively present in the deep bearing sand layers (Gavin et al., 2019). These soft soil layers most often show up as thin lenses in the deep Pleistocene sand and have to ability to drastically affect the end bearing resistance in compression piles. It has been reported in numerous studies that these weak layers do not have a significant impact on the shaft resistance of piles loaded under tension or compression.

Such thin lenses of clay layers are also encountered at the HTT quay wall site and are present within the zone of influence of the compression piles. As discussed before, the influence zone is defined as the zone in which the properties of the soil have an influence on the pile end bearing capacity (Rica & Van Baars, 2018). The thin weak layers have little to no influence on the shaft resistance of these piles, but a major influence on the end bearing capacity (Chai et al., 2022; Imbrechts et al., 2017b; White & Bolton, 2005) . Hence, it is necessary to consider the effect of these subsurface weaknesses on the performance of the screw injection piles at the HTT quay wall and at any other quay wall in general.

This chapter begins with showing the evidence for the presence of weak clay lenses within the zone of influence of the SI piles located in zone B of the HTT quay wall. The method of simulating the effect of the weak layers on the pile end bearing resistance using Plaxis-2D is then explained, followed by the results of the simulations for various positions of the weak layers with respect to the pile tips. This chapter ends with the discussions on the results of simulations.

6.1. Presence of Deep Embedded Clay Layer in Pleistocene Sand

The design report by Imbrechts et al. (2017b) clearly points out the CPTs where the presence of deep weak layers in the Pleistocene sand is recorded, around the zone of influence of the bearing piles in zone B of the HTT quay wall. At the HTT quay wall project, the CPT's were carried out along three main axes, namely X1, X2 and X3. The axis X1 lies 25 meters from the quay wall on the passive side. X2 coincides with the quay wall and X3 lies 25 meters from the quay wall on the active side. The location of the bearing pile tips is between axes X2 and X3, and the thin clay layer lenses were recorded in the CPT's along axis X3 near zone B of the quay wall. The figure 6.1 presents the CPT's that recorded these clay layers in the Pleistocene sand layers, which acts as the bearing stratum for the SI piles. The location of these CPTs around the quay wall in zone B4 is shown in the figure 6.2.

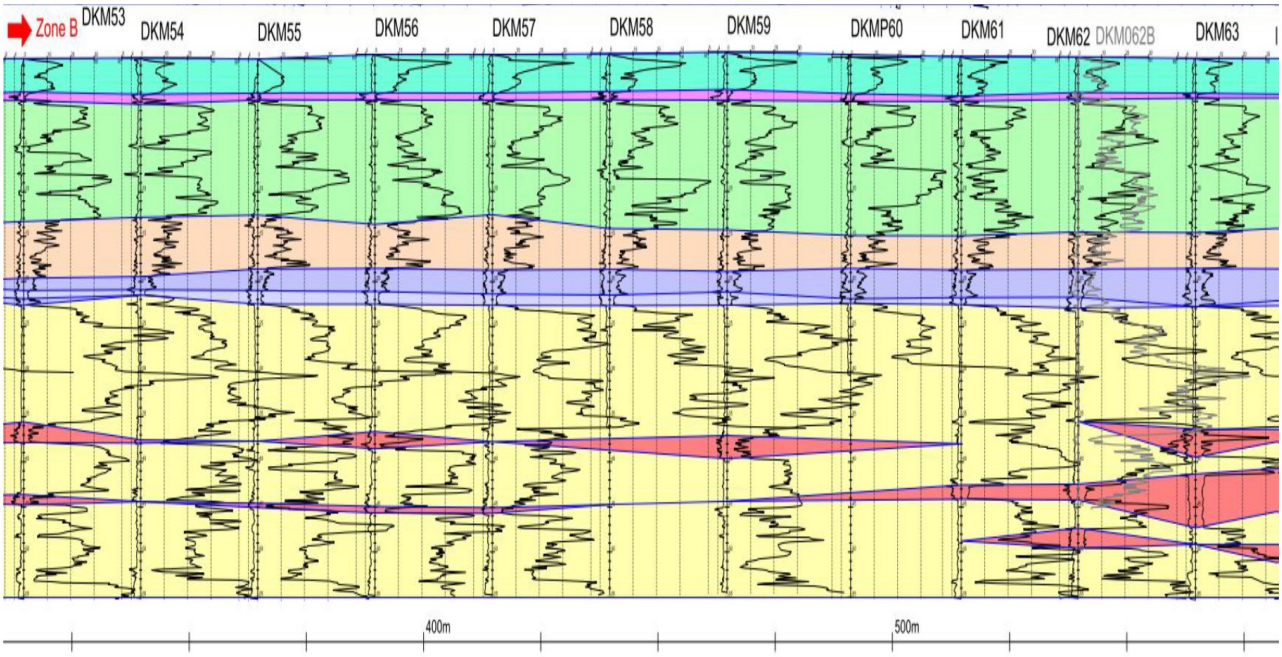

Figure 6.1: CPTs depicting presence of deep weak layers (red) in the Pleistocene sand (Imbrechts et al., 2017b)

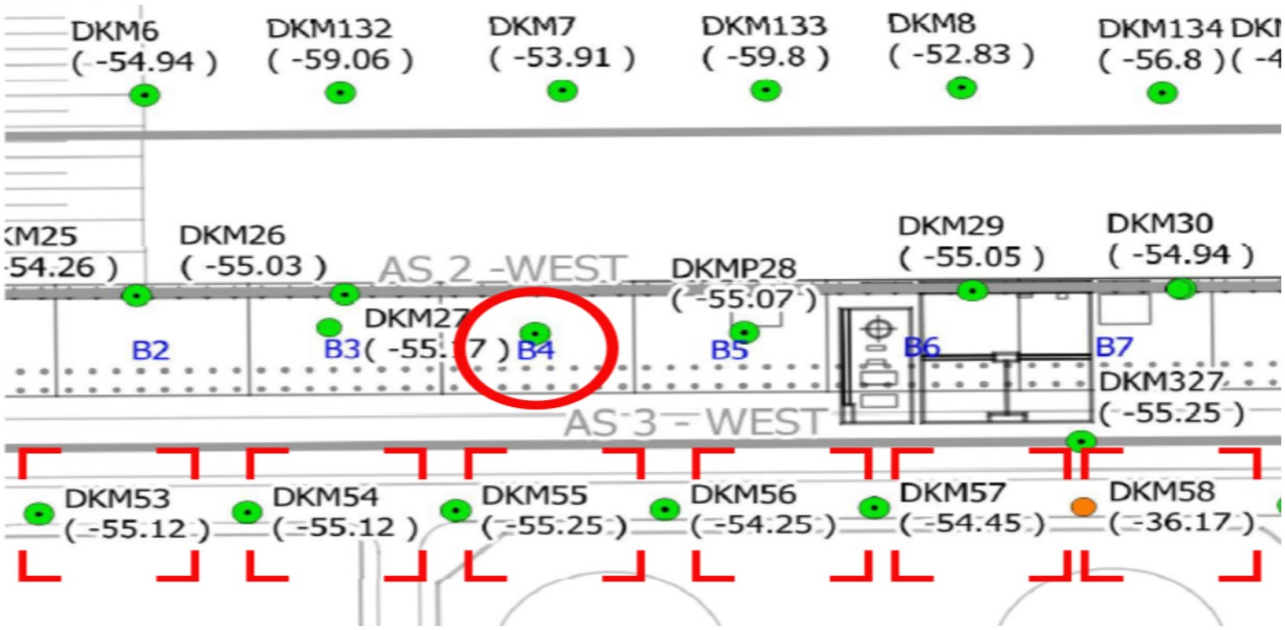

Figure 6.2: Locations of CPTs that recorded deep clay layers around zone B4 (Imbrechts et al., 2017b)

The CPTs presented above are from Axis 3 of the CPT group which lies 25 m away from the wall in the active zone. The clay layers are mostly present around -31 m NAP to -36 m NAP. The zone of influence of the bearing piles as per the Dutch Standard (Koppejan Method) extends to a depth of 4 times the pile equivalent diameter below the pile tip. The pile equivalent diameter is taken as 850 mm, due to the presence of grout around the whole of pile shaft (Duffy et al., 2024b). The pile tips are located at -33 m NAP. The zone of influence extends to -33 – 4*0.850 = -36.4 m NAP. The clay layers are shown to be present within -31 m to -36 m in the CPTs from geotechnical axis 3. There is also a clay layer present around -45 m NAP, but since it is beyond the zone of influence of the bearing piles, it is considered irrelevant in this study. To further support the claim that clay layers are present in the zone of influence of the bearing piles, figure 6.3 presents the CPT DKM53 which lies on geotechnical axis 3 around zone B4. This axis of CPTs is 25 m away from the quay wall in the landside (active) direction.

The CPT DKM53 shows a clay layer within the zone of influence of the pile tips of compression piles. It is clear from the CPT that this clay layer has an average q_c value the same as the Wijchen clay layer. Hence, the same soil parameters as the Wijchen clay layer are adopted to model this clay layer in Plaxis-2D.

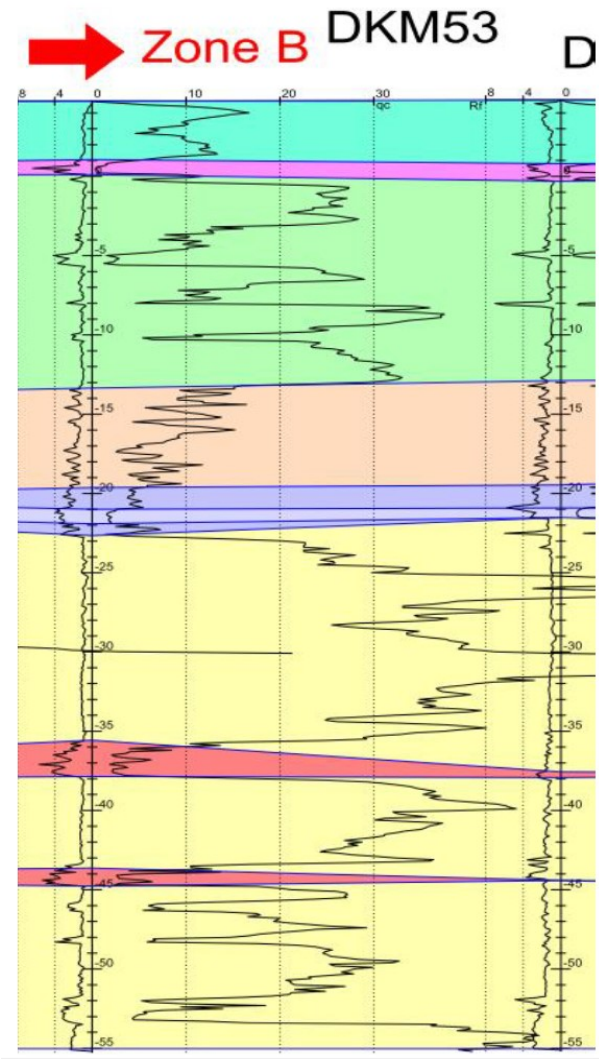

Figure 6.3: CPT DKM53 showing deeply embedded clay layer (red) in Pleistocene sand (Imbrechts et al., 2017b)

The design report by Imbrechts et al. (2017b) also states the possibility of presence of clay layers in geotechnical axis-2 which coincides with the quay wall at section B4, which could have been left undetected by the in-situ soil investigations. The grid of CPTs used for the soil survey of this project was 25 m * 25 m. The spatial extent of the deep weak layers was shown to be less than 25 m by Imbrechts et al. (2017b). Therefore, it is uncertain whether all the weak layers are recorded by the CPTs. Hence, the presence of clay layers in the zone of influence of pile tips makes it necessary for their influence to be analysed on the pile base resistance. In this thesis, the quantity, thickness and depth of weak clay layers will be assumed as it has been done in numerous studies before.

6.2. Method of Simulating Influence of Clay Layer on SI Piles

During a standard load test performed on a compression pile, the end bearing capacity of the pile is checked under 0.1D settlement criterion (Chai et al., 2022; Duffy et al., 2024b; Matic et al., 2019). Under the 0.1D settlement criterion, the pile is considered to have reached failure when the applied load results in the pile

base settlement equal to 10% of the pile equivalent diameter (D_{eq}). The equivalent diameter of the SI piles at HTT quay wall is 850mm (Duffy et al., 2024b; Imbrechts et al., 2017b), this leads to 0.1D displacement value of 85 mm. Under the working loads present at the HTT quay wall, reaching this displacement value of pile tips is not possible. Hence, to check the influence of the clay layer on the pile end bearing resistance, the analysis is carried out on the mobilised base resistance instead of ultimate base resistance.

The influence of clay layer on the base resistance of the SI piles is analysed by checking the reduction in the mobilised base resistance of the SI piles on application of Uniform Surface Load of $40kN/m^2$ on top of the relief floor. This is repeated for different locations of weak clay layer around the pile tip and then compared to the case where no clay layer is present. As per the revised Dutch method stated in the new Dutch standard (NEN 1997-1: EC 7, 2016), the zone of influence of the pile tip is considered from 4D below the pile tip to 8D above the pile tip. The pile tips are located at -33 m NAP and the zone of influence extends to -36.4 m NAP. The clay layers are situated around -31 m NAP to -36 m NAP.

Clay Layer Parameters	Value
γ_{unsat} [kN/m^3]	17.00
γ_{sat} [kN/m^3]	18.10
Φ'_p [°]	30.00
Ψ [°]	0
c' [kPa]	8.70
E_{oed}^{ref} [MPa]	2.80
E_{50}^{ref} [MPa]	2.20
E_{ur}^{ref} [MPa]	11.20
m [-]	1.00
G_0^{ref} [MPa]	33.90
$\gamma_{0.7}$ [-]	$7*10^{-4}$

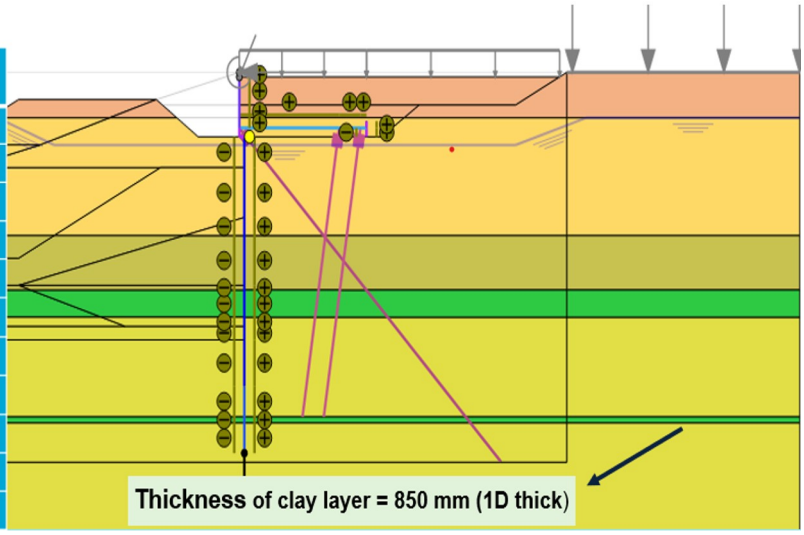

Figure 6.4: Representation of soil parameters for the deep clay layer along with the Plaxis model overview

The figure 6.4 presents the overview of how the clay layer is modeled around the tips of SI piles. It also presents the soil parameters adopted for the deep lying clay layer based on the parameters from Wijchen clay layer due to similar q_c value as can be seen in figure 6.3.

It must be noted that the research conducted to ascertain the zone of influence of axially loaded closed-ended piles, e.g. Chai et al. (2022), are based on either physical load tests or the numerical modeling of single independent axially loaded compression piles. In the case of HTT quay wall, the SI pile structure is more complex due to the connection of two SI piles with the relieving platform and the inclination of the piles which results in bending moments in the piles. This entails that the base resistance of these SI piles in presence of weak clay layer needs to be studied in more detail. For this reason, the influence of the clay layer has been studied on a much larger region starting from 10D below the pile tip to 10D above the pile tip under a load of $40kN/m^2$ on top of the relief floor.

The thickness of the clay layer around the pile tip is taken as one diameter thick, i.e., 850mm. This 850 mm thick clay layer is modeled at different depths around the pile tip as explained above. First, the influence of the clay layer presence is shown for the waterside (left) SI pile and then for the landside (right) SI pile. Later, the combined base resistance of the two piles is checked with respect to different locations of the clay layer.

The distance between the pile tip and the top of the clay layer is normalised with the pile diameter D. The normalised distance is taken as positive when the top of the clay layer is above the pile tip and negative in the inverse condition. The ultimate base capacity of compression piles is tested by loading the pile to failure, which is defined by 10% settlement criterion of the pile base. In the case of HTT quay wall, it was only possible to test the pile behaviour under working loads which the quay wall experiences during its operational phase. Hence, only the mobilised base capacity of the SI piles is analysed.

In plaxis-2D, the SI piles are modeled as embedded beam elements. The base resistance of a compression pile modeled as an embedded beam is directly shown in Plaxis output at the tip of the pile as the reaction

force opposing the axial force. The material properties and the structural model input properties of SI piles are the same as shown in section 4.3.

6.3. Influence of Clay layer on base resistance of SI Piles

The clay layers, 1D thick, are simulated in the vertical space range of -10D to +10D around the tips of the SI piles, D being the equivalent diameter equal to 850 mm. For each position of clay layer around the pile tip, along with the case with no clay layer in the deep sand, the operational load of $40kN/m^2$ is applied on top of the relief floor to mobilise the end bearing resistance of the SI piles. After more than 20 such simulations, the results of mobilised base resistances of both the waterside and landside SI piles are presented and compared with the case where no clay layer is present around the pile tips.

In the case of no clay layer present in the deep sand, the mobilised base resistance of the waterside SI pile is 1015 kN on application of uniform surface load of $40kN/m^2$, as shown in the figure 6.5. In the figure 6.5, the axial forces in the pile are largest at the top due to the load applied on the top. As the pile enters the Pleistocene sand, which is the bearing stratum, the skin friction generated in the deep sand causes the axial forces in the pile to gradually reduce as it is dissipated into the surrounding soil. Plaxis shows the mobilised base capacity of embedded beam elements at the tips of the elements as can be seen in figure 6.5.

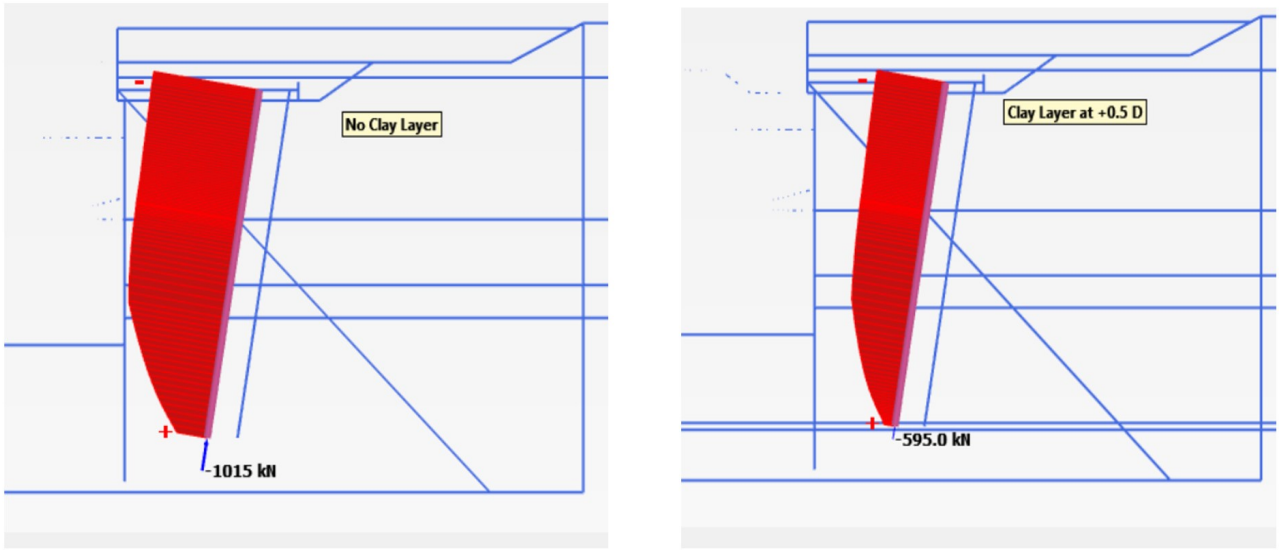

Figure 6.5: Plaxis model output showing axial forces in the waterside SI pile with no clay layer (left) and clay layer at +0.5D from pile tip (right)

The mobilised base resistance of the SI piles in absence of any clay layer is taken as reference value. The mobilised base resistances of these piles in presence of clay layers will be compared to the reference value to determine the reduction due to clay layer. The maximum reduction in the mobilised base resistance is observed when the tip of the pile is in the middle of the clay layer, i.e., at 0.5D. There is a 40% reduction in the mobilised base resistance, from 1015 kN with no clay layer to 595 kN with the clay layer at 0.5D, as shown in figure 6.6. Similar result is seen for the landside SI pile, where the mobilised base resistance in absence of clay layer is 775 kN and in presence of clay layer at 0.5D is 500 kN, which amounts to a 35% reduction. Figure 6.6 and figure 6.7 further elaborate on the results of simulations of a clay layer around the waterside and landside SI pile tips at various locations.

Figure 6.6 shows the influence of clay layer present at various positions around the tip of waterside SI Pile when the quay is loaded with surcharge of $40kN/m^2$ on top of the relief floor.

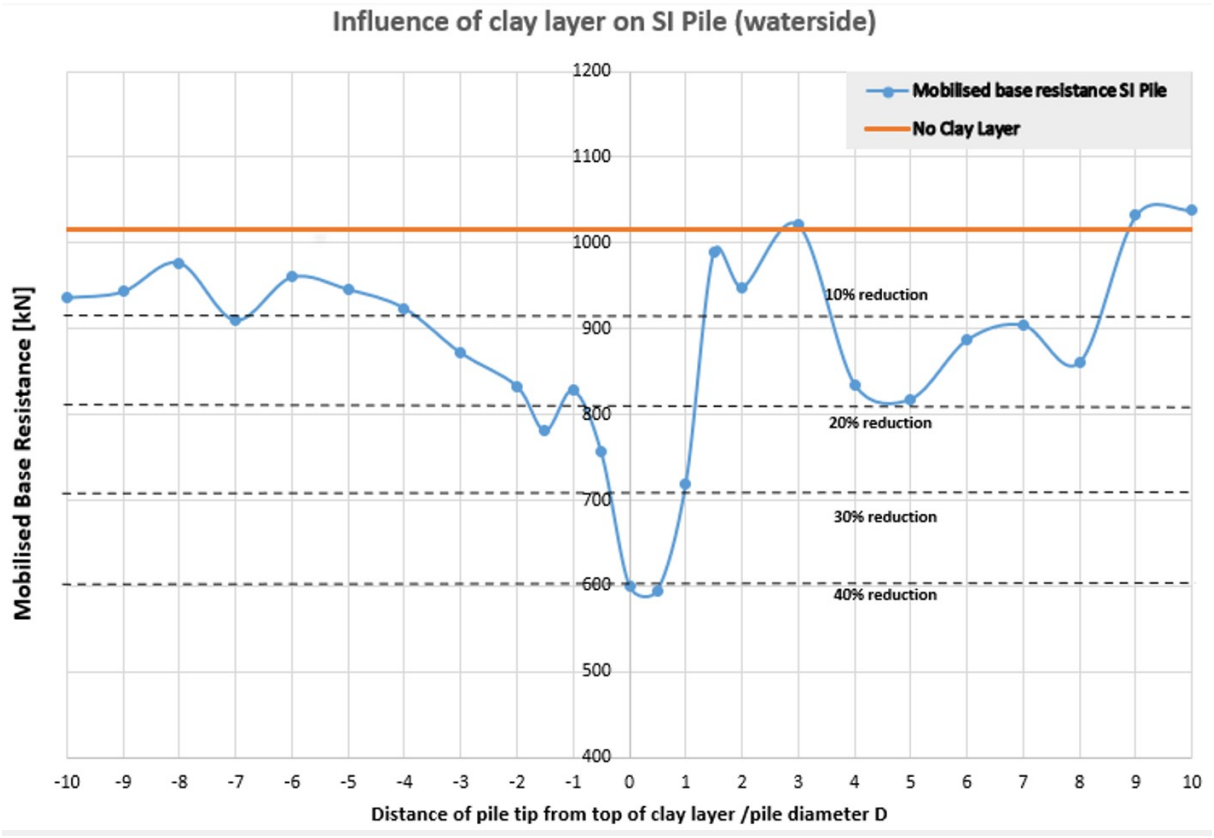

Figure 6.6: Influence of clay layer on the mobilised base resistance of the waterside SI pile

It is clear from the figure that the maximum reduction in the mobilised base resistance is observed when the pile tip is in the middle of the clay layer, i.e., when the top of clay layer is at the distance of 0.5D from the pile tip. A significant influence on the mobilised base capacity can be observed when the top of clay layer is within the range of +8D to -4D, as a minimum reduction of 10% is observed in the mobilised base capacity. The deviation from the trend outside the range of -6D to +8D can be attributed to the inaccuracies in the Plaxis calculations. There is also a possibility that the deeper simulated clay layer (-7D to -10D) might have interfered with the lower boundary of the Plaxis model which lies close to the modelled clay layers. Next, the results for the mobilised base capacity of the landside SI pile in presence of clay layer is discussed.

The figure 6.7 shows the mobilised base resistance of the landside SI pile when the clay layer is around the pile tip. Due to the load applied on the top of the relief floor, the mobilised base capacity of the landside SI pile in absence of clay layer is 775 kN, which will be taken as the reference value. In presence of clay layer around the pile tip, the influence on the mobilised base capacity is clearly seen. The maximum reduction in the mobilised base capacity is seen when the clay layer is at +0.5D from the pile tip, i.e., half of the clay layer is above and half below the pile tip. It also shows a slight increase when the clay layer is 3D and farther upwards from the pile tip. This increase is also validated by the research conducted by Chai et al. (2022) in which he showed a slight increase in the ultimate end bearing capacity when the clay layer was present above the pile tip. The curve follows a regular trend until -4D and shows irregularity below -4D distance from the pile tip. Plaxis calculation inaccuracies and the model boundary effects are probably the reasons for such irregularities in the output.

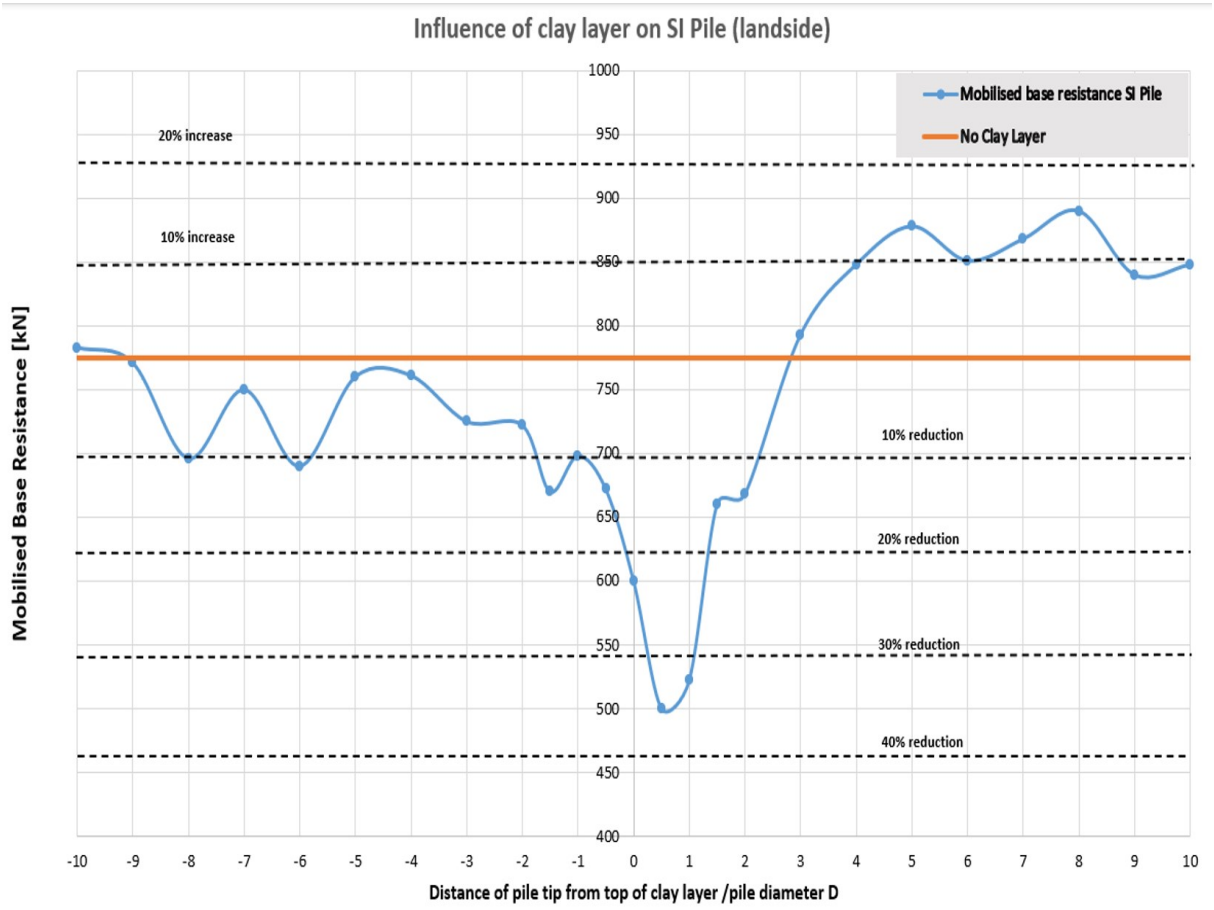

Figure 6.7: Influence of clay layer on the mobilised base resistance of the landside SI pile

Influence of clay layer on both SI piles combined

The inclination of the SI piles leads to oblique eccentric load application at the top of the piles, as the load axis does not coincide with the pile neutral axis. This leads to lateral stresses in the piles and generation of bending moment. This phenomenon together with the connection of these piles with the relieving platform bring complexities that are not considered in standard pile tests such as Duffy et al. (2024a), Duffy et al. (2024b) and Matic et al. (2019). Given the complexity of the quay wall structure in which the two SI piles are connected to each other at their heads through the relieving platform, it is necessary to consider the differences in the pile behaviour at the HTT quay wall and pile behaviour during standard load tests. Hence, it is more reasonable to check the effect of clay layers on the total system of SI piles instead of individual SI piles. To do that, the average base resistance of the two piles combined is studied in presence of the clay layers.

After analysing mobilised base capacities of both the piles, it is seen that in the absence of any clay layer around the pile tips, the average mobilised base capacity of the system is 895 kN. This is taken as the reference for comparisons with the cases where clay layers are present at various location around the pile tips. The maximum reduction in the average mobilised base capacities is observed in the case of clay layer at +0.5D from the pile tips. A reduction of around 38% is observed as the average mobilised base capacity drops from 895 kN to 547 kN.

The figure 6.8 shows the influence of clay layer on the average mobilised base resistance of both SI piles combined, compared to the case with no deep clay layer present.

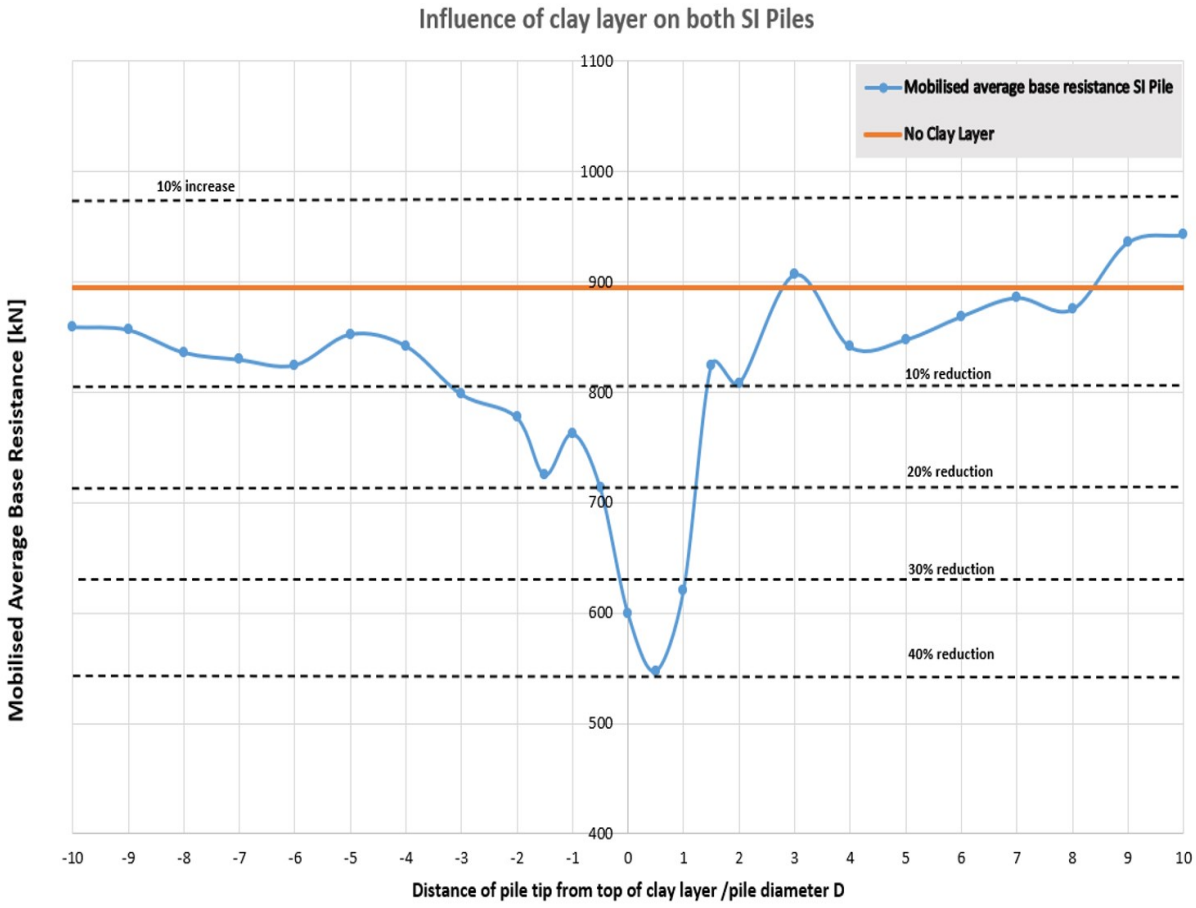

Figure 6.8: Influence of clay layer on the average mobilised base resistance of both SI piles

It is clear in the figure 6.8 that when the influence of clay layers is analysed on both SI piles combined as a system, the curve shows more regularity in trend both when the clay layer is below the pile tip as well as when it is above the pile tip, and can be compared to the reduction curve generated by Chai et al. (2022). The reduction in the mobilised base resistance for both piles is more regular in the interval -5D to +3D. The reduction in the base resistance is most significant in the interval -3D to +1.5 D where at least a 10% reduction in the average mobilised base capacity can be observed. The maximum reduction is observed when the pile tips are lying in the middle of the 1D thick clay layer, meaning, the top of the clay layer is at +0.5D from the pile tips.

It can be concluded that in the case of a quay wall with a relieving platform and a bearing and tension pile trestle with inclined pair of bearing piles, where the complete load bearing capacity is derived only from the deep bearing sand layers, the zone of influence of the pile tips is from -3D to +1.5D around the pile tips. The clay layer or any subsurface weakness has significant influence on the mobilised base capacity when present around the zone of influence of the pile tips. The maximum influence of the subsurface weakness is observed when the weak soil layer is at +0.5D from the pile tip.

6.4. Discussion

Due to the presence of a weak clay layer within the zone of influence of SI piles, a significant reduction in the mobilised base resistance is seen depending on the position of the clay layer around the pile tips. However, at the current working loads experienced by the quay wall, this reduction in the mobilised base resistance was not large enough to be translated to the displacements or bending moments generated in the combined wall. This is due to the mobilisation of greater skin friction in the bearing sand layer which accommodates the

higher load bearing requirement of the SI piles. As explained before in section 2.4, the total load bearing capacity of compression piles consists of the end bearing capacity at the base of the pile and the shaft friction capacity offered by the pile shaft in the bearing stratum. The ultimate shaft friction capacity using the Dutch CPT method was found to be 765 kN/m.

In the case of HTT quay wall under current operational loads and in the absence of subsurface weaknesses, the mobilised shaft friction capacity of the waterside SI pile on application of uniform surface load of $40kN/m^2$ on top of the relief floor is 209 kN/m. This amounts to 27% of the shaft friction capacity. When the clay layer is present in the closest proximity (+0.5D) to the pile base, the reduction in the mobilised base resistance leads to an increase in the mobilised shaft capacity to 381 kN/m, which amounts to an 80% increase in the mobilised shaft capacity compared to the case where no clay layer was present in the zone of influence of the SI piles. The total increase in the mobilised shaft capacity increased to 50% when the clay layer was at +0.5D from the pile tips.

Figure 6.9 illustrates the Plaxis output of waterside SI pile embedded beam element, presenting the comparison in the mobilised shaft capacity in absence of the clay layer and in presence of clay layer at 0.5D from the pile base.

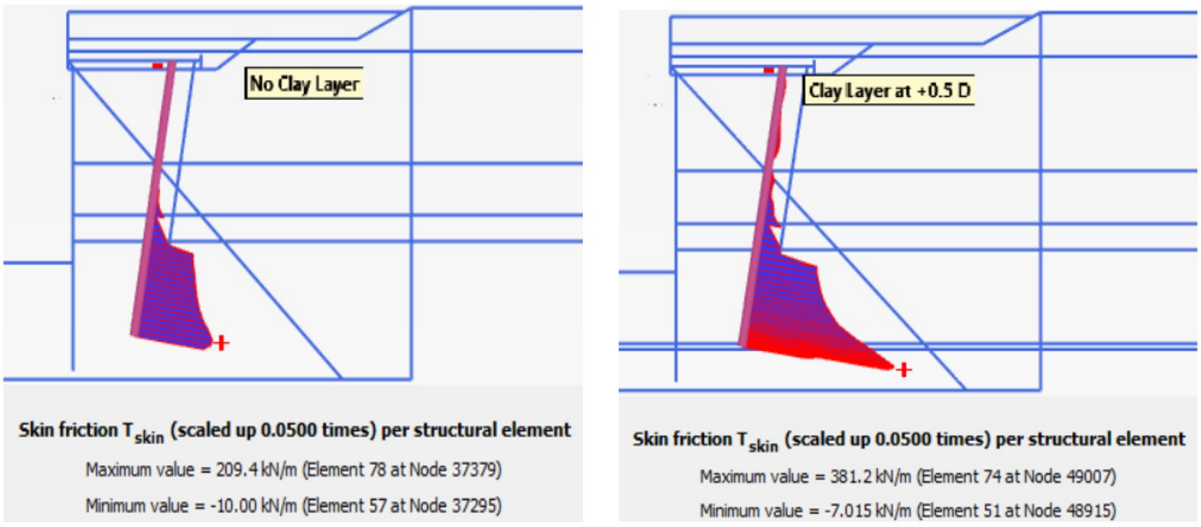

Figure 6.9: Skin fiction generated along SI piles for the case of no deep clay layer (left) and a clay layer at +0.5 D (right)

This increased mobilised shaft capacity is much closer to the ultimate shaft capacity and is equal to 50% of the ultimate shaft capacity. This drastic increase in the mobilised shaft capacity poses a serious concern for analysing the pile behaviour in presence of subsurface weaknesses.

It is important to point out some major differences between the SI piles at the HTT quay wall and the closed ended compression piles that have been either physically load tested e.g. Duffy et al. (2024a), Duffy et al. (2024b) and Matic et al. (2019) or tested with finite element simulations such as Chai et al. (2022).

Points of difference between available literature on pile behaviour and the SI piles at HTT quay wall

The most influential researches considered in this section of thesis are the reports on the load tests performed by Duffy et al. (2024a), Duffy et al. (2024b) and Matic et al. (2019) on the behaviour of SI piles at the Port of Rotterdam, along with the finite element software analysis on the behaviour of compression piles, such as ‘The influence of a thin weak clay layer on closed-ended piles in sand (Chai et al., 2022).’

- In the finite element analysis carried out by Chai et al. (2022) the ultimate base capacity of a closed ended pile in sand in presence of a deeply located clay layer was analysed. The conditions of the experiment were very controlled and ideal in terms of the soil profile, the geometry of the pile, pile behaviour at the base and the shaft, and the load applied at the pile head, etc. The whole soil profile consisted of a dense sand with an embedment of a clay layer in the vicinity of the pile tip as shown in

the figure 6.10 below. In the case of the SI piles at the HTT quay wall however, the soil profile is not a single layer of soil but multiple different layers.

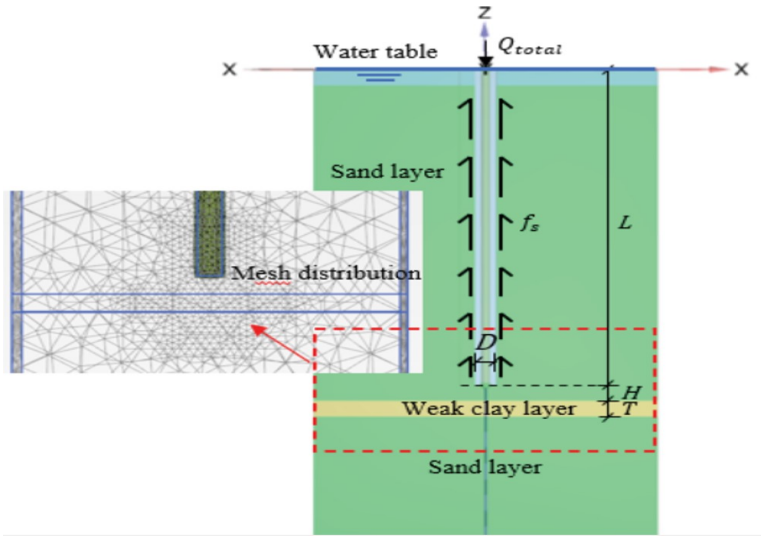

Figure 6.10: Overview of the Plaxis 3D model created to simulate pile load test in presence of weak soil layer (Chai et al., 2022)

- It is also worth noting that the shaft friction around the pile develops positively throughout the depth of the pile in the study carried out by Chai et al. (2022), whereas, in the case of SI piles at HTT quay wall, the positive shaft friction only develops in the deep Pleistocene sand layer as is also stated in the design report by Imbrechts et al. (2017b) and in the report of load tests on prefabricated concrete piles in a steel casing by Matic et al. (2019). The possible reasons for this are the negative skin friction generated in the clay layer above the deep sand layer and due to the influence of the active zone in the soil behind the retaining wall. Also, in the Plaxis 2D model of the HTT quay wall created for this thesis, the shaft friction along the SI piles only develops in the bearing sand layers as shown in the figure 6.9.
- Another major difference lies in the fact that the closed ended pile in the research mentioned above was a vertical independent pile loaded perfectly axially on the top to failure, which is 0.1D settlement of the pile base. Similar set-up of piles was also seen in the physical load tests performed by Duffy et al. (2024a), Duffy et al. (2024b) and Matic et al. (2019), as shown in figure 6.11. However, the SI piles in the HTT quay wall are connected to the relieving platform which distributes the loads to the two SI piles in an unequal manner and hence have a more complex structural response.

Figure 6.11: Load frame for pile load tests of 4 SI piles (Matic et al., 2019)

- The SI piles at the HTT quay wall are not vertically installed but at an inclination which leads to eccentricity of the load at the top. In the load tests performed by Duffy et al. (2024b) and Matic et al. (2019), the test piles were vertically installed and the loading on top of them was purely axial, as shown

in figure 6.11. In the case of the SI piles at the HTT quay wall, the load axis does not coincide with the neutral axis of the pile, but, has a lateral component also, which generates bending moments in the pile, especially a high head bending moment. Therefore, the vertical settlement of 0.1D is not the only failure mechanism to be considered. The lateral displacement along with the generated bending moments also play a role in the failure mechanisms.

Due to the loading limitations as per the actual loading scenario at the HTT site, it was not possible to check the ultimate base capacity of the piles (0.1D settlement criterion) but rather mobilised base resistance in the given working loads at the quay structure. Due to all the fundamental differences from the standard load tests, the zone of influence of the SI piles at the HTT quay wall could not be determined definitively for individual piles but had to be determined for both the piles together. The zone of influence in this study has been considered for the region around the pile tips where the clay layer presence has a significant impact on the end bearing resistance offered by the SI piles i.e., at least a 10% change in the mobilised base capacity. Hence, the zone of influence of the SI piles at the HTT quay wall, in presence of a weak clay layer, is -3D to +1.5D around the pile tips.

Chapter 7

Conclusions and Recommendations

7.1. Conclusions

This research studied the impact of cyclic loads, including cyclic operational surcharge loads and the cyclic water loads due to water level fluctuations, on the long-term behaviour of the deep-sea quay wall situated at zone B4 of the Hartel Tank Terminal in the Port of Rotterdam. Additionally, it analysed the impact of subsurface weaknesses on the end bearing resistance mobilised in the SI piles. The subsurface weaknesses were recorded during the site investigations in the form of clay layers deeply embedded in the bearing stratum.

This study used the finite element modeling software Plaxis-2D for analysing the quay wall behaviour under cyclic loading and in the presence of subsurface weaknesses. To analyse the quay wall behaviour under said conditions, an a priori finite element model of the quay wall was created. This model simulated the construction phases of the quay wall using data available in the design reports by Mariteam and the Port of Rotterdam such as Putteman et al. (2017) and Imbrechts et al. (2017a, 2017c, 2017b), and the site investigation data from third party testing such as Dijkstra (2016). The construction phases of the model were validated using the real time sensor data from the project site such as wall horizontal displacement readings from the inclinometers installed along the combined wall, and anchor force readings from the anchor sensors installed along the MV piles. After validating the a priori model, adjustments were made in the model to simulate the conditions of the cyclic loads and subsurface weaknesses. The following research question was then pursued,

”How do cyclic loading and subsurface weaknesses influence the structural performance of a deep-sea quay wall?”

The main research question was divided into two sub-questions:

1. **The impact of cyclic surcharge loads and cyclic water loads on the structural response of the quay wall.**
2. **The influence of deeply embedded clay layers on the base resistance of SI piles.**

The next section will summarize the two research sub-questions and the results that were obtained from each research sub-question. This chapter will end with some recommendations on the considerations necessary for design of future quay wall projects.

7.1.1. Impact of Cyclic Loads

The impact of cyclic loads was analysed for two cases, namely, cyclic surcharge loading and cyclic water loading due to water level fluctuations. In both these cases of cyclic loading, the deformation behaviour of the quay wall was analysed over a long-term period.

Cyclic Surcharge Loads

The operational loads applied as surcharge on the quay wall were analysed with a frequency of unload-reload of 30 days based on the data available from a similarly functioning quay wall at the Port of Rotterdam as stated in De Gijt et al. (2011). The surcharge load combinations were classified in two loading scenarios namely current loading scenario and the future loading scenario where the crane load is introduced on the quay wall, as reported in the design reports of the project. A total of 40 load cycles were simulated in each loading scenario.

The two major structural responses observed in the behaviour of the quay wall are the **accumulation of horizontal wall displacements** and **continuously increasing anchor forces** in the tension piles over long-term application of these cyclic loads.

Accumulation of horizontal wall displacement

The wall showed significant accumulation of wall displacements in both loading scenarios. In the current loading scenario, the total accumulation in horizontal wall displacement was 22.2 mm at a depth of 11 m along the combined wall. Following the last unload phase in the current scenario, the future scenario load cycles were simulated. The total accumulation in the displacement after 40 cycles of loading turned out to be 24 mm at the top of the front wall where the crane load and bollard load were applied.

The maximum allowed horizontal displacement of the wall is 1% of the retaining height, which amounts to 306 mm (Imbrechts et al., 2017a). The accumulation of 22 mm in the wall displacement during current scenario loading cycles took the overall wall displacement value to 20% of the maximum allowed displacement. The addition of 24 mm in the accumulation in wall displacement in the future scenario load cycles took the overall value of wall displacement to around 33% of the maximum allowed displacement.

In both the current and the future loading scenarios, the first load cycle led to maximum increments in the wall displacements. The first load cycle led to an accumulation of 12.7 mm in the current loading scenario and 15.8 mm in the future loading scenario. The rate of increments in successive cycles dropped exponentially to 0.1 mm per load cycle in the current scenario and 0.2 mm per load cycle in the future scenario, making future loading scenario more critical in the assessment of deformation behaviour of the quay wall.

As stated by De Gijt et al. (2011) and Tolba et al. (2020), on unloading the surcharge on top of the quay wall, the quay wall does not return to the original position, instead, irreversible deformations occur in the wall due to the plastic strains generated in the soil behind the wall. Each load cycle generates new plastic points in the soil and redistributes the stresses in the soil which leads to progressive accumulation of plastic strains in the soil and ultimately to accumulation of horizontal wall displacements. However, the rate of generation of new plastic points and the rate of redistribution of stresses in the soil decreases after initial load cycles due to densification in the soil fabric. This was also validated with the simulated load cycles in Plaxis, where the assessment of wall displacement output showed that the rate of increments in the wall displacements reduced exponentially after initial load cycles in both the current and future loading scenarios.

The observed correlation between the rate of accumulation of wall displacement and the progression of surcharge load cycles matches well with the analytical findings as reported by De Gijt et al. (2011). The cyclic loading of surcharge on the quay wall is a major factor in continuously developing horizontal wall displacements in the quay wall as shown by De Gijt et al. (2011) and Tolba et al. (2020).

Accumulation of anchor force

Similar observations were recorded for the anchor forces generated in the tension piles. The progressive

increase in the anchor forces with the load cycles coincided with the increase in wall displacements and followed the same trend as the accumulation in wall displacements. The maximum allowed anchor force value is 6399 kN (Imbrechts et al., 2017c). The shaft friction capacity of the MV pile is 554 kN/m near the toe of the pile and 244 kN/m at the top of the deep bearing sand layer. Like the horizontal wall displacements, maximum anchor forces in MV pile were also larger in the future loading scenario compared to the current scenario because of the additional horizontal load applied by the crane on top of the wall.

At the end of construction phases, the anchor force generated in the MV pile was 1111 kN, which was 17% of the design anchor capacity, along with 20% mobilisation of shaft capacity at the tip of anchor in Pleistocene sand. On first load cycle application from current scenario, 41% of design anchor force capacity was mobilised along with 47% mobilisation of shaft capacity at the pile tip. By the end of 40 load cycles in current scenario, 46% of anchor force capacity and 56% of shaft capacity were mobilised in the tension pile.

Due to additional horizontal load from the crane, the first load application from future scenario increased the mobilised anchor force to 62% of anchor capacity and the mobilised shaft capacity to 60% of shaft capacity. By the end of 40 load cycles, the anchor force was mobilised to 73% of its capacity and the shaft friction was mobilised to 64% of its capacity.

The rate of increment in the anchor forces per load cycle follow the same trend as the rate of increment in wall displacement per load cycle. The future scenario again turned out to be more critical in the structural analysis of the tension piles with around 700 kN anchor force being accumulated in the future scenario compared to 318 kN accumulation in current scenario.

Finally, with 40 load cycles in each loading scenario, the accumulation of wall displacement may not seem critical, but the accumulation in mobilisation of anchor forces and shaft friction, close to ultimate capacities, poses a serious concern for the stability of the quay wall under cyclic loading of surcharge over its lifespan.

Cyclic Water Loads

The fluctuating water levels recorded at the HTT quay wall were modeled as cyclic water loads to investigate the impact of changing stress levels in the soil on the deformation behaviour of the quay wall. The measurement data from the installed piezometer at the zone B4 of the HTT quay wall provided information on the fluctuating ground water levels, which also coincided with the fluctuating harbour water levels. A high groundwater level of +1.25 m NAP and a low groundwater level of -0.5 m NAP were simulated in alternate phases in the Plaxis model with 20 cycles.

No significant changes in the horizontal displacement of the combined wall were observed with changing ground water levels. There were also no changes in the anchor forces generated in the MV piles. The reason for this is the small scale of water level fluctuations along with the fact that most of the soil profile was dominated by highly permeable cohesionless soils which did not allow any excess pore pressure to build up in the soil behind the wall, and hence keeping the stress states in the soil nearly steady.

In the case where there is no difference in the water levels of the harbour (free water) and groundwater level, such as the HTT quay wall, the fluctuation in the global water level do not pose any serious concern for long-term assessment of stability of the quay wall.

7.1.2. Influence of Subsurface Weakness on SI Piles

The deltaic geological nature of The Netherlands has led to widespread deposits of cohesive soils in the Holocene sand and in the deep bearing Pleistocene sand layer. Such subsurface weaknesses were also recorded at the project site of the HTT quay wall in the form of thin clay lenses around the zone of influence of the bearing piles in the deep sand layer. These weak soil layers affect the end bearing resistance in the compression piles. A thin clay layer, one pile diameter thick, was modeled in Plaxis around the tips of the SI piles in a large vertical space range to ensure the correct site-specific zone of influence of the bearing piles. Due to load constraints, the ultimate base capacity of the SI piles could not be ascertained with the 0.1D settlement criterion. Instead, given the working loads on top of the quay structure, the mobilised base capacity of the SI piles was analysed in the presence of a deep clay layer in the bearing stratum.

After studying the individual piles for their behaviour in presence of deep clay layers, different zones of influences were recorded for each pile. Due to the complex structure and installation of the SI piles, it was deemed necessary to investigate the behaviour for both piles together as a system of piles.

A significant reduction, at least a 10% reduction, in the average mobilised base capacity of both SI piles was observed when the clay layer was present in the zone -3D to +1.5D around the SI pile tips, D being the pile diameter. The maximum reduction of 38% was observed when the tips of the piles were in the middle of the clay layer i.e., the top of the clay layer at +0.5D from the pile tips.

Given the small magnitude of loads on top of the quay structure, the effect of this reduction in mobilised base capacity was not translated to the deformation behaviour of the quay wall and neither to the generation of extra bending moments. However, the reduced end bearing resistance was compensated with an increase in the mobilised shaft capacity near the toe of the piles. The mobilised shaft capacity of waterside SI pile increased from 27% in absence of a clay layer to 50% in presence of the clay layer at +0.5D from the pile tip.

This drastic increase in the mobilised shaft capacity poses a serious concern for the stability of the pile system. In the case of presence of a thicker clay layer, or the presence of multiple clay layers around the pile tips, the mobilised shaft capacity could reach the failure point which would lead to plunging of the SI piles leading to large settlements of the relieving platform and possibly to larger bending moments generated in the combined wall.

7.2. Recommendations

Based on the observations made in this investigation, several recommendations are posed for the design of future quay walls and the future research related to the quay walls and their structural members.

7.2.1. Design Considerations for Cyclic Loading

Cyclic Surcharge Loads

Variable loads on the quay wall are generally considered during the planning and design phase with an extra partial safety factor as per different design approaches. However, the accumulating effects of cyclic loading of these operational loads, especially the ones with a very low frequency of up to a month, are neglected in most designs.

The cyclic surcharge loads proved to be quite critical in the long-term behaviour of quay walls, both in terms of the horizontal displacement of the combined wall and consequently in terms of the anchor forces generated in the tension piles. The phenomenon of accumulation of plastic strains in the soil that lead to continuous development of wall deformations needs to be included in the design.

Changes in the operational functionality of the quay walls may introduce critical loads which can severely affect the deformation behaviour of the wall, especially over a long-term cyclic loading of the new loads.

Cyclic Water Loads

Caution is required in the projects where there is a difference between the free water level and the ground water level due to presence of impermeable soil layers. The build up of excess pore pressure can lead to significant changes in the effective stress state of the soil and may result in larger changes in the deformation behaviour of the quay wall.

Continuous long-term monitoring of the water levels is required even in cases where the cohesionless soils

are dominant. In cases of large differences between the high tide and low tide water levels, the changes in the soil stresses can lead to more significant impact on the wall deformations.

7.2.2. Design Considerations for Subsurface Weaknesses

In the regions where weak soil layers are common to be present in the deep bearing strata, such as coastal regions along the North Sea, the resolution of the soil investigations should be improved, meaning, smaller grids of Cone Penetration Tests and Boreholes must be adopted in order to not miss out on the detection of smaller clay lenses deeply interbedded in the Pleistocene sand layers.

The design of the pile embedment length should account for possible reduction in the load bearing capacity due to the subsurface weaknesses. The position of pile tips must also be adjusted in a way that these weaknesses in the subsurface do not coincide with the zone of influence of these bearing piles.

In already existing projects where these local weaknesses are present in the bearing stratum, soil improvement techniques such as grouting can be adopted as a remedial measure.

7.2.3. Future Research

Most of the current finite element analyses on retaining wall projects are carried out with two-dimensional modelling software such as Plaxis-2D. A two-dimensional model makes the complex structures such as quay walls with relieving platforms easier to simulate. However, a three-dimensional FEM software will capture the intricate soil-structure interactions in more detail.

This study was focused on simplified assumptions for the frequency of cyclic loading of operational loads. More refined modelling needs to be carried out to assess the impact of irregularly unloaded and reloaded loads with varying magnitudes.

In projects where cohesive soil layers dominate the soil profile, time dependent calculations need to be carried out to account for consolidation and creep related deformations in the soil and in the combined wall.

Bibliography

Benz, T. (2007). *Small-strain stiffness of soils and its numerical consequences* (PhD Thesis). Institut für Geotechnik, University of Stuttgart.

Bolton, M. D. (1986). Strength and dilatancy of sands. *Geotechnique*, *36*(1), 65–78.

Brinkgreve, R. B. J. (2019). *Hardening soil model* (tech. rep.) [Reader CIE4361 Behaviour of Soils and Rocks]. Delft University of Technology.

Brinkgreve, R. B. J. (2019a). *Plaxis material models manual*. PLAXIS BV. Netherlands.

Brinkgreve, R. B. J. (2019c). *Plaxis reference manual*. PLAXIS BV. Netherlands.

Brinkgreve, R. B. J., Engin, E., & Engin, H. K. (2010). Validation of empirical formulas to derive model parameters for sands. In T. Benz & S. Nordal (Eds.), *Numerical methods in geotechnical engineering (numge 2010)* (pp. 137–142). CRC Press.

Bustamante, M., & Gianeselli, L. (1982). Pile bearing capacity prediction by means of static penetrometer cpt. *Proceedings of the Second European Symposium on Penetration Testing/ Amsterdam*.

Chai, F., Duffy, K., Gavin, K., & Tian, F.-B. (2022). The influence of a thin weak clay layer on closed-ended piles in sand. *Proceedings of the 8th International Symposium on Geotechnical Safety and Risk (ISGSR)*. https://doi.org/10.3850/978-981-18-5182-7_05-010-cd

CUR 166: Part-2. (2008). *Design of sheet piles-part 2* [Fifth edition]. CURNET. https://archief.briswarenhuis.nl/docs/cur/rapport166-deel2

CUR 2001-4. (2003). *Design rules for tension piles* [CUR Report 2001-4]. CURNET. https://www.briswarenhuis.nl/docs/cur/rapport2001-4/3

De Gijt, J., Grotegoed, D., & Van Heel, D. D. (2011). *Research into the causes of the measured displacements of a quay wall* (tech. rep.). Delft University of Technology and Engineering Department of Public Works of Rotterdam.

De Gijt, J., & Brassinga, H. E. (1990). Geotechnische aspecten van de zeekade en de bewerkingskade voor de euroterminal op de maasvlakte. *Polytechnisch Tijdschrift Civiele Techniek*.

De Gijt, J., & Broeken, M. (2013). *Handbook quay walls* (Second). CRC Press.

Dijkstra, A. (2016). *Geotechnisch onderzoek, project hartel tank terminal te rotterdam* (Technical Report). Wiertsema & Partners Raadgevend Ingenieurs.

Duffy, K., Gavin, K., Korff, M., & de Lange, D. (2024b). Base resistance of screw displacement piles in sand. *Journal of Geotechnical and Geoenvironmental Engineering*, *150*(8), 04024070. https://doi.org/10.1061/JGGEFK.GTENG-12340

Duffy, K., Gavin, K., Korff, M., de Lange, D., & Roubos, A. (2024a). Influence of installation method on the axial capacity of piles in very dense sand. *Journal of Geotechnical and Geoenvironmental Engineering*, *150*(6), 04024043. https://doi.org/10.1061/JGGEFK.GTENG-12026

Duncan, J. M., & Chang, C. Y. (1970). Nonlinear analysis of stress and strain in soil. *ASCE Journal of the Soil Mechanics and Foundations Division*, *96*, 1629–1653.

EAU 2004. (2005). *Recommendations of the committee for waterfront structures - harbours and waterways (eau 2004)* (8, revised). Ernst & Sohn.

Galema, A. (2013). *Shielding effect of piles on quay walls* (Master's thesis). Delft University of Technology.

Gavin, K., Cadogan, D., & Casey, P. (2009). Shaft capacity of continuous flight auger piles in sand. *Journal of Geotechnical and Geoenvironmental Engineering*, *135*(6), 790–798. https://doi.org/10.1061/(ASCE)GT.1943-5606.0000073

Gavin, K., Kovacevic, M. S., & Igoe, D. (2019). A review of cpt based axial pile design in the netherlands. *Underground Space*, *6*, 85–99. https://doi.org/10.1016/j.undsp.2019.09.002

Imbrechts, T., Putteman, J., Meersschaert, J., & Tuunter, L. (2017a). *Hhtt-dzk-rap-do-0301 hoofdberekening onderbouw zone b. design report* (tech. rep.) [HES Hartel Tank Terminal]. Mariteam.

Imbrechts, T., Putteman, J., Meersschaert, J., & Tuunter, L. (2017c). *Hhtt-dzk-rap-do-0302 draagvermogen mv-palen zone b. design report* (tech. rep.) [HES Hartel Tank Terminal]. Mariteam.

Imbrechts, T., Putteman, J., Meersschaert, J., & Tuunter, L. (2017b). *Hhtt-dzk-rap-do-0303 geotechnisch draagvermogen drukpalen zone b. design report* (tech. rep.) [HES Hartel Tank Terminal]. Mariteam.

Kondner, R. L. (1963). A hyperbolic stress-strain formulation for sands. *Proceedings of the 2nd Pan-American Conference on Soil Mechanics and Foundation Engineering (ICOSFE)*, *1*, 289–324.

Korff, M. (2018). *Deep excavations: Design, execution and monitoring of deep excavations with retaining walls*. Delft University of Technology.

Liao, T., & Mayne, P. W. (2007). Stratigraphic delineation by three-dimensional clustering of piezocone data. *Georisk: Assessment and Management of Risk for Engineered Systems and Geohazards*, *1*(2), 102–119. https://doi.org/10.1080/17499510701345175

Matic, I., de Nijs, R. E. P., De Vos, M., & Roubos, A. (2019). Full-scale load testing on long prefabricated concrete piles in the port of rotterdam. *Proceedings of the XVII ECSMGE-2019: Geotechnical Engineering Foundation of the Future*.

Mayne, P. W., & Kulhawy, F. H. (1990). *Manual on estimating soil properties for foundation design* (tech. rep. EL-6800) [Research Project 1493-6, Final Report. Prepared by Cornell University, Geotechnical Engineering Group]. Electric Power Research Institute.

Młynarek, Z., Gogolik, S., & Połtorak, J. (2012). The effect of varied stiffness of soil layers on interpretation of cptu penetration characteristics. *Archives of Civil and Mechanical Engineering*, *12*, 253–264. https://doi.org/10.1016/j.acme.2012.03.013

Murphy, G., Igoe, D., Doherty, P., & Gavin, K. G. (2018). 3d fem approach for laterally loaded monopile design. *Computers and Geotechnics*, *100*, 76–83. https://doi.org/10.1016/j.compgeo.2018.03.006

NEN 1997-1: EC 7. (2016). *Geotechnical design - Part 1: General rules* [Dutch implementation of EN 1997-1:2004+A1:2013+C1:2019]. Nederlands Normalisatie-instituut (NEN).

Obrzud, R. F., & Truty, A. (2018). *The hardening soil model – a practical guidebook* (Technical Report). Zace Services Ltd.

Putteman, J., Gootjes, G., & Tuunter, L. (2017). *Hhtt-dzk-rap-do-0001 uitgangspuntennota diepzeekade. design report* (tech. rep.) [HES Hartel Tank Terminal]. Mariteam.

Qiu, G., & Grabe, J. (2012). Active earth pressure shielding in quay wall construction: Numerical modelling. *Acta Geotechnica*, *7*, 343–355.

Rica, S., & Van Baars, S. (2018). The influence of a thin weak soil layer on the pile bearing capacity. *International Conference on Deep Foundations and Ground Improvement, Urbanization and Infrastructure Development: Future Challenges, DFI*, 308–317. http://hdl.handle.net/10993/36070

Robertson, P. K., & Cabal, K. L. (2010). Estimating soil unit weight from cpt. *Proceedings of the 2nd International Symposium on Cone Penetration Testing (CPT'10)*.

Schanz, T., Vermeer, P. A., & Bonnier, P. G. (1999). Formulation and verification of the hardening-soil model. *Beyond 2000 in Computational Geotechnics*.

Schmudderich, C., Shahrabi, M. M., Taiebat, M., & Lavasan, A. A. (2020). Strategies for numerical simulation of cast-in-place piles under axial loading. *Computers and Geotechnics*, *125*, 103656. https://doi.org/10.1016/j.compgeo.2020.103656

Schouten, O. (2020). *Optimising the functionality of smart quay walls using measurement data obtained during the construction process: A case study in the port of rotterdam: Hhtt-quay* (Master's thesis) [Master's thesis]. Delft University of Technology.

Spruit, R., Putteman, J., Broos, E. J., Brassinga, H. E., De Vos, M., & Timmermans, A. L. J. (2019). Mv tension pile load tests in the port of rotterdam: Practical aspects and geotechnical behaviour. *Proceedings of the XVII ECSMGE-2019: Geotechnical Engineering Foundation of the Future*. https://doi.org/10.32075/17ECSMGE-2019-0247

Tolba, E., Ellah, S., Galal, E. M., Ezzat Ahmed Sallam, E. A., & Kamal, M. A. (2020). Comparative analyses of quay wall case study using plaxis 3d. *International Journal of Applied Science and Research*, *3*.

van Paassen, B. P. H., & van Dalen, J. H. (2009). High load tests on vm-piles for the quay wall euromax. In M. H. et al. (Ed.), *Proceedings of the 17th international conference on soil mechanics and geotechnical engineering* (pp. 1143–1146). IOS Press. https://doi.org/10.3233/978-1-60750-031-5-1143

White, D. J., & Bolton, M. D. (2005). Comparing cpt and pile base resistance in sand [Paper 13342]. *Proceedings of the Institution of Civil Engineers - Geotechnical Engineering*, *158*(GE1), 3–14. https://doi.org/10.1680/geng.2005.158.1.3

Xu, X., & Lehane, B. M. (2008). Pile and penetrometer end bearing resistance in two-layered soil profiles. *Géotechnique*, *58*(3), 187–197.

Yang, J. (2006). Influence zone for end bearing of piles in sand. *Journal of Geotechnical and Geoenvironmental Engineering*, *132*(9), 1229–1235. https://doi.org/10.1061/(ASCE)1090-0241(2006)132:9(1229)

Chapter A

Drawing of Section B4

The cross-sectional drawing of section B4, with a relief floor, is presented.

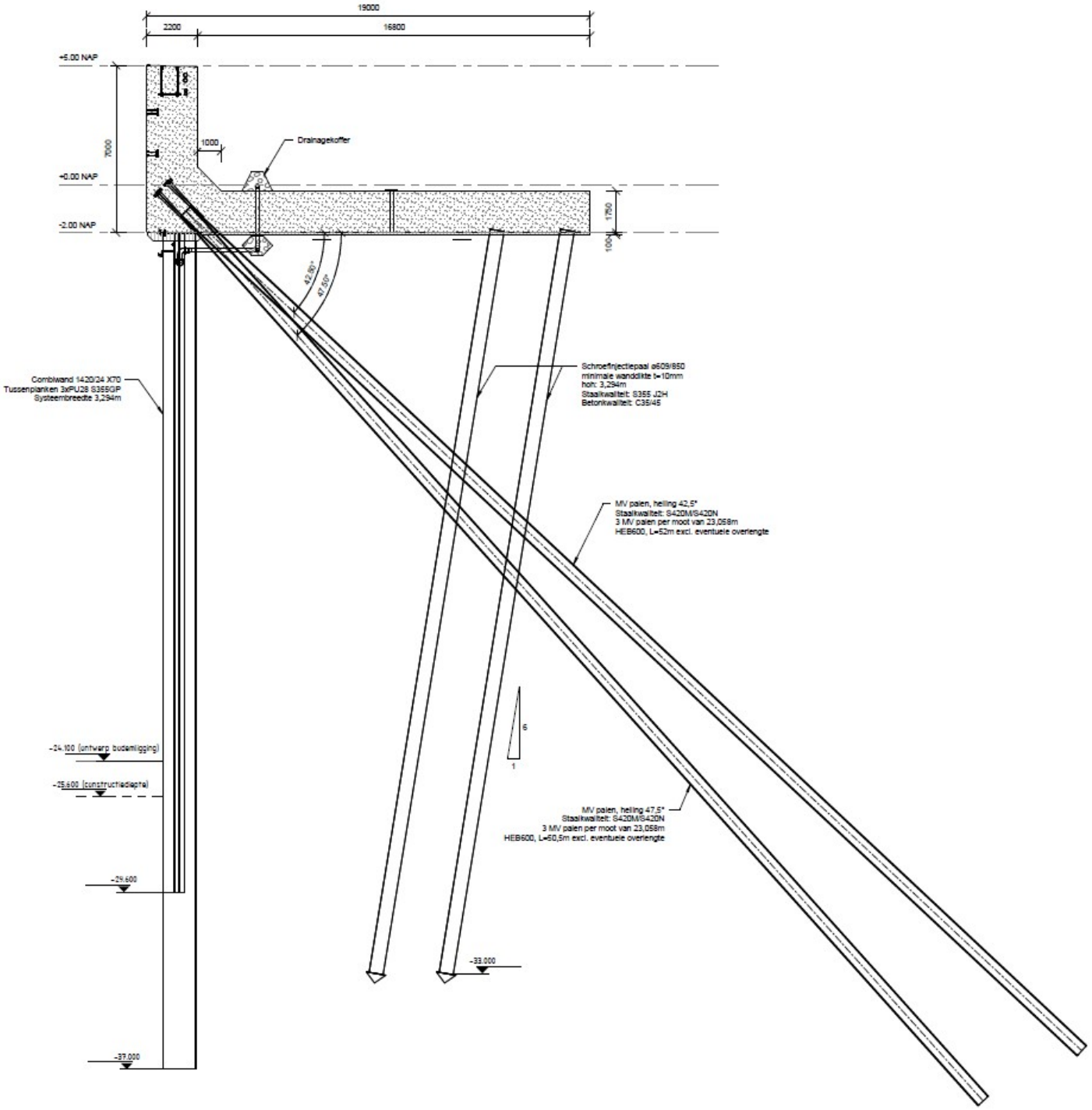
19000
2200
16800
+5.00 NAP
7000
1000
Drainagekoffer
+0.00 NAP
-2.00 NAP
1750
1000
42,50°
47,50°
Combiwand 1420/24 X70
Tussenplanken 3xPU28 S355GP
Systeembreedte 3,294m
Schroefinjectiepaal ø609/850
minimale wanddikte t=10mm
hart: 3,294m
Staalkwaliteit: S355 J2H
Betonkwaliteit: C35/45
MV palen, helling 42,5°
Staalkwaliteit: S420M/S420N
3 MV palen per moot van 23,058m
HEB600, L=52m excl. eventuele overlengte
6
1
-24.100 (ontwerp bodemligging)
-25.600 (constructiediepte)
-29.600
-33.000
MV palen, helling 47,5°
Staalkwaliteit: S420M/S420N
3 MV palen per moot van 23,058m
HEB600, L=50,5m excl. eventuele overlengte
-37.000

Chapter B

Cone Penetration Test Data

B.1. CPTs used for soil parameter determination

CPT DKM132 from axis-1 on the passive side of the wall

CPT DKM032B from axis-2 coinciding with the wall axis

CPT DKM327 from axis-3 on the active side of the wall

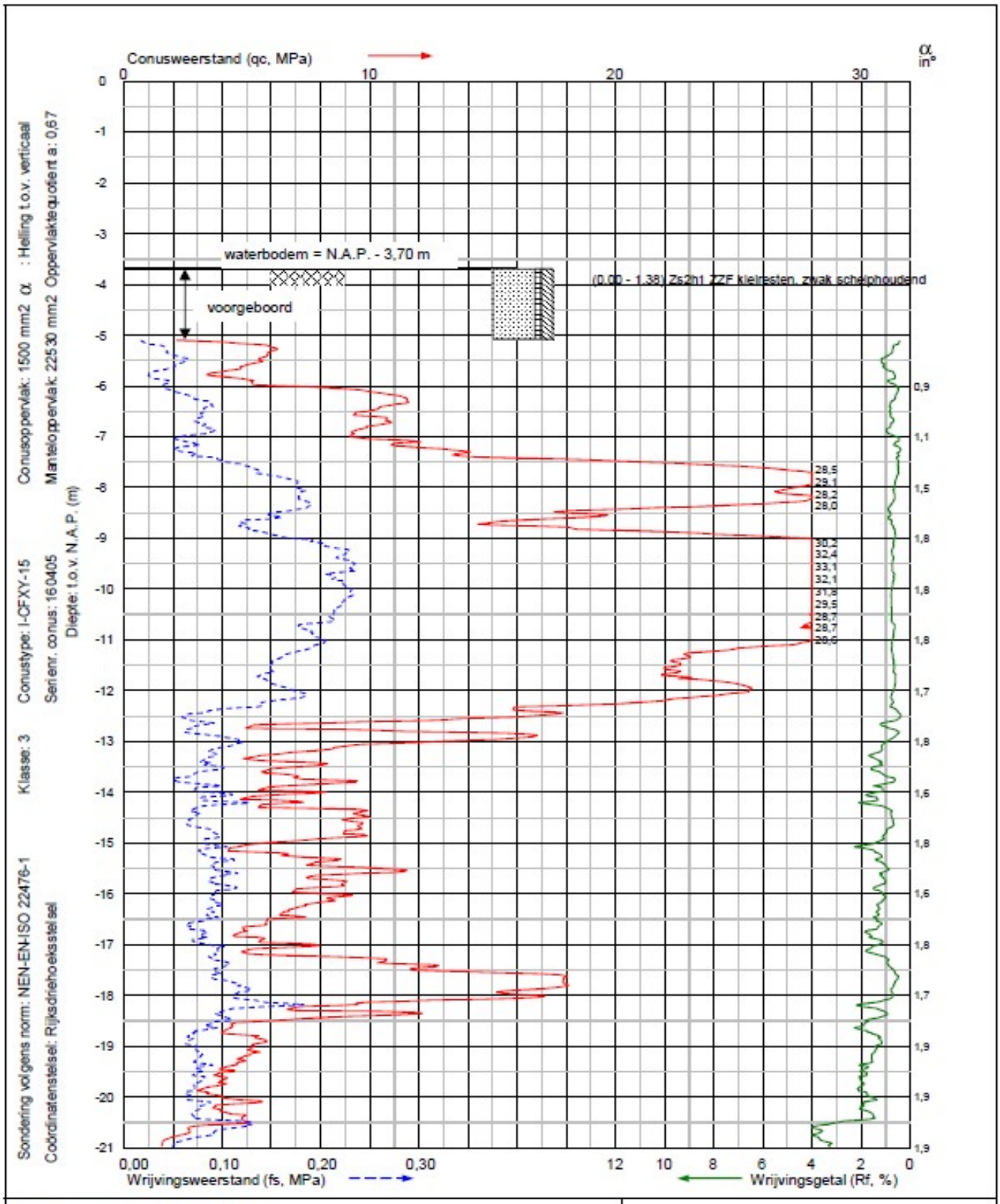

Project: Project Hartel Tank Terminal
Projectplaats: Rotterdam

Sondering: DKM132

Wiertsema & Partners
RAADGEVEND INGENIEURS

X = 63.937
Y = 439.476

Opdrachtnr.: VN-66080-1

Blad: 1 van 3

Datum: 14-11-2016

AKKOORD UITV

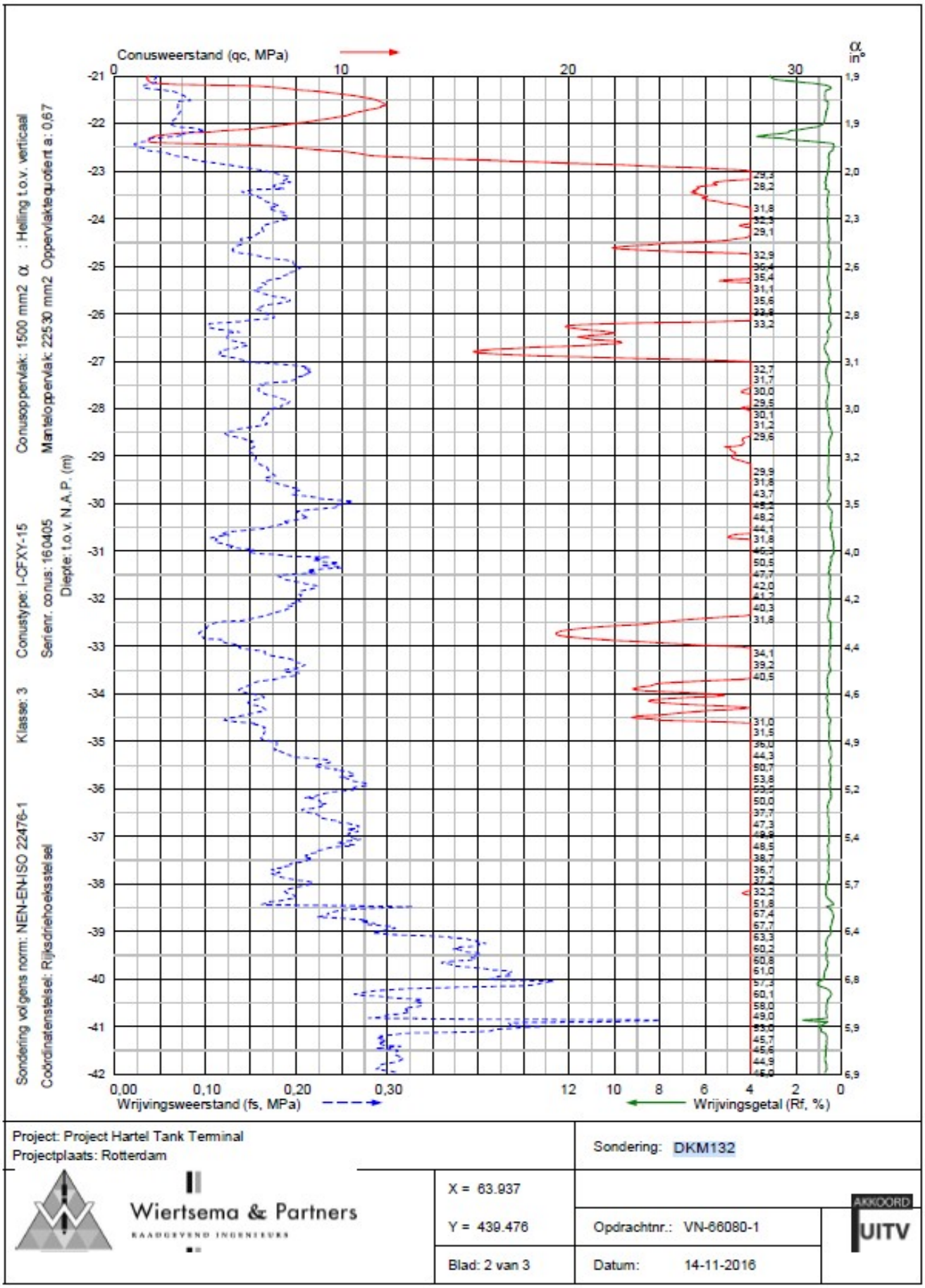
Conusweerstand (qc, MPa)
α in°
Wrijvingsweerstand (fs, MPa)
Wrijvingsgetal (Rf, %)
Sondering volgens norm: NEN-EN-ISO 22476-1
Klasse: 3
Conustype: I-CFXY-15
Serienr. conus: 160405
Coördinatenstelsel: Rijksdriehoeksstelsel
Diepte: t.o.v. N.A.P. (m)
Conusoppervlak: 1500 mm2
Mantelopervlak: 22530 mm2
α : Helling t.o.v. verticaal
Oppervlaktequotient a: 0,67
Project: Project Hartel Tank Terminal
Projectplaats: Rotterdam
Sondering: DKM132
Wiertsema & Partners
X = 63.937
Y = 439.476
Blad: 2 van 3
Opdrachtnr.: VN-66080-1
Datum: 14-11-2016
AKKOORD
UITV

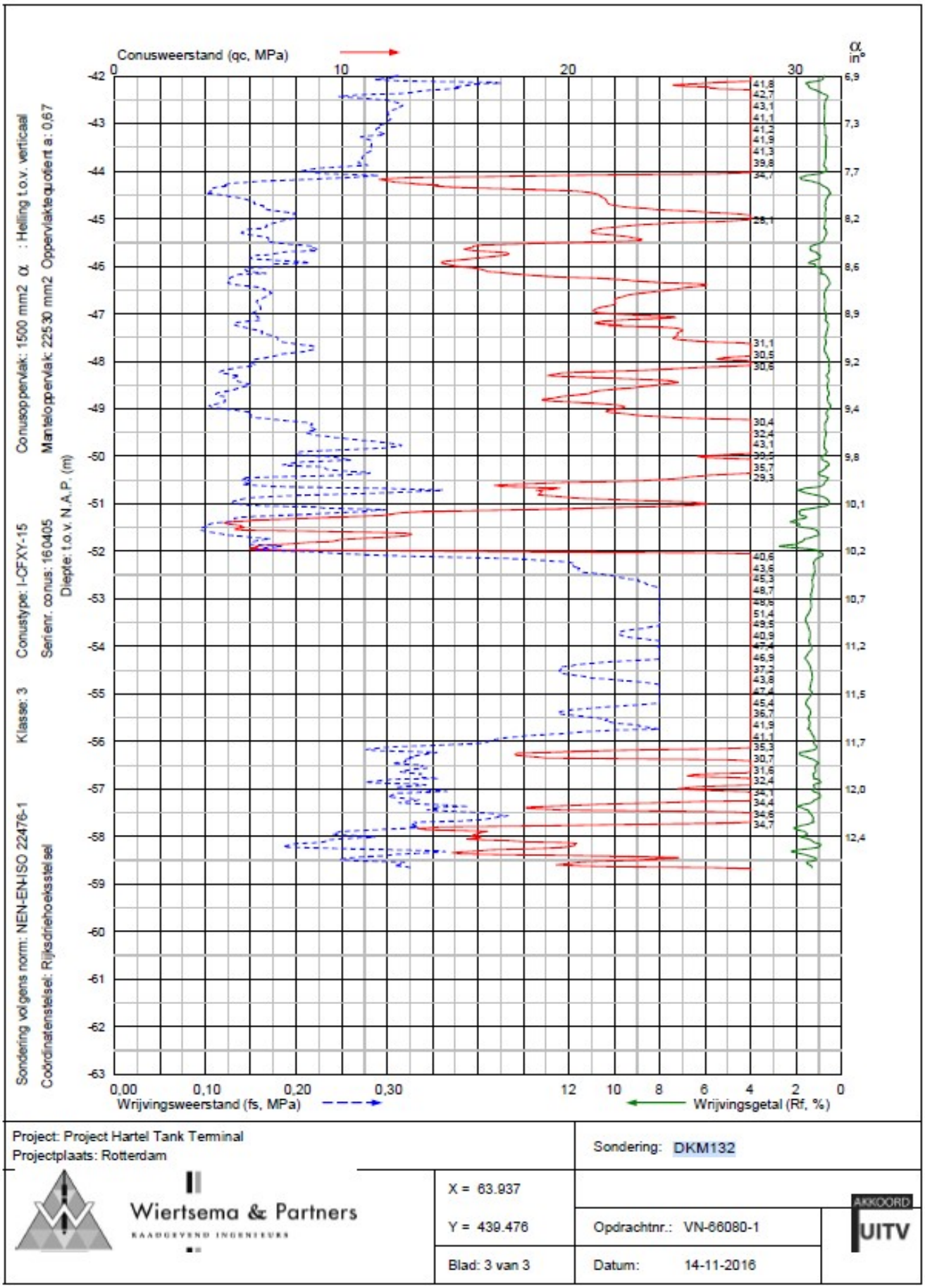
Conusweerstand (qc, MPa)
α in°
Conusoppervlak: 1500 mm2 α : Helling t.o.v. verticaal
Manteloppervlak: 22530 mm2 Oppervlaktequotient a: 0,67
Conustype: I-CFXY-15
Serienr. conus: 160405
Diepte: t.o.v. N.A.P. (m)
Klasse: 3
Sondering volgens norm: NEN-EN-ISO 22476-1
Coördinatenstelsel: Rijksdriehoeksstelsel
Wrijvingsweerstand (fs, MPa)
Wrijvingsgetal (Rf, %)
Project: Project Hartel Tank Terminal
Projectplaats: Rotterdam
Sondering: DKM132
Wiertsema & Partners
RAADGEVEND INGENIEURS
X = 63.937
Y = 439.476
Blad: 3 van 3
Opdrachtnr.: VN-66080-1
Datum: 14-11-2016
AKKOORD
UITV

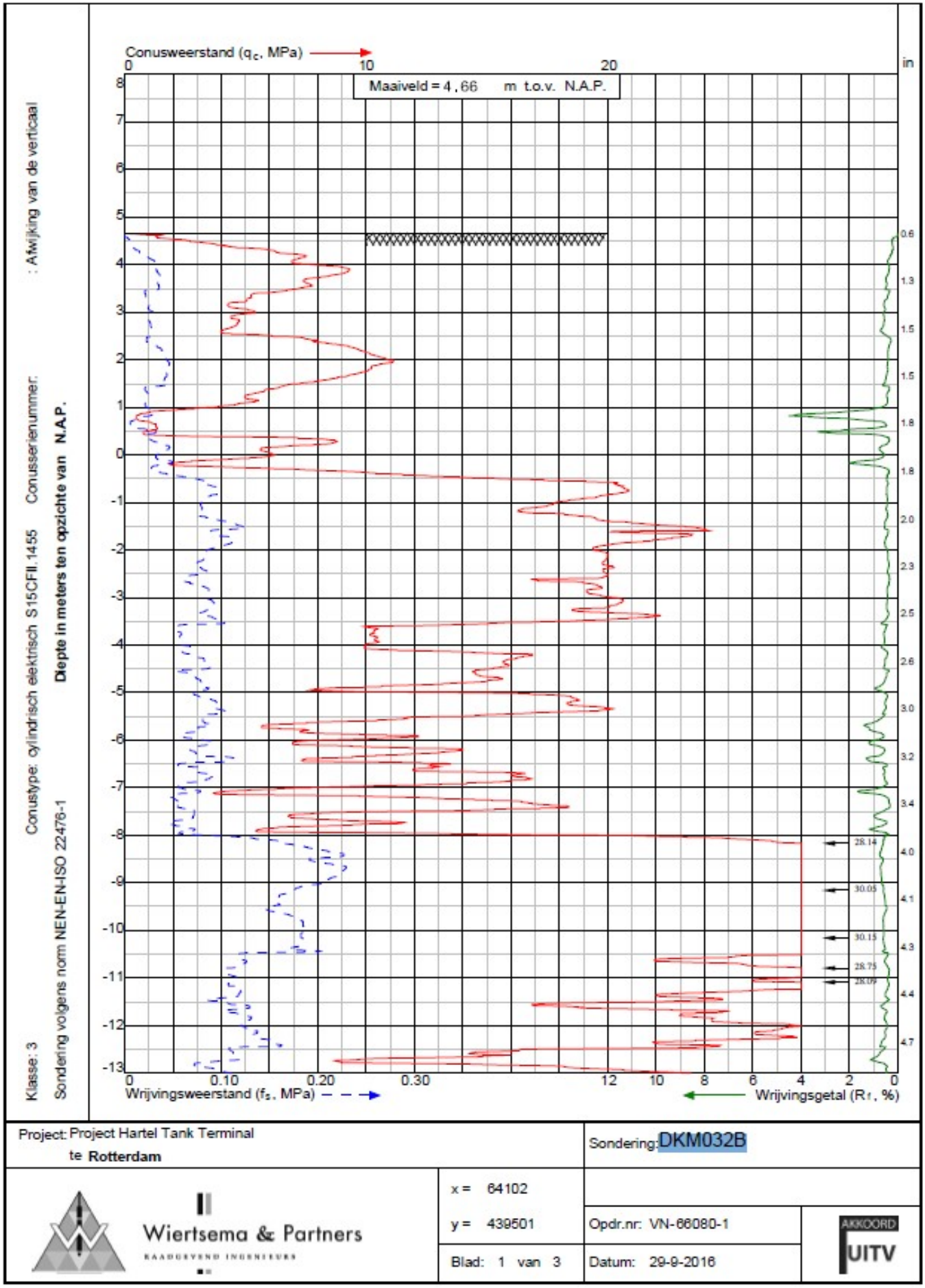
Conusweerstand (q_c, MPa)
0
10
20
in
Maaiveld = 4,66 m t.o.v. N.A.P.
Conustype: cylindrisch elektrisch S15CFII.1455 Conusserienummer: : Afwijking van de verticaal
Sondering volgens norm NEN-EN-ISO 22476-1 Diepte in meters ten opzichte van N.A.P.
Klasse: 3
28.14
30.05
30.15
28.75
28.09
0
0.10
0.20
0.30
Wrijvingsweerstand (f_s, MPa)
12
10
8
6
4
2
0
Wrijvingsgetal (R_f, %)
Project: Project Hartel Tank Terminal
te Rotterdam
Sondering: DKM032B
Wiertsema & Partners
RAADGEVEND INGENIEURS
x = 64102
y = 439501
Opdr.nr: VN-66080-1
Blad: 1 van 3
Datum: 29-9-2016
AKKOORD
UITV

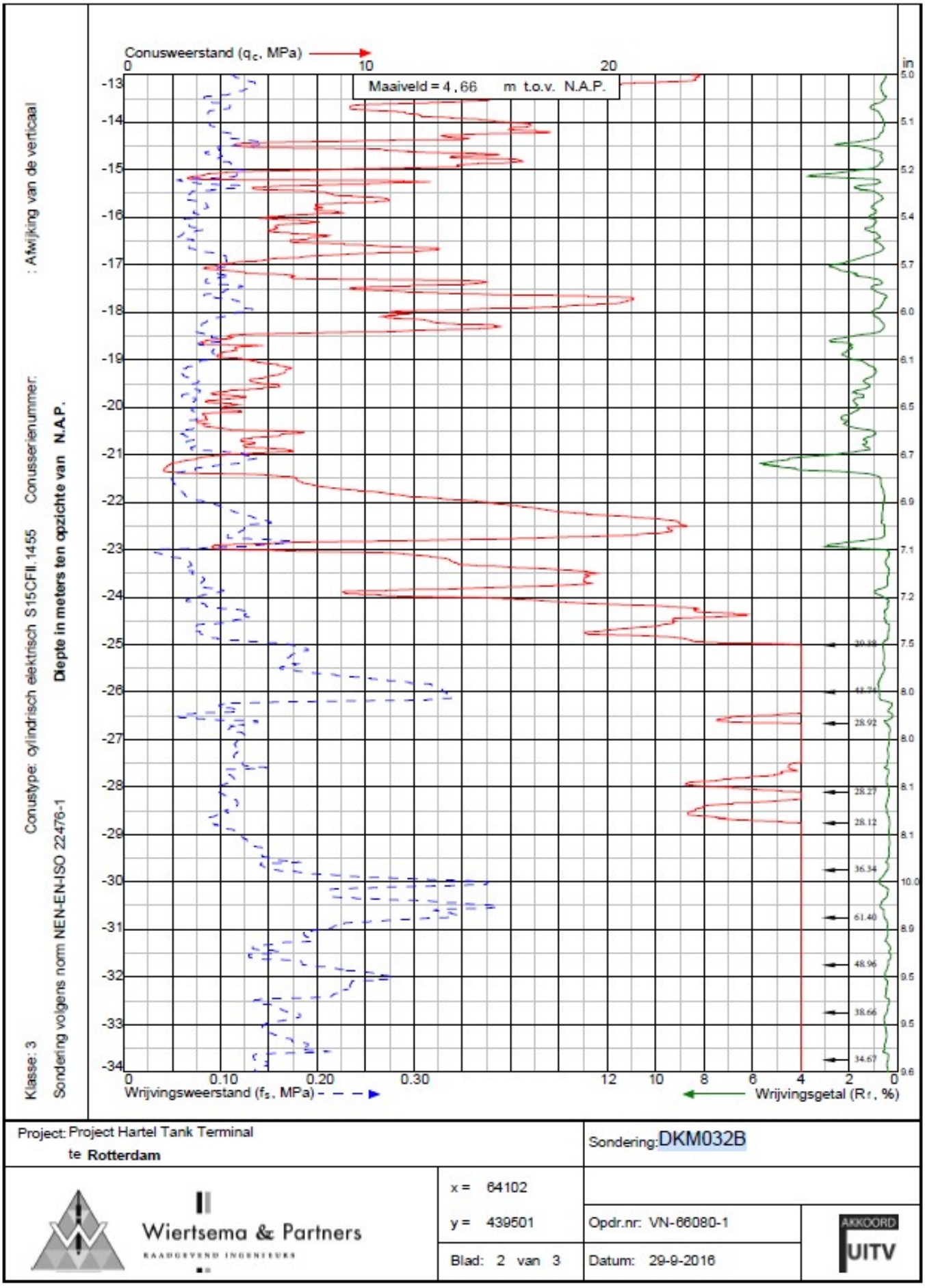

Project: Project Hartel Tank Terminal te Rotterdam		Sondering: DKM032B
Wiertsema & Partners RAADGEVEND INGENIEURS	x = 64102 y = 439501	Opdr.nr: VN-66080-1
	Blad: 2 van 3	Datum: 29-9-2016
		AKKOORD UITV

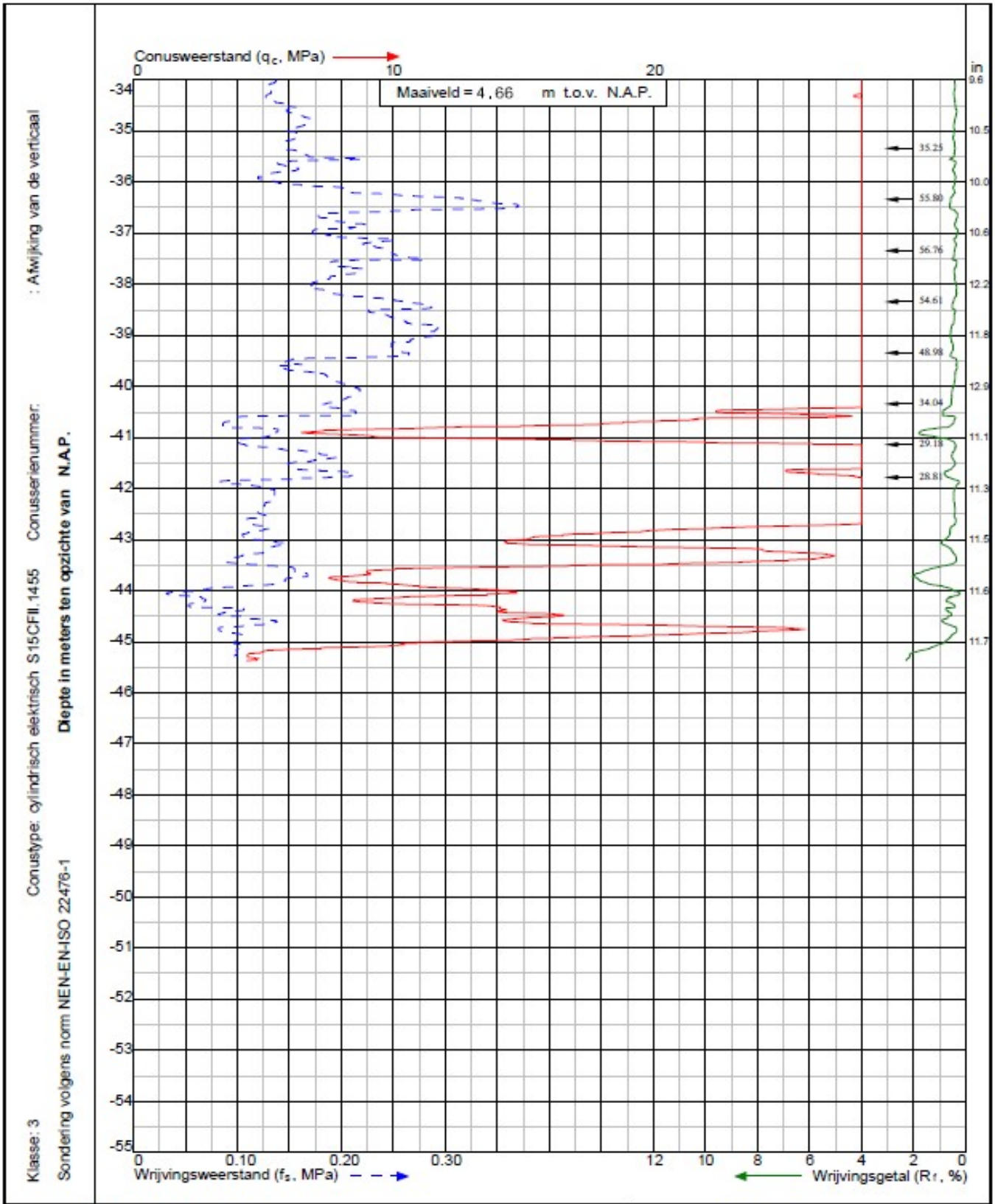

Project: Project Hartel Tank Terminal te **Rotterdam**		Sondering: DKM032B
Wiertsema & Partners RAADGEVEND INGENIEURS	x = 64102 y = 439501	Opdr.nr: VN-66080-1
	Blad: 3 van 3	Datum: 29-9-2016
		AKKOORD UITV

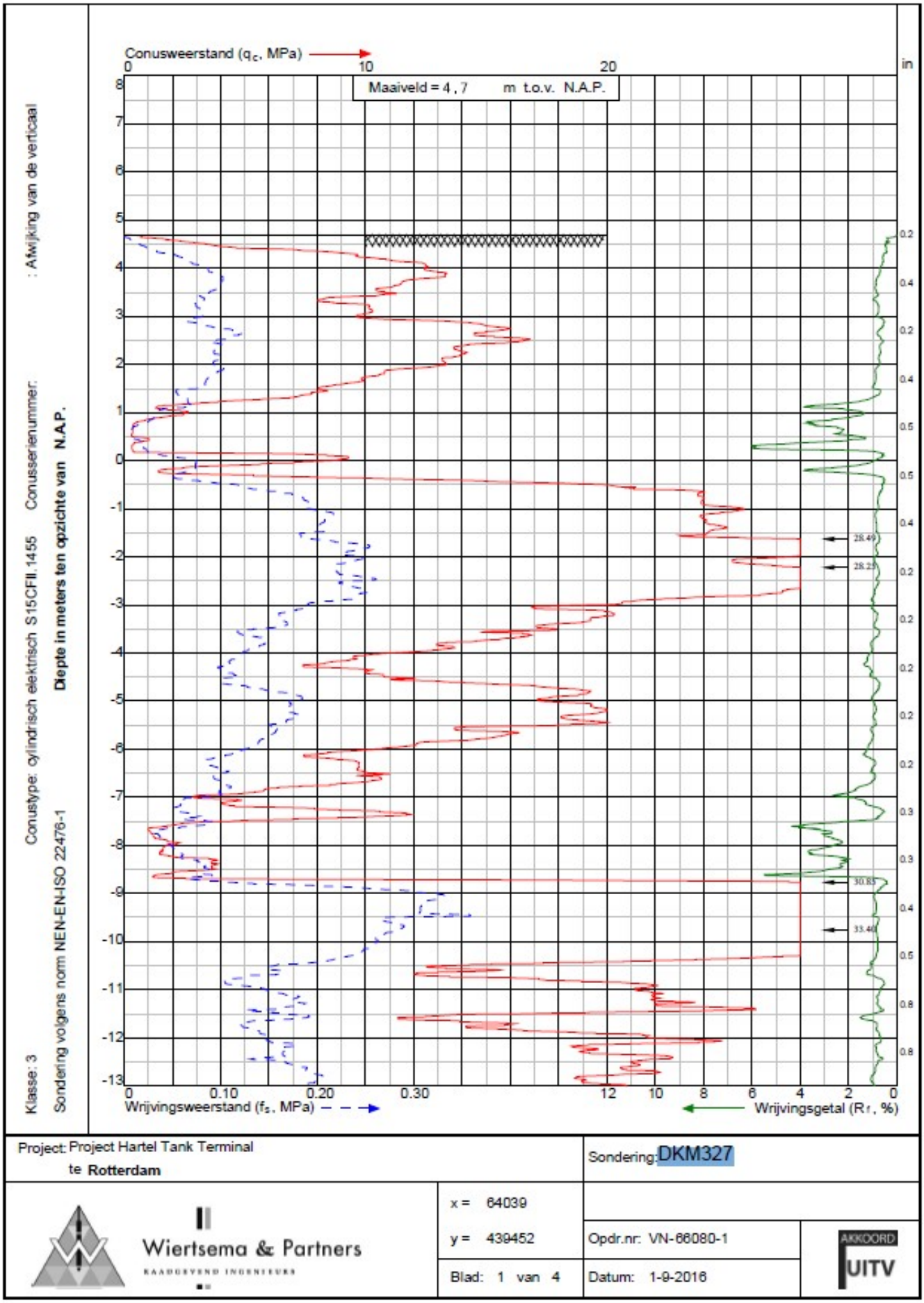

Project: Project Hartel Tank Terminal te **Rotterdam**

Sondering: DKM327

Wiertsema & Partners
RAADGEVEND INGENIEURS

x = 64039

y = 439452

Blad: 1 van 4

Opdr.nr: VN-66080-1

Datum: 1-9-2016

AKKOORD UITV

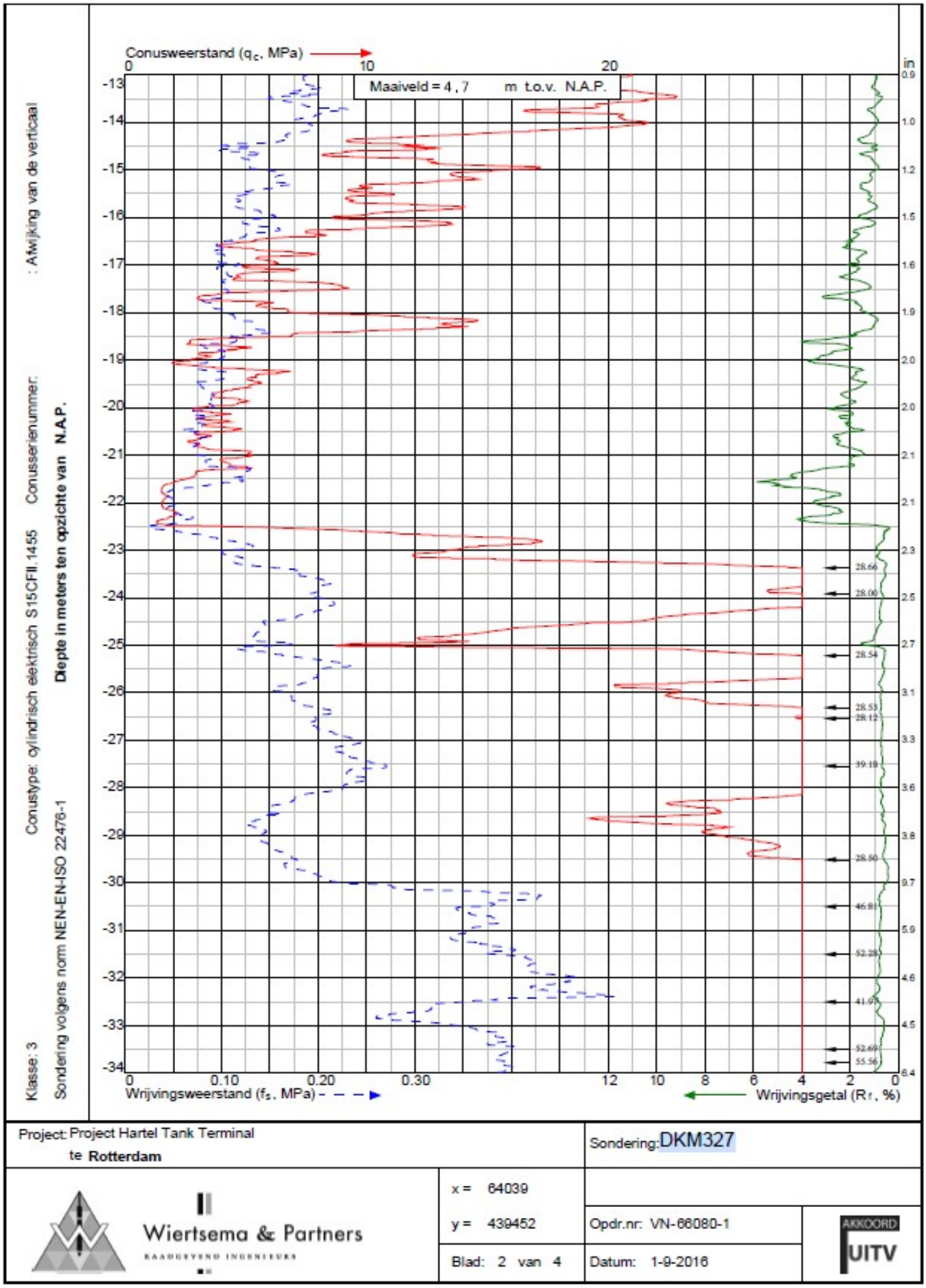

Project: Project Hartel Tank Terminal te **Rotterdam**		Sondering: DKM327
Wiertsema & Partners RAADGEVEND INGENIEURS	x = 64039 y = 439452 Blad: 2 van 4	Opdr.nr: VN-66080-1 Datum: 1-9-2016
		AKKOORD UITV

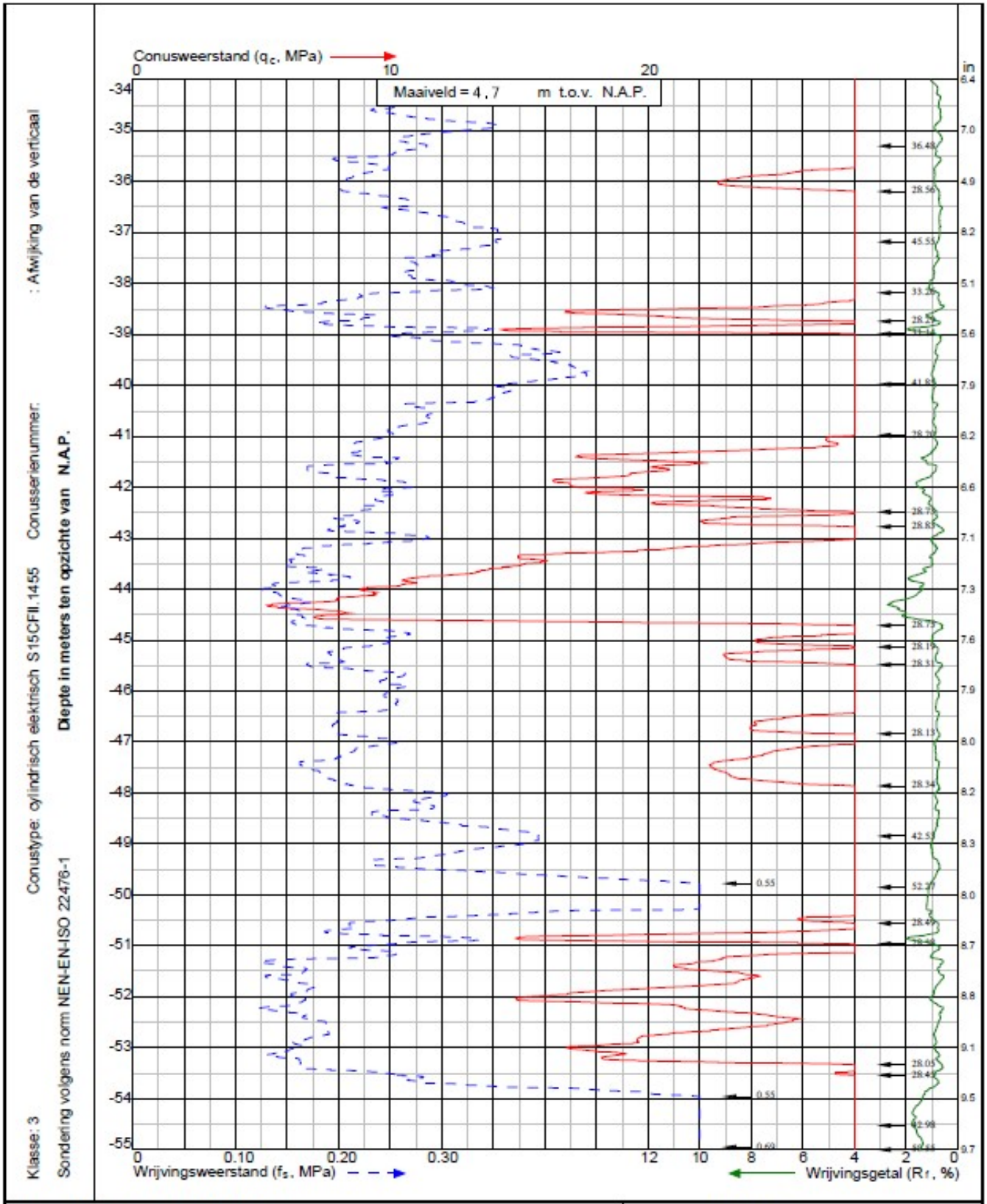

Project: Project Hartel Tank Terminal te **Rotterdam**

Sondering: DKM327

Wiertsema & Partners
RAADGEVEND INGENIEURS

x = 64039

y = 439452

Opdr.nr: VN-66080-1

Blad: 3 van 4

Datum: 1-9-2016

AKKOORD UITV

B.2. CPTs from zone B showing presence of deep clay layer

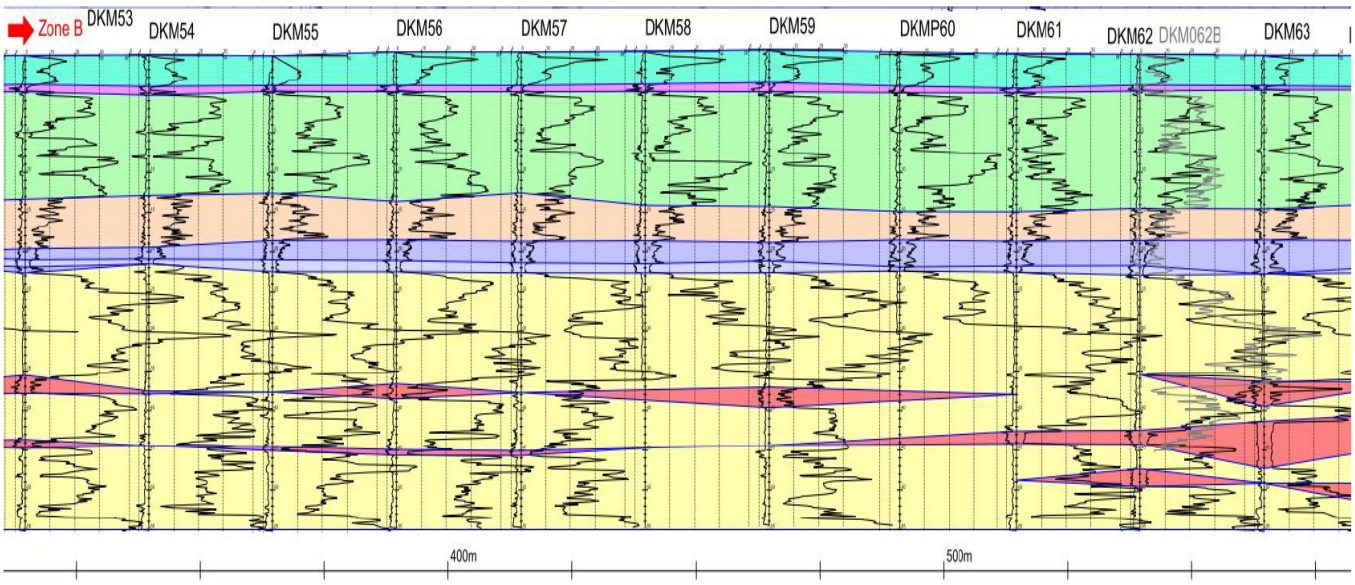

Figure B.1: CPTs along axis-3 with deep clay layers [red] recorded around zone B of HTT quay wall (Imbrechts et al., 2017b)

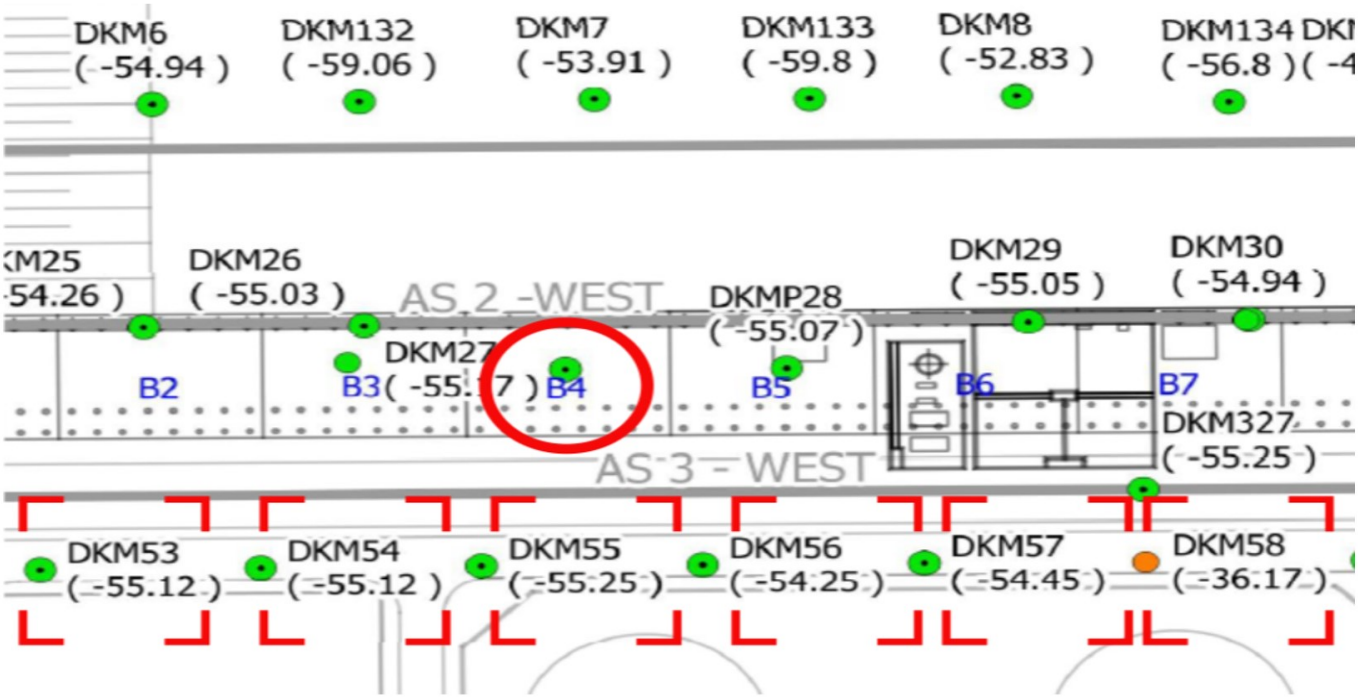

Figure B.2: Locations of CPTs that recorded deep clay layers around zone B4 (Imbrechts et al., 2017b)

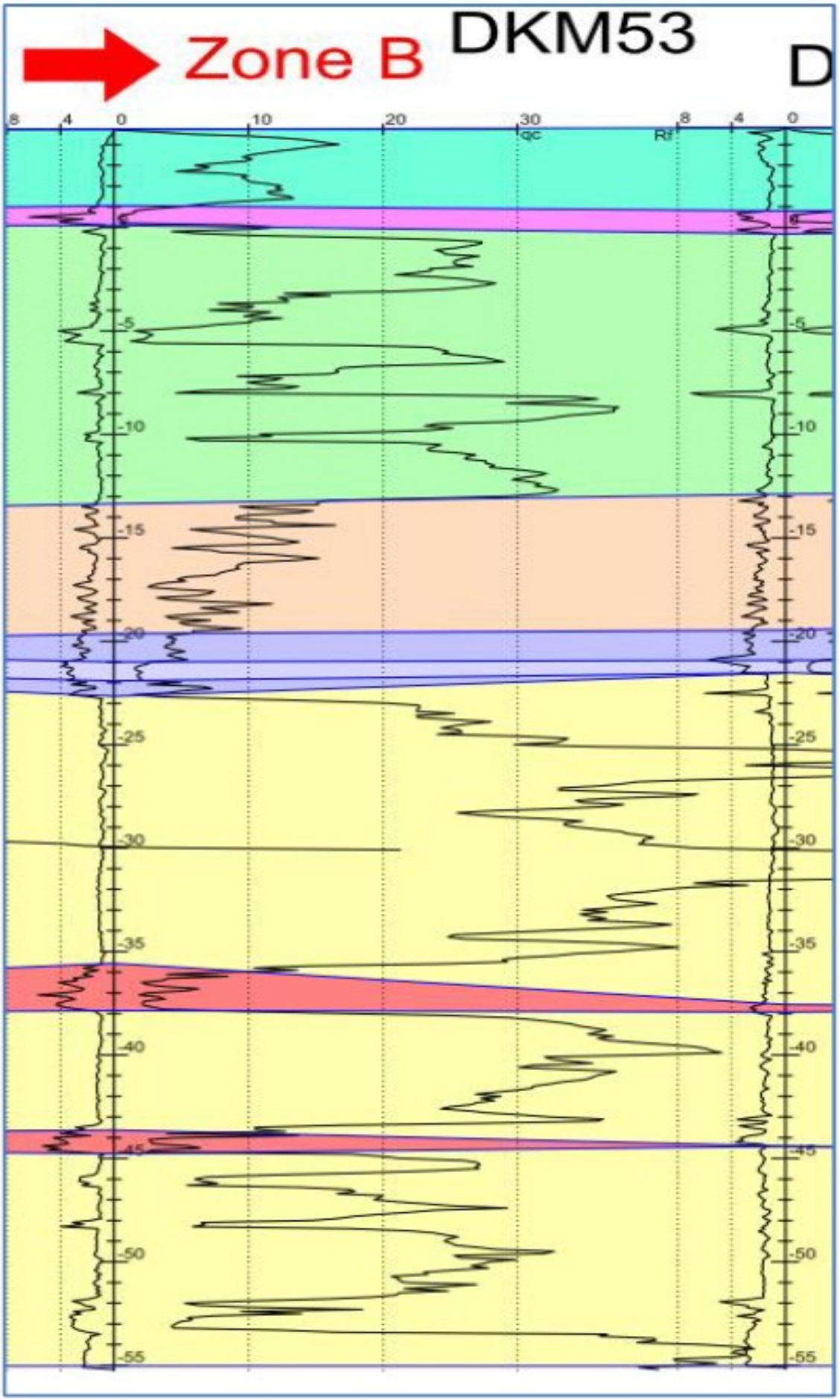
Zone B
DKM53
D
8
4
0
10
20
30
qc
8
4
0
Rf
-5
-10
-15
-20
-25
-30
-35
-40
-45
-50
-55

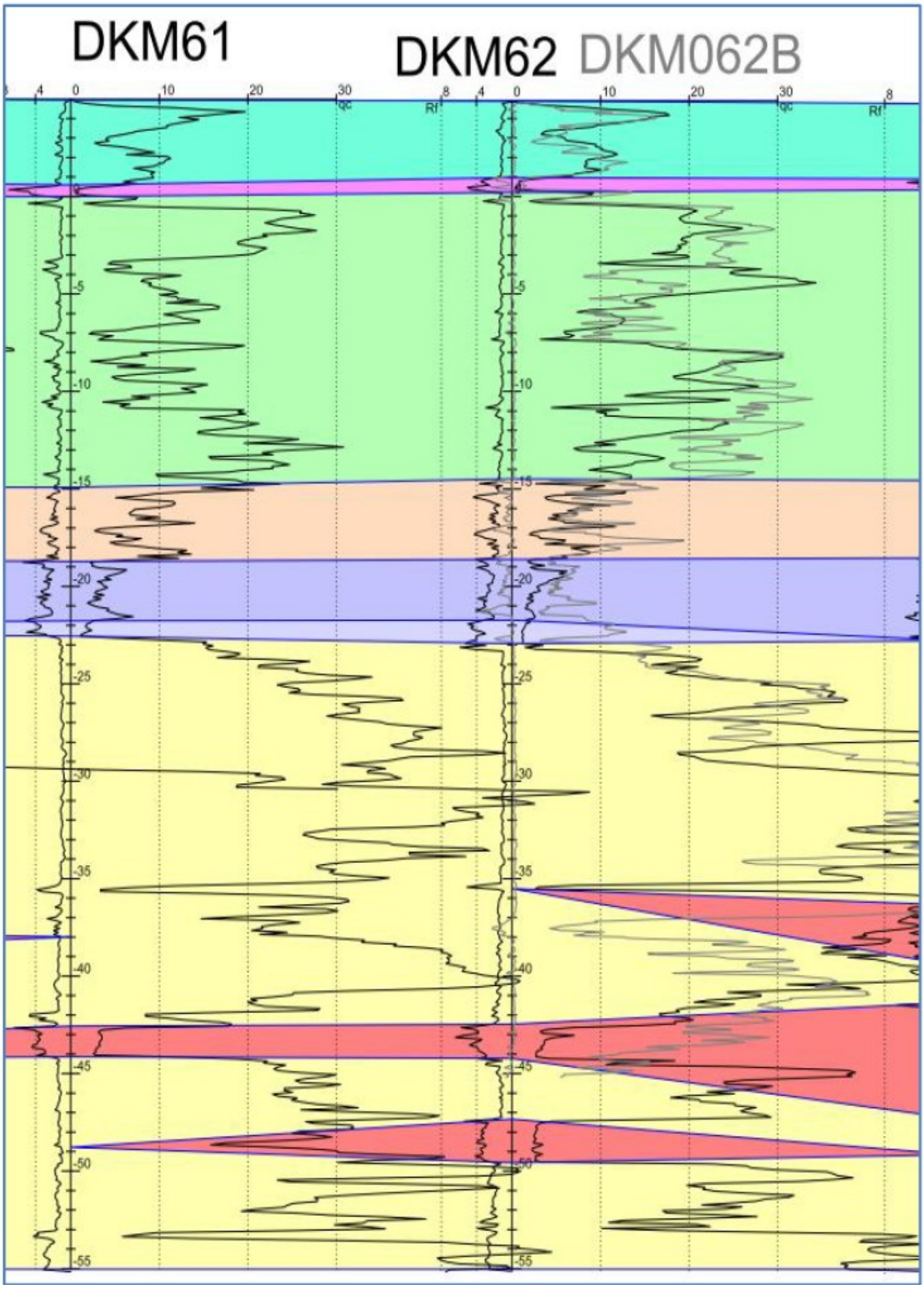
DKM61
DKM62
DKM062B
qc
Rf
-5
-10
-15
-20
-25
-30
-35
-40
-45
-50
-55